Identification of genes regulated by the *Drosophila* transcription factor Hindsight

by

Olivia Yang Du

A thesis
presented to the University of Waterloo
in fulfillment of the
thesis requirement for the degree of
Master of Science
in
Biology

Waterloo, Ontario, Canada, 2013

© Olivia Yang Du

Declaration Page

I hereby declare that I am the sole author of this thesis. This is a true copy of the thesis, including any required final revisions, as accepted by my examiners.

I understand that my thesis may be made electronically available to the public.

Abstract

Hindsight (HNT) is a zinc finger transcription factor that is required for morphogenesis of the *Drosophila* embryo, having roles in germ band retraction (GBR) as well as dorsal closure (DC). HNT expression is also found in sensory organ precursors (SOP) of the developing pupal peripheral nervous system, and muscle progenitor cells, but the role of HNT in neurogenesis and myogenesis during embryogenesis has not been investigated in any depth. Microarray analysis of embryos over-expressing HNT during GBR and DC identified 1290 genes with significant changes in expression. This data set included many potential HNT targets, including genes associated with myogensis, and a disruption of muscle development was observed in embryos over-expressing HNT. It is possible that HNT may function to repress muscle identity genes in muscle founder cells. In addition, HNT over expressing embryos were found to resemble the neurogenic class of mutants. Among the potential target genes, *D-Pax2* (*shaven, sparkling,* CG11049) expression, which is known to be expressed in the developing peripheral nervous system, was confirmed to be up-regulated following HNT over-expression. Interestingly, *D-Pax2* and *HNT* expression were found to co-localize at the onset of their expression at stages 10-12 in embryos, but were not co-localized in later stages of embryogenesis. The up-regulation of D-Pax2 by HNT over-expression was further characterized and was found to be associated with strong ectopic HNT expression. The relevance of HNT to the regulation of *D-Pax2* during normal development remains to be determined, but it is possible that endogenous expression of HNT is involved in D-Pax2 repression.

Acknowledgements

First of all, I would like to thank my supervisor Dr. Bruce Reed, for his support and guidance throughout my Masters. His knowledge and advice has not only helped me complete my project, but has also allowed me to develop extensive research skills that will aid me in my future endeavours. I would also like to thank Dr. Brendan McConkey and Dr. Matt Vijayan for their support and for serving on my supervisory committee.

In addition I want to thank the past and present graduate students and lab members, whose friendships and enthusiasm have made my Master's an enjoyable and stimulating experience. Special thanks to Olga Cormier, Brittany Baechler, Minhee Kim, April Pawluck, and Elissa Downey.

Lastly, I am forever grateful to my friends and loved ones, especially Rachelle Kanippayoor and Daniele Hohol, who believed in me and supported me throughout my Masters; and to my family, especially my father Caigan Du, who has not only supported me financially, but has always motivated and guided me to realize this achievement.

Table of Contents

Declaration ii

Abstract iii

Acknowledgements iv

Table of Contents v

List of Figures viii

List of Tables x

List of Abbreviations xi

Chapter 1. Introduction 1

1.1 Morphogenesis 1

1.2 *Hindsight* 4

1.3 *Hindsight*'s role in the amnioserosa during Germ Band Retraction and Dorsal Closure 5

1.4 Notch signaling 6

1.5 *Hindsight* in the sensory organ precursor 9

1.6 *Hindsight* in muscle progenitor cells 12

1.7 Objective 15

Chapter 2. Materials and Methods 16

2.1 *Drosophila* Stocks and Fly Husbandry 16

2.2 *GAL4*/*UAS* system 16

2.3 $GAL80^{ts}$ 19

2.4 Overnight embryo collection for Microarray Analysis and Fluorescent *In situ* hybridization 19

2.5 Embryo Fixation and Dechorionation 19

2.6 Phalloidin stain 20

2.7 Immunostaining: Double and Single Antibody stain 20

2.8 RNA extraction 21

2.9 Microarray 21

2.9.1 Bioinformatics Analysis of Microarray Results 21

2.10 Fluorescent *In situ* hybridization 22

2.11 Confocal microscopy 23
2.12 Cell count 23
Chapter 3. Results 26
3.1 Design of experimental *Drosophila* models for the analysis of embryos in which Hindsight is over-expressed or depleted 26
3.1.1 Phenotypic consequences of a variety of *GAL4*-driver>*UAS*-reporter combinations 26
3.1.2 Hindsight expression in the experimental models 30
3.2 Microarray Analysis of *Hindsight* targeted genes 32
3.2.1 Confirmation of Hindsight expression in experimental models (Hindsight over-expression versus RNAi depletion) 37
3.3 Association of Hindsight expression with Muscle Development 39
3.3.1 The regulation of muscle formation by *Hindsight* 42
3.3.2 The regulation of muscle strand development by *Hindsight* 44
3.3.3 Investigation of the sensitivity of muscle development to Hindsight over-expression during development 46
3.3.4 Hindsight expression in Muscle founder cells 49
3.3.5 The effect of inducing Hindsight expression in Muscle founder cells 51
3.3.6 Summary: the roles of *Hindsight* in muscle development 54
3.4 The association of *Hindsight* with Neuron development, and Notch signaling 55
3.4.1 *Shaven/D-Pax2* 58
3.4.2 The relationship between Hindsight and D-Pax2 expression in wild type embryos 58
3.4.3 The analysis of neurogenesis defects associated with Hindsight over-expression 62
3.4.4 The co-localization of D-Pax2 and Hindsight in different experimental models 64
3.5 D-Pax2 expression may be dependent on the level of Hindsight expression 70
3.5.1 D-Pax2 expression is not robustly increased using the *hnt* reporter line *EP55* 70
3.5.2 Hindsight over-expression via the *UAS-GFP-HNT* reporter is greater

than the *EP55* reporter 74
3.5.3 Increasing Hindsight expression in *EP55* embryos is unable to give strong D-Pax2 expression 76
3.5.4 Reducing Hindsight expression in the *UAS-GFP-HNT* line has little effect on D-Pax2 expression 79
3.5.5 The UAS-GFP-HNT construct is not the cause of the strong D-Pax2 expression 83
3.6 Summary: the role of *Hindsight* in Neuron development 87
Chapter 4. Discussion 88
4.1 Muscle Development during embryogenesis 88
4.1.1 Down-regulation of muscle identity genes by *Hindsight* 88
4.1.2 Down-regulating muscle identity genes by *Hindsight* through *Jelly Belly* 90
4.2 Neuron Development during embryogenesis 91
4.2.1 How *Hindsight* could be affecting Neural development 93
4.2.2 How *Hindsight* may be affecting D-Pax2 expression 94
4.3 Conclusion 96
Chapter 5. Future Directions 97
5.1 Further directions with Microarray Data 97
5.2 Muscle development 97
5.3 Neuron development 98
References 100
Appendix A. Stock List 106
Appendix B. Hindsight Over-expression Microarray Results 107
Appendix C. Hindsight Depletion Microarray Results 144

List of Figures

Figure 1.1	Stages of *Drosophila* embryogenesis	3
Figure 1.2	Notch signaling	8
Figure 1.3	Sensory organ precursor specification and differentiation	11
Figure 1.4	Muscle progenitor specification and differentiation	14
Figure 2.1	*GAL4/UAS* System	18
Figure 2.2	Cell count sections of the *Drosophila* embryo	25
Figure 3.1	Hindsight Antibody stain of Control, Hindsight over-expression and depleted embryos	31
Figure 3.2	Microarray analysis of developmental systems affected by Hindsight over-expression	34
Figure 3.3	Microarray analysis of developmental systems affected by Hindsight depletion	35
Figure 3.4	Comparison of linear Hindsight expression between the control and Hindsight over-expression and depletion	38
Figure 3.5	The Fluorescent *in-situ* hybridization expression of *Pox meso*	41
Figure 3.6	TRITC-Phalloidin stain	43
Figure 3.7	Confocal live imagining with the *DmefGAL4>UASmoesinCherry/TM3* stock	45
Figure 3.8	Induced Hindsight over-expression with the *DmefGAL4>UASmoesinCherry/TM3* stock	48
Figure 3.9	Hindsight Antibody stain of the *RP298-GAL4* muscle founder driver	50
Figure 3.10	TRITIC-Phalloidin stain of *RP298-GAL4* early staged embryos	52
Figure 3.11	TRITIC-Phalloidin stain of *RP298-GAL4* late staged embryos	53
Figure 3.12	The Fluorescent *in-situ* hybridization expression of candidate neural genes	57
Figure 3.13	Double antibody stain with Anti-Hindsight and Anti-D-Pax2 of control embryos	58
Figure 3.14	Hindsight expressing cells in the control embryos at different developmental stages	61
Figure 3.15	22C10 stain	63

Figure 3.16 Double antibody stain with Anti-Hindsight and Anti-D-Pax2 on control, Hindsight over-expression and Notch null embryos 67
Figure 3.17 Hindsight antibody stain of Notch null and Delta mutant embryos 68
Figure 3.18 Regulation of Hindsight/D-Pax2 co-localization in embryos of Hindsight over-expression and Notch null 69
Figure 3.19 Double antibody stain with Anti-HNT and Anti-D-Pax2 on *EP55* embryos 72
Figure 3.20 Hindsight and/or D-Pax2 expression in control embryos versus *EP55*, Hindsight over-expression embryos 73
Figure 3.21 Hindsight expression level comparison between *EP55* and *UAS-GFP-HNT* embryos 75
Figure 3.22 Double antibody stain with Anti-Hindsight and Anti-D-Pax2 comparing *EP55* at 29^{o}C to *UAS-GFP-HNT* embryos 77
Figure 3.23 Regulation of Hindsight and/or D-Pax2 expression in the embryos by different levels of Hindsight over-expression 78
Figure 3.24 Double antibody stain with Anti-Hindsight and Anti-D-Pax2 on *UAS-GFP-HNT* embryos at 18^{o}C 81
Figure 3.25 Hindsight and/or D-Pax2 expression in the embryos by modulating different levels of Hindsight expression 82
Figure 3.26 Double antibody stain with Anti-Hindsight and Anti-D-Pax2 on *UAS-GFP-HNT^{J18}* embryos 83
Figure 3.27 Regulation of Hindsight and/or D-Pax2 expression in the embryos in different Hindsight over-expression stocks 86

List of Tables

Table 3.1	Testing a variety of *GAL4*-drivers>*UAS*-reporter combinations	29
Table 3.2	Validating the microarray data based on *yellow* and *white* gene copies	36
Table 3.3	Candidate genes from the Hindsight over-expression microarray data that are involved in muscle development	40
Table 3.4	Candidate genes from the Hindsight over-expression microarray data that are involved in neural development	56

List of Abbreviations

ac	*Achaete*
bHLH	basic helix-loop-helix
Brd	*Bearded*
Ch	Chordotonal organs
da	*daughterless*
DC	Dorsal Closure
es	External sense
F-actin	Filamentous actin
FBtr	FlyBase identifier
FC	Founder cells
FCM	Fusion competent myoblasts
FDR	False Discovery Rate
FISH	Fluorescent in situ hybridization
GAL4	Galactose 4 transcription factor from *Saccharomyces cerevisiae*
GBR	Germ Band Retraction
GFP	Green Fluorescent Protein
HNT	*Hindsight*
Jeb	*Jelly Belly*
JNK	c-Jun N-terminal kinase
l'sc	*lethal of scute*
MD	Multiple Dendritic
NICD	Notch intracellular domain
PBS	Phosphate buffered saline
PNC	Proneural cluster
PNS	Peripheral nervous system
RREB1	Ras responsive element binding protein
sc	*scute*
SOP	Sensory organ precursor
UAS	Upstream Activating Sequence
w	*white*
y	*yellow*

Chapter 1. Introduction

1.1 Morphogenesis

Morphogenesis is the formation of tissues and organisms through the precise control of cell shape, cell proliferation, cell death, and cell-cell adhesion, which are an integral part of *Drosophila* development (Stronach & Perrimon, 2001). During *Drosophila* embryogenesis there are four major morphogenetic movements occurring at stages 11 to 15 of development: germ-band extension, germ-band retraction (GBR), dorsal closure (DC) and head involution (Irvine & Wieschaus, 1994).

Due to the restriction imparted by the vitelline membrane that surrounds the developing embryo, the germ-band folds over itself on the dorsal side as its length increases in the anterior-posterior axis (Schock & Perrimon, 2002) (Figure 1.1 A). This results in the germ-band extended state that persists for approximately 3.5 hours during normal development. GBR follows, whereby cell shape changes in the lateral epidermis allow the amnioserosa (an extra-embryonic epithelium that forms a covering connecting the developing lateral epidermis) to unfold on the dorsal side of the embryo (Figure 1.1 B-C). Immediately after GBR, DC is initiated; the lateral epidermal cells flanking the amnioserosa migrate and fuse along the dorsal midline, internalizing the amnioserosa that is subsequently degenerated by programmed cell death (Hartenstein, 1993; Scuderi & Letsou, 2005) (Figure 1.1 D). Lastly, head involution involves the progression of the epidermis over the head segments that simultaneously regress into the embryo (VanHook & Letsou, 2008).

In addition to these morphogenetic movements, the specification of muscle progenitors and sensory organ precursors (SOP) from the mesoderm also occur during stages 11 to 14 of

development. One of the genes that has been known to be involved in the proper completion of GBR and DC, and most recently has been found in muscle and SOP is Hindsight (HNT).

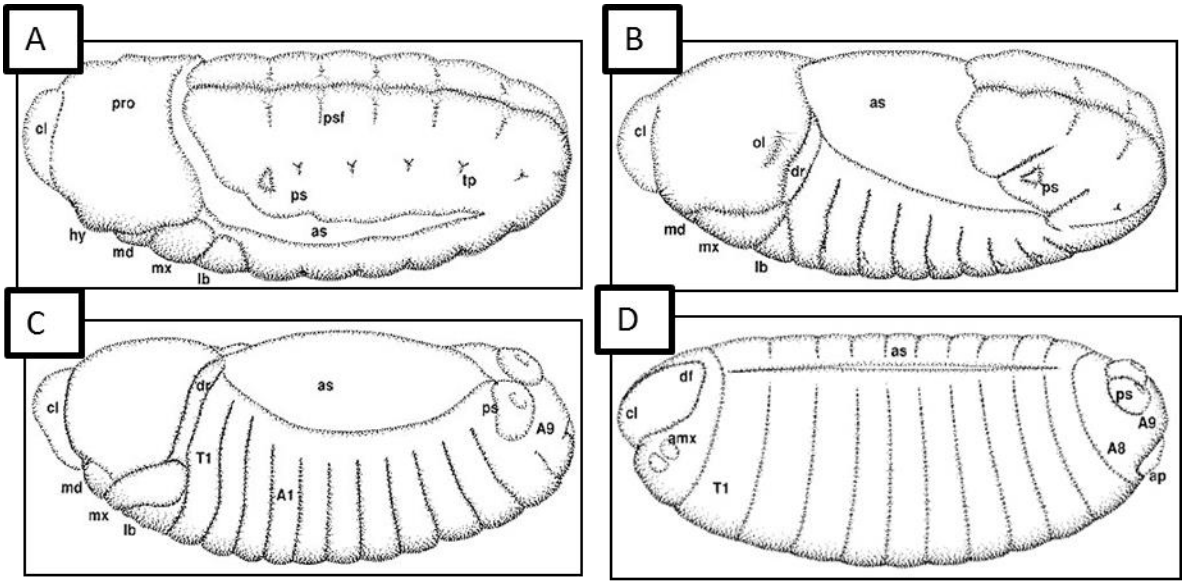


Figure 1.1

Stages of *Drosophila* embryogenesis consist of **(A)** Germ band extended stage of development (stage 11, 5:20-7:20 hr:min), **(B)** Germ band retraction stage of development (stage 12, 7:20-9:20 hr:min), **(C)** Dorsal closure stage of development (stage 14, 10:20-11:20 hr:min), **(D)** Completion of Dorsal closure (stage 15, 11:20-13:00 hr:min). Images adapted Hartenstein, V. 1993

1.2 *Hindsight*

HNT encodes a large nuclear protein with fourteen C_2H_2-type zinc fingers whose functions suggest it acts as a transcription factor, specifically as a repressor. The human/mammalian homolog of HNT is known as Ras responsive element binding protein 1 (RREB1). RREB1 has been suggested to regulate prostate cancer by down-regulating the zinc transporter hZIP1, and in response to DNA damage, RREB1 has been implicated in modulating the expression of the p53 tumour suppressor and its target genes (Irvine & Wieschaus, 1994; Milon, Agyapong, Bautista, Costello, & Franklin, 2010). RREB1 and HNT have a conserved role in regulating dynamic morphological changes, cell-cell adhesion, and the collective migration of epithelial cells (Melani, Simpson, Brugge, & Montell, 2008). HNT is also expressed in the amnioserosa, midgut and tracheae during *Drosophila* embryogenesis, and is required for the proper completion of GBR, DC, and the programmed degradation of the amnioserosa (Reed, Wilk, & Lipshitz, 2001). In addition, HNT is expressed in the ovary and retina of adult flies, where it has been implicated in the regulation of cell-cell adhesion, coordination of the F-actin cytoskeleton, and regulation of these processes by the Notch signalling pathway; in addition, HNT is also involved in the regulation of the mitotic-to-endocycle switch in adult follicle cells (Melani et al., 2008; Pickup, Lamka, Sun, Yip, & Lipshitz, 2002; Sun & Deng, 2007).

1.3 *Hindsight's* role in the amnioserosa during Germ Band Retraction and Dorsal Closure

HNT expression in the amnioserosa has been found to down-regulate the c-Jun N-terminal kinase (JNK) pathway, and this has been suggested to be required for successful completion of GBR and DC (Reed et al., 2001; Yip, Lamka, & Lipshitz, 1997). Without HNT, mutant embryos display head involution defects and undergo premature amnioserosa loss, indicating that the amnioserosa is associated with a failure in GBR and DC (Frank & Rushlow, 1996). Nullomorphic *hnt* mutants are embryonic lethal and fail in GBR. A hypomorphic mutation of HNT (hnt^{308}) successfully completes GBR, but subsequently fails in DC (Reed et al., 2001). *hnt* loss-of-function mutants have been found to show persistent activation of the JNK signaling pathway in the amnioserosa, while an inactivation of JNK signaling is essential for DC. Studies have found that HNT expression in those amnioserosal cells that abut the leading edge of the epidermis is required to direct the epidermal cells to undergo the shape changes that drive GBR (Lamka & Lipshitz, 1999). The premature loss of the amnioserosa may be due to the disruption of cell-cell communication from the amnioserosa to the adjacent epidermis, which suggests a consequence of an underlying defect in the amnioserosal epithelium (Wilk, Reed, Tepass, & Lipshitz, 2000). While cell-cell communication may be the cause of premature amnioserosa loss, failure in DC is linked to HNT'*s* inability to inactivate the JNK signaling pathway, resulting in the disruption of the JNK pathway in the amnioserosa (Reed et al., 2001).

1.4 Notch signaling

As mentioned above, HNT has been implicated in the regulation of processes in the ovary and retina of adult flies through the Notch signalling pathway. Notch signalling is a simple but highly conserved framework that controls the development of cell fates and allows cell differentiation. The basis of Notch signalling, as seen in Figure 1.2, is achieved through cell-cell communication between its ligands Delta and Serrate (known as Jagged in mammals), and the Notch receptor on an adjacent cell. Both the receptor and ligands are transmembrane proteins with large extracellular domains that consist primarily of epidermal growth factor (EGF) repeats. Ligand binding triggers two proteolytic cleavages of the Notch receptor. The second cleavage, by γ-secretase, releases the notch intracellular domain (NICD) which translocates into the nucleus. Upon entering the nucleus, the NICD promotes transcription by activating the DNA-binding protein complex CSL (named after the C-promoter binding factor-1 (CBF1), Suppressor of Hairless (Su(H)), and LAG-1, and its co-activator Mastermind (Mam)) (S. Bray, 1998; S. J. Bray, 2006; Eric C Lai, 2004).

Notch signaling appears to act through three different modes: lineage decisions, establishing boundaries, and lateral inhibition. Lineage decisions are a type of directional inhibitory Notch signaling that occurs during asymmetric cell divisions. In this situation, two daughter cells are capable of sending and receiving Notch signals, but directionality is imposed by the asymmetric segregation of regulators that influence Notch signaling, such as Numb, and as a result the daughter cells adopt different fates from one another (Eric C Lai, 2004). Notch signaling is also involved in establishing boundaries. In this process Notch is activated in cells at the interface between two regions, creating an organizer at the boundary. The organizer is involved in cell-cell communication between the two regions that keeps them distinct. The

positive outcome of this Notch signaling function contrasts Notch's inhibitory role in other signaling functions (Neumann & Cohen, 1997).

Lastly, Notch signaling is involved in lateral inhibition. Lateral inhibition is a process by which one cell is selected from a group of equivalent precursors. In the group, all cells initially express the Notch ligand and receptor, and have the capacity to signal to one another; however, subtle differences between the cells become reinforced through a feedback loop. This process ensures that the cell with the least amount of Notch activation is singled out as the 'source' of the ligand, which sends inhibitory signals to all of the surrounding cells (Simpson, 1997). Lateral inhibition is of particular interest since it is involved in the selection of SOP and muscle progenitors from clusters in the embryonic epithelium.

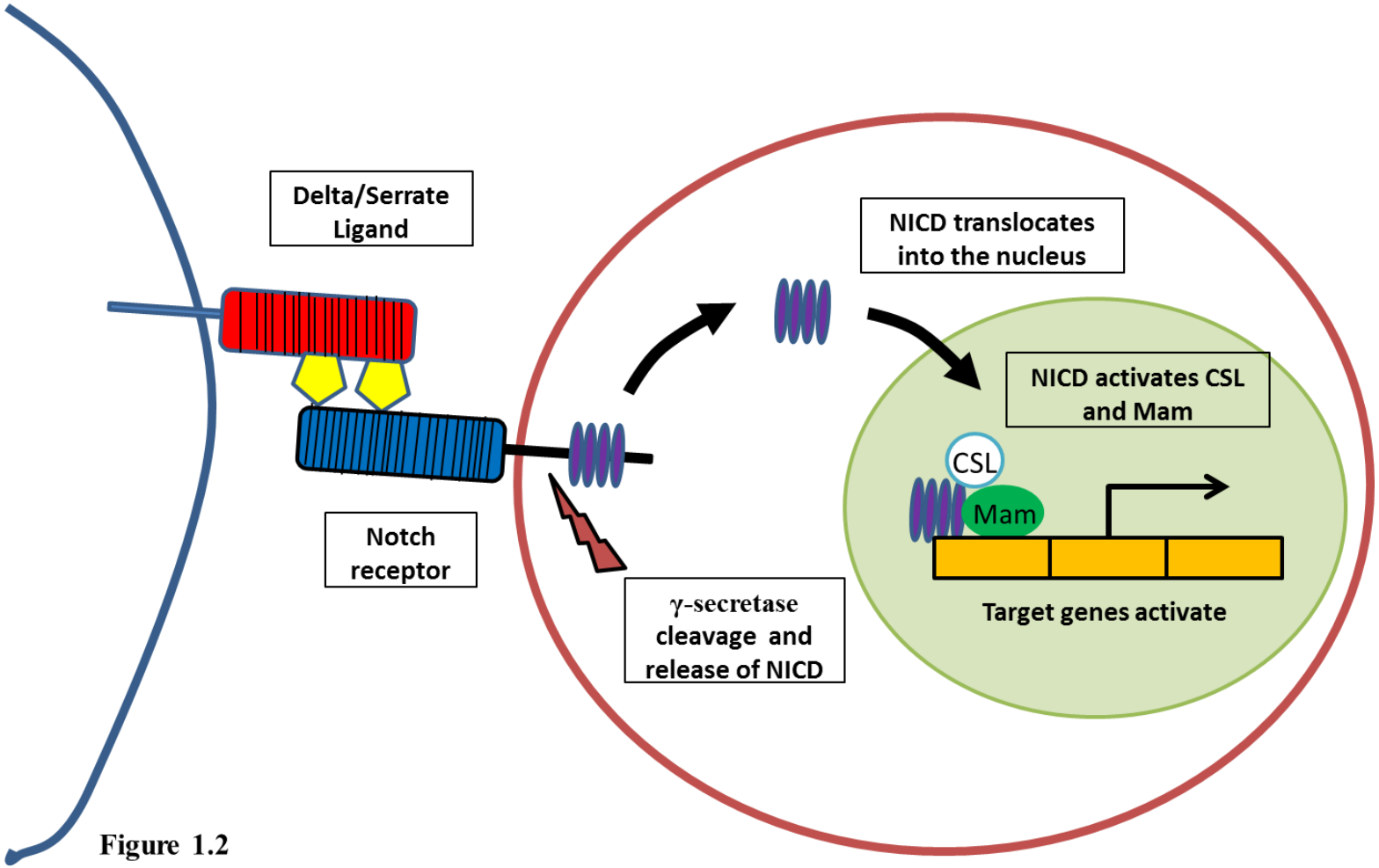


Figure 1.2

Notch signaling is based upon cell-cell communication between the Delta/Serrate ligand and the Notch receptor, on the adjacent cell. Cleavage by γ-secretase releases the Notch intracellular domain (NICD), which translocates into the nucleus. Upon entering the nucleus, the NICD activates the CSL, which is named after the C-promoter binding factor-1 (CBF1), Suppressor of Hairless (Su(H)), and LAG-1. NICD also binds CSL's co-activator Mastermind (Mam) to activate target gene expression.

1.5 *Hindsight* in the sensory organ precursor

Most recently, in a genome-wide transcriptome analysis of SOP's that were isolated using laser microdissection from the dorsal epithelium of *Drosophila* pupae, HNT was found to be highly expressed (Buffin & Gho, 2010). The early cell fate specification of the SOPs in pupae into microchaetes, is not unlike the SOP selection during other forms of *Drosophila* development, such the peripheral nervous system (PNS) during embryogenesis (Pi & Chien, 2007). In both cases, the SOPs are selected from a small group of cells, termed the proneural cluster (PNC). The PNC is defined by the expression of members of the so-called proneural genes, including *lethal of scute* (*l'sc*). Early in the establishment of the SOP, all cells of the PNC have the potential to adopt neural cells fates. Eventually, however, only one cell of the PNC is selected as the SOP, and as shown in Figure 1.3, the SOP will generate all cells of the microchaetes, of the pupae, also known as external sense (es) organs. The expression of proneural proteins of basic helix-loop-helix (bHLH) transcription factors is required in the PNC to initiate and execute neurogenic programs (Villares & Cabrera, 1987). *Achaete* (*ac)* and *scute (sc)*, from the achaete-scute complex, are the first identified members of the bHLH proteins, and are required for cells in the PNC to develop into SOPs, through a process called lateral inhibition mediated by the Notch signaling pathway.

Lateral inhibition is a key process by which a single SOP is selected from the proneural cluster. A popular model for SOP selection involves a single cell within a PNC that expresses more Delta ligand than its surrounding cells. This cell then activates Notch in adjacent cells to trigger an intracellular signalling cascade that leads to the inhibition of proneural gene expression and results the acquisition of non-noneural neighbouring cells, as outlined in Figure 1.3 (Artavanis-Tsakonas et al., 1990; Artavanis-Tsakonas, Rand, & Lake, 1999).The SOP then

proceeds to divide to produce five cell types, four of which mature into es organs (Campuzano & Modolell, 1992).

The embryonic PNS consists of three types of sensory organs: es organs, chordotonal (Ch) organs, and multiple dendritic (MD) neurons. The mechanism of their cell specification is similar to the specification of microchaetes of the pupae. The major difference being that *ac* and *sc* are required for the formation of es organs, whereas *atonal* directs the formation of Ch organs (Campuzano & Modolell, 1992; Jarman, Grau, Jan, & Jan, 1993). The MD neurons are derived in two different ways; the most common way is from either es or Ch organ lineages, while the remaining MD neurons, also known as solo-MD neurons derive directly from SOP cells (Brewster & Bodmer, 1995). While HNT was found to be expressed in the SOPs of pupae, the role of HNT has yet to be determined, nor has HNT's function in embryonic SOPs, of the PNS, been investigated.

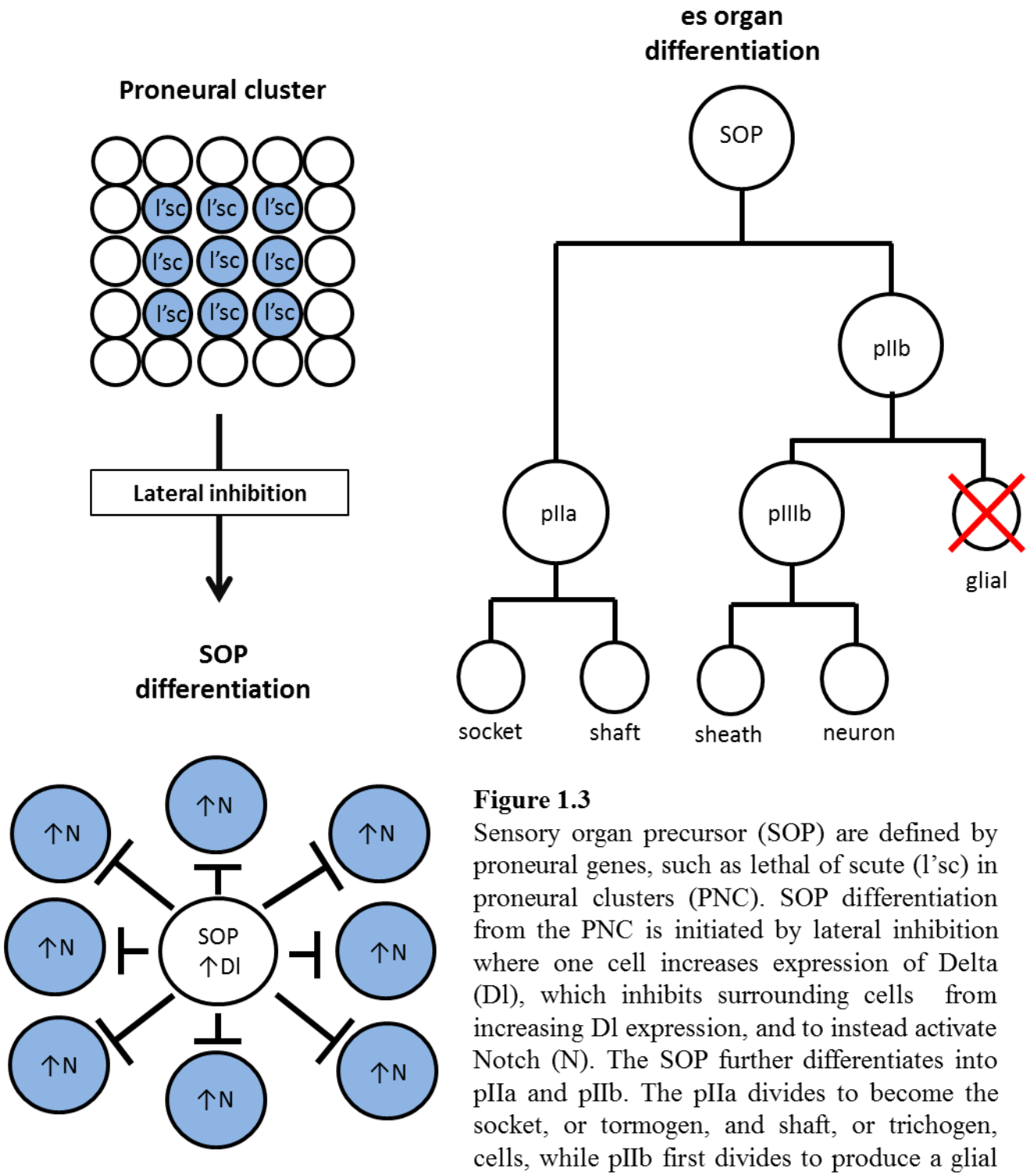


Figure 1.3
Sensory organ precursor (SOP) are defined by proneural genes, such as lethal of scute (l'sc) in proneural clusters (PNC). SOP differentiation from the PNC is initiated by lateral inhibition where one cell increases expression of Delta (Dl), which inhibits surrounding cells from increasing Dl expression, and to instead activate Notch (N). The SOP further differentiates into pIIa and pIIb. The pIIa divides to become the socket, or tormogen, and shaft, or trichogen, cells, while pIIb first divides to produce a glial cell that undergoes programmed cell death (PCD), and pIIIb, which divides into the sheath, or thecogen, and neuron cells.

1.6 *Hindsight* in muscle progenitor cells

An additional recent study investigating short term transcriptional responses to Notch in a *Drosophila* cell line similar to adult muscle progenitor cells also identified HNT as a direct transcriptional target of the Notch signaling pathway. HNT was confirmed to be present in adult myoblasts, and determined to have an effect on differentiation in adult muscle progenitors (Krejci, Bernard, Housden, Collins, & Bray, 2009). The process of muscle progenitor differentiation and development is shown in Figure 1.4. During embryogenesis, muscle development starts with the segregation of progenitor cells from an area of the mesoderm expressing high levels of *twist* (Borkowski, Brown, & Bate, 1995; Carmena, Bate, & Jimenez, 1995). Muscle progenitors are singled out from clusters of the mesoderm that expresses a proneural gene, such as *l'sc*, by a process of lateral inhibition (Bate, Rushton, & Frasch, 1993; Carmena et al., 1995; Corbin et al., 1991). The muscle progenitor cells are then specified into two types of myoblasts, founder cells (FCs), which contain information required for morphogenesis, and fusion competent myoblasts (FCM). Muscles develop from the fusion of the FC with the FCM, and the characteristics of the muscle are specified by the specific identity gene expressed in the FC (Bate, 1990; Dohrmann, Azpiazu, & Frasch, 1990). Identity genes expressed in the FCs include *apterous* (*ap*), *even skipped* (*eve*), *kruppel* (*kr*), *ladybird* (*lb*) and *nautilus* (*nau*) and *slouch* (*slou*) (Tixier, Bataille, & Jagla, 2010).

Similar to the selection of SOP's within the PNC, the process by which progenitor cells become FCs, or FCMs, also occurs by lateral inhibition coupled to mitogen-activated protein kinase signalling through multiple feedback loops. This process allows only one cell to express the specific muscle identity gene thereby becoming a FC, while the other remaining cells become FCMs (Carmena & Baylies, 2006). Following the initial diversification steps, each FC fuses with

the FCM and this is thought to enable the formation of functional muscles with unique features. However, the exact role of HNT in embryonic muscle development has yet to be investigated.

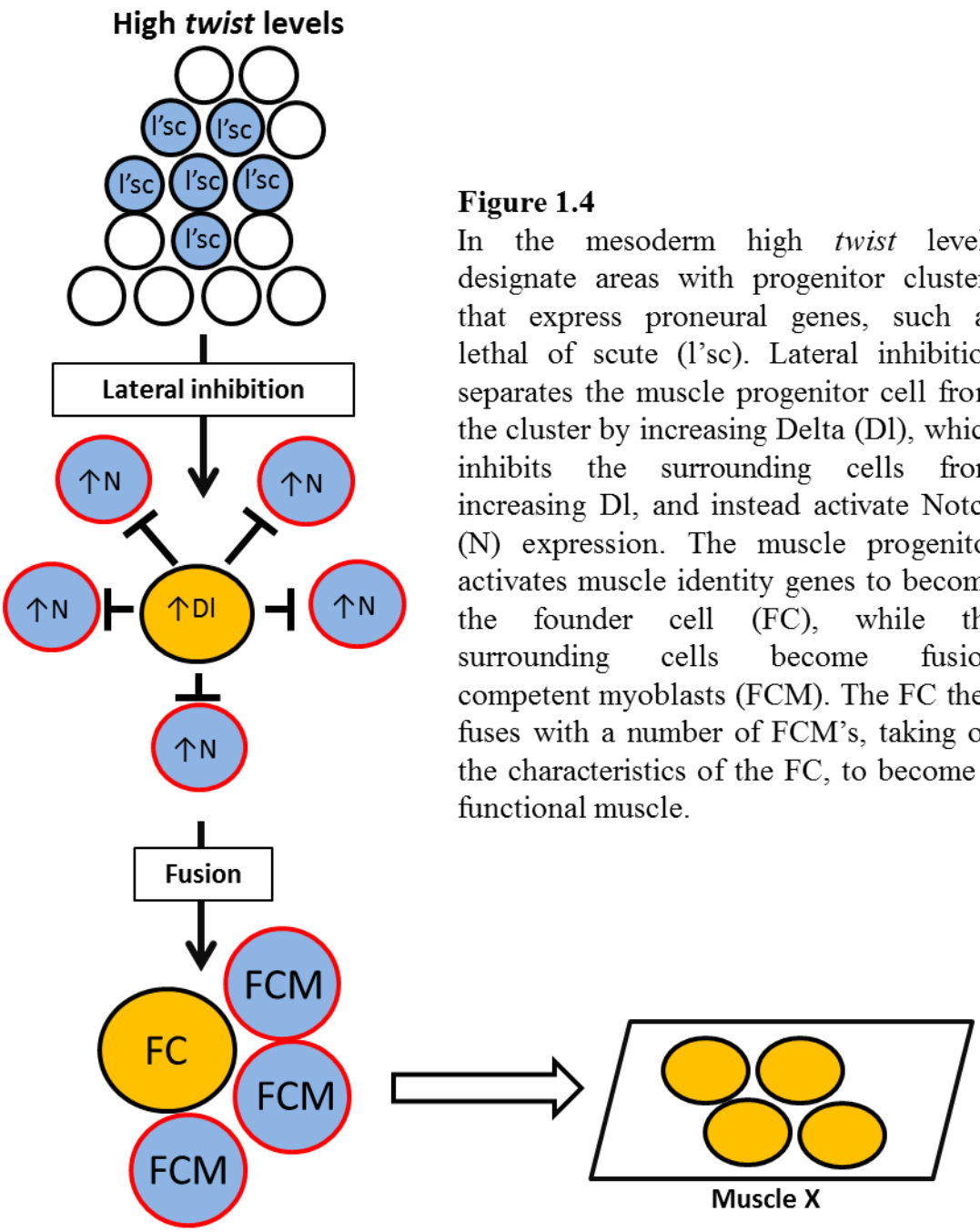


Figure 1.4
In the mesoderm high *twist* levels designate areas with progenitor clusters that express proneural genes, such as lethal of scute (l'sc). Lateral inhibition separates the muscle progenitor cell from the cluster by increasing Delta (Dl), which inhibits the surrounding cells from increasing Dl, and instead activate Notch (N) expression. The muscle progenitor activates muscle identity genes to become the founder cell (FC), while the surrounding cells become fusion competent myoblasts (FCM). The FC then fuses with a number of FCM's, taking on the characteristics of the FC, to become a functional muscle.

1.7 Objective

Previous studies have demonstrated that HNT plays a potential role in SOP's isolated from the dorsal epithelium of pupae as well as in muscle precursors isolated from adult muscle precursor cells; however, the function of HNT in these precursors remains unknown. This project was designed to identify HNT's direct and/or indirect targets in muscle progenitors and SOPs during embryogenesis, and to determine if HNT may play a role in their development. The approach involved microarray analysis of stage 13-16 embryos in which HNT was either over-expressed or depleted by RNAi.

Chapter 2: Materials and Methods

2.1 *Drosophila* Stocks and Fly Husbandry

Drosophila stocks were obtained from the Bloomington *Drosophila* Stock Centre (Department of Biology, Indiana University), the Kyoto *Drosophila* Genetic Resource Center (Kyoto Institute of Technology, Kyoto, Japan), from other *Drosophila* research labs, or were created previously in our laboratory. A list of all genetic stocks used, including sources and full genetic nomenclature is found in Appendix A. *Drosophila* cultures were raised on standard *Drosophila* media at 25^{o}C on a 12 hour light/dark cycle.

2.2 *GAL4/UAS* system

The GAL4/UAS system serves as a standard technique for inducing gene expression in *Drosophila*. As outlined in Figure 2.1 the GAL4/UAS system commonly involves the use of two stocks: the first stock expresses the yeast Galactose 4 (GAL4) transcription factor in a specific spatiotemporal pattern, while the second stock possesses a target gene located downstream of the GAL4 binding site, otherwise known as the Upstream Activating Sequence (UAS). Such stocks are stable transgenic lines and carry the GAL4 and UAS sequences within engineered forms of the highly studied *Drosophila* transposable genetic element known as the P element. GAL4 expressing lines or associated GAL4 insertions are frequently referred to as "GAL4 drivers" and their counterpart UAS lines (or the UAS insertions) are often called "UAS reporters". The transcription of the gene of interest, on the UAS line, requires GAL4 to activate transcription. Thus, in the absence of GAL4 expression, the gene of interest on the reporter line remains silent. To activate transcription of the gene of interest, individuals possessing the UAS reporter gene are

mated with an individual from the GAL4 transgenic line. The resulting offspring will, therefore, express the gene of interest, in only those cells that express the GAL4 driver (Duffy, 2002). Many GAL4 lines are available, each associated with a unique spatiotemporal pattern of GAL4 expression. In many cases, however, a particular GAL4 driver and UAS reporter combination may be carried together as a viable genetic stock. For example, many GAL4 lines are readily maintained with UAS-GFP reporters and these have become very useful for a variety of live imaging strategies. In addition, the GAL4/UAS system is mildly responsive to temperature. The level of UAS reporter gene expression is routinely increased by raising the temperature to 29^{o}C degrees, or decreased by reducing the temperature to 18^{o}C degrees (Kramer & Staveley, 2003).

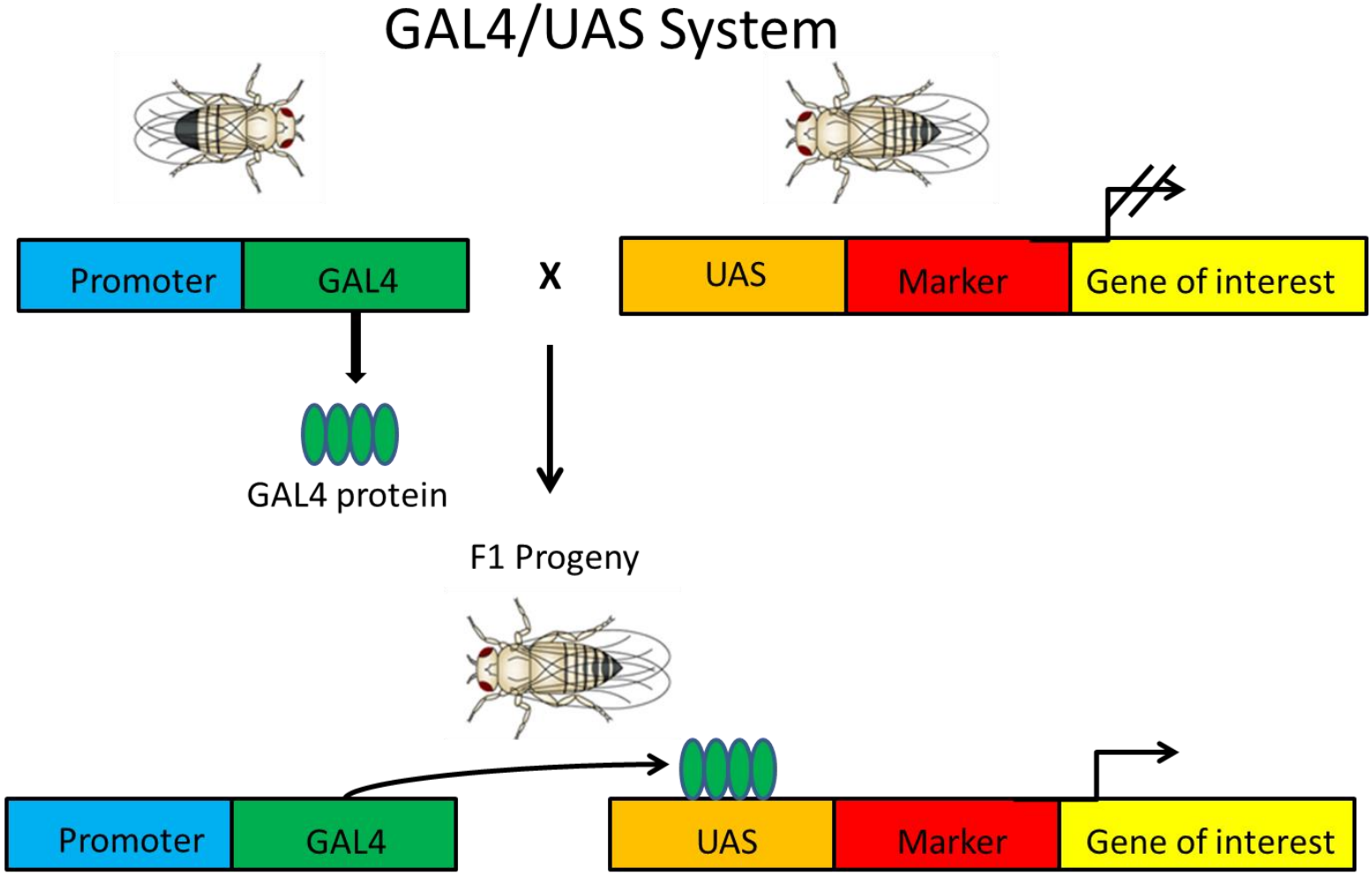


Figure 2.1
The GAL4/UAS method consists of one genetic line containing a GAL4 driver, and another genetic line containing the gene of interest downstream of multiple copies of the GAL4 binding domain, otherwise known as the UAS binding site. When the two genetic lines are crossed the GAL4 protein binds the UAS binding sites and activates transcription of the gene of interest.

2.3 *GAL80*^{ts}

Within the GAL4/UAS system another technique arises: repression via GAL80. GAL80 is a yeast repressor under the control of a tissue-specific enhancer alongside the GAL4 driver. When co-expressed with GAL4, GAL80 blocks GAL4 activity by binding to its transcriptional activation domain (Suster, Seugnet, Bate, & Sokolowski, 2004). GAL80^{ts} is a temperature sensitive form of the GAL80 repressor. At 25^{o}C degrees, the GAL80^{ts} represses the activity of GAL4; however, when the temperature is shifted to 29^{o}C degrees, the GAL80^{ts} is inactivated, allowing for the GAL4 transcription factor to bind to the UAS binding sites and express the gene of interest (Zeidler et al., 2004).

2.4 Overnight embryo collection for Microarray Analysis and Fluorescent In-Situ Hybridization

To ensure that embryos collected for Microarray Analysis and *in situ* hybridization were at the same developmental stage, 3 hour collections of embryos on grape agar dishes were aged for 10 hours. Incubation at 25^{o}C for 10 hours ensures that the embryos are between stages 13-16 of development (Campos-Ortega & Hartenstein, 1997).

2.5 Embryo Fixation and Dechorionation

Dechorionation is the removal of the outer chorion layer (Pascucci, Perrino, Mahowald, & Waring, 1996). Embryos were dechorionated in a mixture of 50% bleach and 50% water with PBT (0.1% Triton X-100 in 1xPBS) for 3 minutes. After thoroughly washing the embryos with water, they were fixed in a solution of 5 mL of heptane and 5 mL of 3.7% formaldehyde in PBS for 20 minutes. The formaldehyde and PBS mixture was replaced with either methanol or

absolute ethanol, and the embryos were shaken until they separated from their vitelline membrane.

2.6 Phalloidin stain

Phalloidin is a high-affinity, filamentous (F) actin stain, and was used for the visualization of muscle strands. Since phalloidin actin binding sites are degraded in the presence of methanol during fixation, absolute ethanol was used as a replacement (Narasimha & Brown, 2006). The fixed embryos were stained with 0.1mg/ml phalloidin diluted with PBS at a 1:1000 dilution for 30 minutes, and then scanned using Confocal Imaging (section 2.11).

2.7 Immunostaining: Double and Single Antibody stain

Protocols for double and single antibody staining were modified from Nipam H. Patel's Imaging *Drosophila* Embryos and Larvae using antibody probes (Patel, 1994). Modifications included blocking the embryos for 1 hour in 5% Bovine serum albumin (BSA) and normal goat serum. In addition, after removing the secondary antibody and PBT washes, the embryos were hydrated with a glycerol/PBS series.

Primary antibodies used were rabbit anti-D-Pax2 polyclonal at 1:2000 (Joshua Kavaler, Colby College, Maine), mouse monoclonal anti-HNT antibody at 1:25 (Howard Lipshitz ,University of Toronto), and mouse monoclonal anti-22C10 at 1:500 (Developmental studies Hybridoma Bank, University of Iowa). The secondary antibodies were Alexa Flour® 488 goat anti-mouse and goat anti-rabbit, and TRITC goat anti-mouse (Cedarlane Labs); used at a 1:1000 dilution.

2.8 RNA extraction

RNA extraction from embryos followed a modified Medium scale RNA extraction using TRIZOL protocol from FlyChip, Functional Genomics for *Drosophila* at the University of Cambridge. Before the addition of isopropanol, the supernatant was centrifuged at 13,000 RPM for 10 minutes at 4^{o}C degrees, and the supernatant was removed while leaving behind a small amount at the bottom. This was done to ensure that any potential contamination that may have been in the supernatant was centrifuged and discarded.

2.9 Microarray

cDNA production, labelling, hybridization and scanning of the microarray plates were conducted at the Microarray Centre at the University of Toronto, Mississauga campus. Before cDNA production, RNA samples were analysed in a Bioanalyzer to determine RNA purity and quantity. A Molecular Devices (Axon) GenePix 4000B scanner was used. The arrays used were a custom version of the Nimblegen *Drosophila melanogaster* 4 x 72K array. There were 72,000 oligo probes on each of the sub-arrays of the 4-plex array with each gene having 2-5 probes per gene. The probes used in the array represent the coding sequence of approximately 17,000 different transcripts of the version 4.3 of the *Drosophila melanogaster* genome. A single channel scan was used, and the levels of expressions were compared to one another.

2.9.1 Bioinformatics Analysis of Microarray Results

For the microarray analysis, a total of 4 sample sets were used for comparison, with each set consisting of a control cross, daGAL4 x *yw*, a HNT over-expression cross, daGAL4 x UAS-GFP-HNT, and a HNT RNAi depleted cross, daGAL4 x UAS-HNT-RNAi2A;UAS-HNT-

RNAi2B. The resulting data were analyzed using the program ArrayStar. The expression values of the control and mutants were averaged. The HNT over-expression and depleted results were compared to the Control in a Scatter plot, and Student's t-test with false discovery rate (FDR) correction (Benjamini and Hochberg procedure) was used to test for significance. Genes with at least a two-fold change in expression and a FDR corrected p-value < 0.05 were retained as significant; to produce a list of genes with 2-fold, 4-fold, and 8-fold changes in expression, along with genes that had an 99% 95% and 90% confidence range.

The data were isolated based on at least a 2-fold change in expression, along with a 95% confidence. The FlyBase identifier (FBtr) code was used to find the gene symbol the code represented using the FlyBase *Drosophila* data website (http://flybase.org). The HNT over-expression data is presented in Appendix B, and the HNT RNAi depleted data is represented in Appendix C.

2.10 Fluorescent *In situ* hybridization

Embryo fixation followed the Fluorescent in situ Hybridization (FISH) protocols in *Drosophila* embryos and tissues by Eric Lécuyer, Neela Parthasarathy and Henry M. Krause (Lecuyer, Parthasarathy, & Krause, 2008).

The Single FISH, along with post-fixation, hybridization, post-hybridization and scans were performed by Ronit Wilk from the Krause Lab at the University of Toronto. Probes for the FISH were acquired from either the Krause lab or the *Drosophila* Genomics Resource Center (Indiana University). Both HNT over-expression and control embryos were probed for MyO10A (CG43657), scabrous (CG17579), AP-2 (CG7807), Scute (CG3827), Slowpoke binding protein

(CG6772), Nplp1 (CG3441), Enhancer of split mγ, helix-loop-helix (CG8333), shaven/D-Pax2 (CG11049), Pox Meso (CG9610), unpaired 3 (CG33542), and CENP-ana (CG33695).

2.11 Confocal microscopy

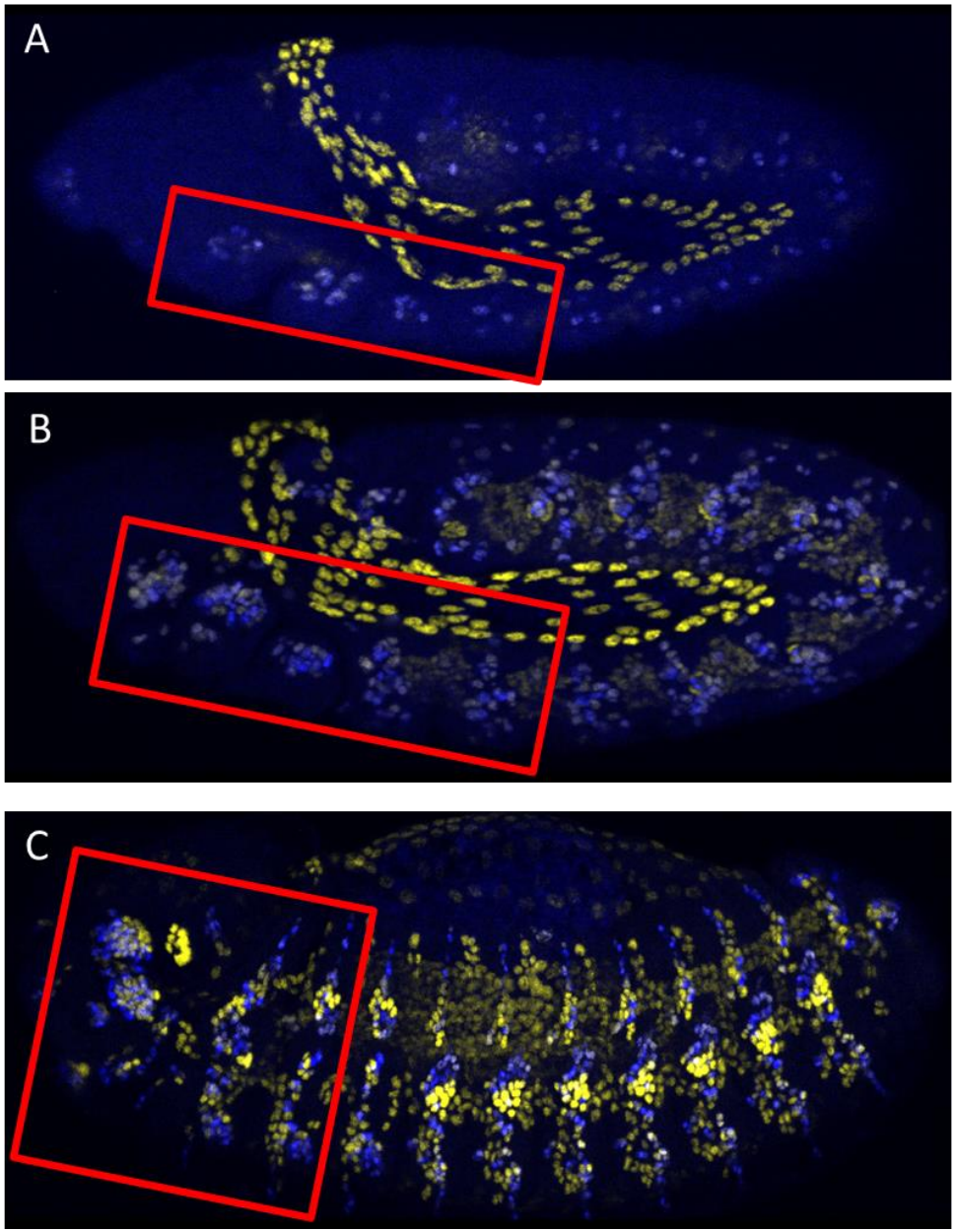
All stained embryos were imaged using a Nikon Eclipse 90i microscope fitted with a Nikon D-eclipse C1 scan head, Nikon EZ-C1 software and a 20x objective Nikon CFI Plan Apo VC lens, unless stated otherwise. Z-stack scans through embryos used slices averaging between 0.40 µm – 2.00 µm. Z-stack projections were obtained with using the Nikon EZ-C1 or the NIH ImageJ software. Live imaging was performed as previously described (Reed, McMillan, & Chaudhary, 2009; Reed, Wilk, Schock, & Lipshitz, 2004).

2.12 Cell count

To compare the amount of cells with co-localized expression or cell expressing either one of the antibodies from the double antibody stain, confocal images of embryos were taken that represented each co-localized and individual antibody expression of the genetic crosses. The number of confocal images for each developmental stage, of each genetic cross, contained at least 5 embryos; the exact number of embryos is represented as an "n" value within the graphical comparisons. To count the number of cells, each confocal image had a section cropped out for cell counting. Sections, as outlined in Figure 2.2 denote the area where the numbers of co-localized and single antibody expressing cells were counted. Lining the sections up in parallel aided in determining which cells had co-localized expression or just expressed a single antibody. The cell counts from each developmental stage, of a genetic cross, were averaged using the MEAN function on the Excel program. The standard deviation for each mean was calculated

using the Excel STDEV function. p-values were determined using a type 2 student T-test with 2 tails, and trends in the graph were analyzed using one- or two-way ANOVA.

For each stain, embryos were compared on the stage of development: early stage, stage 11, a middle stage, stage 12, and a late stage, stages 13-14 (Campos-Ortega & Hartenstein, 1997). If the developmental stage of the embryo was undetermined, based on the appearance of a severe phenotype that has arrested development, the embryos were denoted as having only one stage, since early, middle, or late stages were indistinguishable.



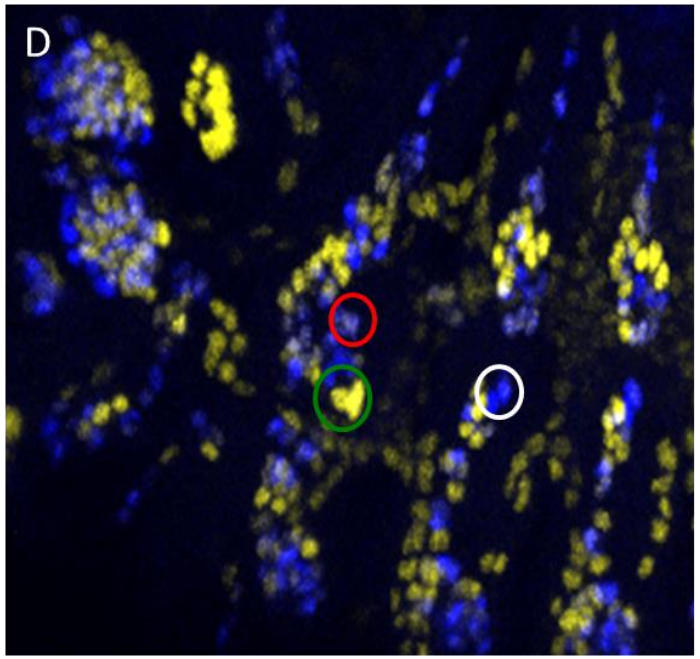


Figure 2.2
Wildtype embryos were double antibody stained with anti-HNT, as seen in yellow, and anti-D-Pax2, as seen in blue, antibodies. **A-C** display sections, outlined in red, of the embryo used for the cell counts during the early (**A**, stage 11), middle (**B**, stage 12), and late (**C**, stage 13-14) developmental stages.

D Denotes what is considered a cell expressing co-localization (red ring), expressing only HNT (green ring) and only D-Pax2 (white ring)

Chapter 3. Results

3.1 Design of experimental *Drosophila* models for the analysis of embryos in which HNT is over-expressed or depleted

To identify genes as potential targets of HNT during embryogenesis, a variety of GAL4 drivers were tested in combination with UAS-HNT (over-expression) or UAS-HNT-RNAi (depletion) reporters. In order to proceed with a microarray analysis, it was necessary to use driver and reporter lines that were homozygous viable; it was also desirable to identify driver>reporter combinations that were associated with a disruption of normal development, which would enhance any chance of identifying genes affected by the over-expression and depletion of HNT.

3.1.1 Phenotypic consequences of a variety of *GAL4*-driver>*UAS*-reporter combinations

A variety of GAL4-driver>UAS-reporter combinations were tested to determine the best available experimental model for microarray analysis. Two GAL4 drivers were tested: NP3312 and daGAL4, which drive expression of GAL4 under control of the promoters for the genes *hnt* and *daughterless* (da), respectively. Table 3.1 compares the severity of the mutant phenotypes associated with each GAL4-driver>UAS-reporter combination. The genetic stock NP3312+Apoliner/FM7 carries a GAL4 driver and the apoliner reporter that expresses a GFP-mCherry fusion protein which normally serves as a biosensor for caspase activity, but is simply used here as a reporter for the NP3312 driver. In addition, the UAS-DT is a mCherry-GFP-

DrAtg8a construct that simply serves as a reporter for the NP3312 driver, although it is normally used to detect autophagy. When the NP3312 driver was crossed with the HNT over-expression line UAS-GFP-HNT, progeny displayed a strong embryonic lethal phenotype that included a failure in DC and a persistent amnioserosa tissue. A second HNT over-expression reporter line, EP55, was also tested with the NP3312 driver. NP3312>EP55 embryos displayed a mild embryonic phenotype where there was a persistent amnioserosa tissue, but was ultimately not associated with embryonic lethality. The HNT RNAi depleted line tested was UAS-HNT-RNAi2A; UAS-HNT-RNAi2B, which also produced a mild embryonic phenotype that did cause lethality.

Despite the strong phenotypes observed, the NP3312 driver, which maps to the X chromosome, was also found to be associated with strong dosage compensation. As a consequence, the NP3312 driver displayed a twofold increase in expression in male embryos compared to female embryos. Such a lack of homogeneity in resulting embryonic phenotypes was deemed undesirable and the NP3312 driver was not used.

The other driver tested was daGAL4. When crossed with another HNT depleted line (UAS-Dicer; UAS-HNT-RNAi2B), embryos displayed an embryonic phenotype most similar to wild type, which will be designated as an weak embryonic phenotype, where no obvious phenotype was detected and was not embryonic lethal. The daGAL4>EP55 embryos were associated with a persistent amnioserosa tissue, but were not embryonic lethal. Lastly, daGAL4>UAS-GFP-HNT displayed a strong embryonic mutant phenotype that ended in embryonic lethality, while the HNT depleted line: UAS-HNT-RNAi2A; UAS-HNT-RNAi2B embryos displayed a mild mutant embryonic phenotype that did not end in lethality. Given the phenotypes seen with the daGAL4 driver and the HNT over-expression line: UAS-GFP-HNT,

and HNT depleted line: UAS-HNT-RNAi2A; UAS-HNT-RNAi2B, this combination of GAL4-driver>UAS-reporters was selected for microarray analysis.

Table 3.1 Comparison of phenotypes for GAL4-drivers>UAS-reporter combinations.

The two main drivers tested is a Hindsight NP3312 driver, and a daGAL4. The reporters consisted of two HNT over-expression lines: UAS-GFP-HNT and EP55, and two HNT RNAi depleted reporter lines: UAS-HNT-RNAi2A; UAS-HNT-RNAi2B and UAS-Dicer; UAS-HNT-RNAi2B. The severity of the mutant phenotype is denoted as being weak: +, mild: ++, and strong: +++.

***GAL4*-drivers>*UAS*-reporter Combinations**	**Degree of Mutant Phenotype**
***NP3312* driver**	
NP3312 + Apoliner/FM7	
> UAS-GFP-HNT	+++
> UAS-HNT-RNAi2A; UAS-HNT-RNAi2B	++
> EP55	++
NP3312; Dp/+	
> UAS-GFP-HNT	+++
NP3312; (Dp)/(UAS-DT)	
> EP55	++
da*GAL4* driver	
KrGAL4+UASGFPClc5/TM3	
> UAS-Dicer; UAS-HNT-RNAi2B	+
w; (YET1); daGAL4	
> EP55; dpplacZ/CYO	++
w; UAS-mCherry-DrAtg8a;daGAL4+Spider/TM3,Ser	
> UAS-GFP-HNT	+++
> UAS-HNT-RNAi2A; UAS-HNT-RNAi2B	++

3.1.2 Hindsight expression in the experimental models

To confirm HNT expression with the daGAL4 driver during GBP and DC, an HNT antibody stain, as shown in Figure 3.1, was conducted on HNT over-expression embryos using the reporter line UAS-GFP-HNT and on HNT RNAi depleted embryos using the reporter line UAS-HNT-RNAi2A; UAS-HNT-RNAi2B. As seen in Figure 3.1 B, the daGAL4>UAS-GFP-HNT embryos had greater HNT expression throughout the embryo, than in the control, *yw*, embryos (Figure 3.1 A). In the UAS-HNT-RNAi2A;UAS-HNT-RNAi2B RNAi depleted line, when compared to the control, there was less HNT expression (Figure 3.1 C), but the expression of HNT was not reduced completely, which indicated that there was not a constant depletion of HNT. However, since the reporter line was still able to reduce HNT expression, it was used as a part of the experimental model for the study of HNT using microarray analysis.

In summary, the experimental models for this study consisted of a reporter-less control, *yw*, and the driver daGAL4 driving expression of the HNT over-expression, UAS-GFP-HNT, and the HNT RNAi depleted, UAS-HNT-RNAi2A; UAS-HNT-RNAi2B, reporter lines.

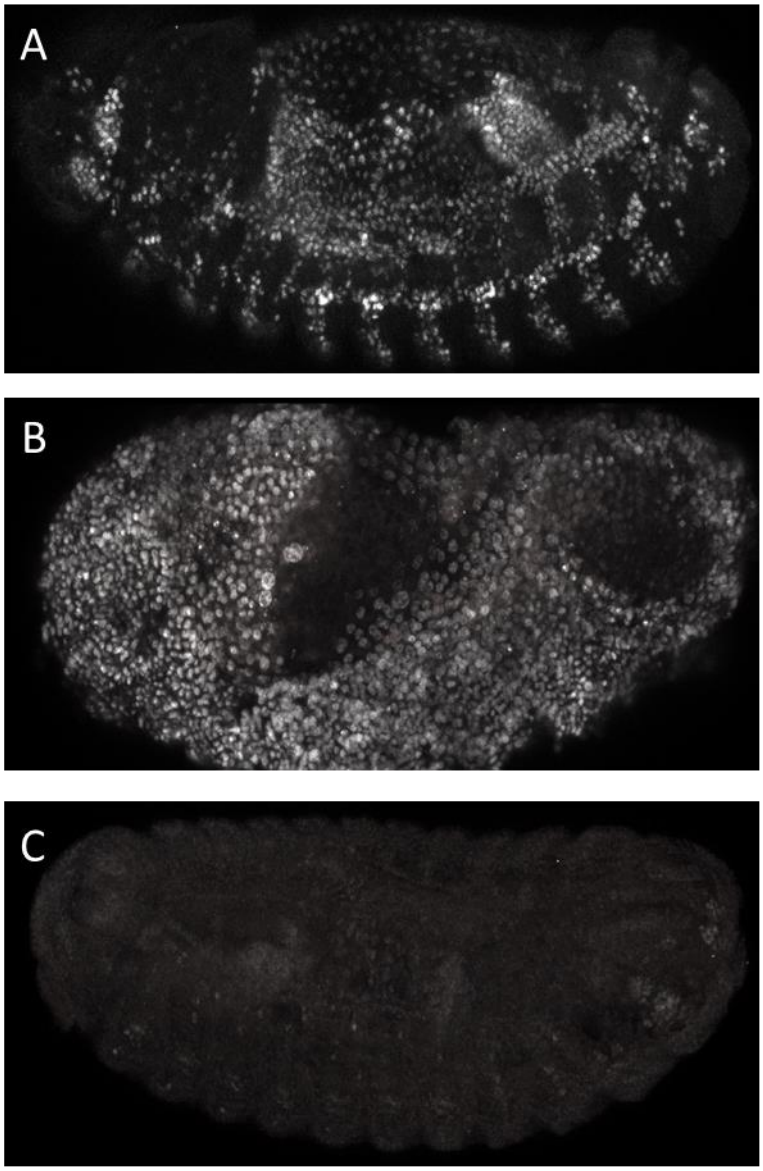


Figure 3.1
Immunostaining of embryos using Anti-HNT monoclonal antibody 276B10. (A) Control embryos from the standard control stain y w. (B) Embryo over expressing HNT of the genotype UAS-GFP-HNT/+; daGAL4/+ (C) Embryos in which HNT expression was depleted, have the genotype UAS-HNT-RNAi^{2A}/+; UAS-HNT-RNAi^{2B}/ daGAL4.

3.2 Microarray Analysis of *Hindsight* targeted genes

In the comparison of the HNT over-expression microarray analysis profile with the control, approximately 1,300 cDNA transcripts were identified as having at least a 2-fold change in expression, along with 95% confidence rate with p values of less than 0.05 after False Discovery Rate (FDR) correction, as shown in Appendix B. The number and functions of these under-expressed or over-expressed genes in each developmental category is presented in Figure 3.2. Genes whose transcriptional activity is affected by HNT over-expression are involved in a number of different processes including neurogenesis and eye development, transmembrane transport, morphogenesis, and myogenesis systems of development. These gene ontology assignments were based upon gene ontology terms from the FlyBase database.

In the HNT RNAi depleted line, when compared to the control, approximately 100 cDNA transcripts demonstrated a minimum 2-fold change in their expression, along with 95% confidence rate with p values of less than 0.05 before and after the False Discovery Rate (FDR) correction, as seen in Appendix C. The categorized genes are shown in Figure 3.3, which indicates that most genes affected by reduced HNT expression are associated with transmembrane transport, reproduction, morphogenesis, and sensory/olfactory related development.

Previous studies have shown that HNT plays a role in down-regulating the JNK signaling pathway in the amnioserosa, which is needed for the proper completion of GBR and DC (Reed et al., 2001; Yip et al., 1997). Surprisingly though, only two genes were found to be involved in the JNK pathway: *omega* (*ome*) and *cln3*, and only one gene, aside from HNT, was found to be involved in DC: *Myosin binding subunit* (*Mbs*). However, other data confirm the validity of the microarray data, such as the up-regulation of *pebbled*/HNT, *yellow* (*y*), and *white* (*w*). *y* and *w*

can act as controls for the HNT over-expression microarray analysis since the control and the HNT over-expression embryos are associated with dosage differences for the wild-type copies of these loci: Control embryos carry only single copies of y^+ and w^+, whereas the experimental HNT over-expression embryos carry two copies of y^+ and w^+. Therefore, when the HNT over-expression is compared to control embryos in the microarray data, *y* and *w* would be expected to be up-regulated (Table 3.2), which is also seen when comparing the microarray linear expression values of *yellow* and *white* between the control and the HNT over-expression.

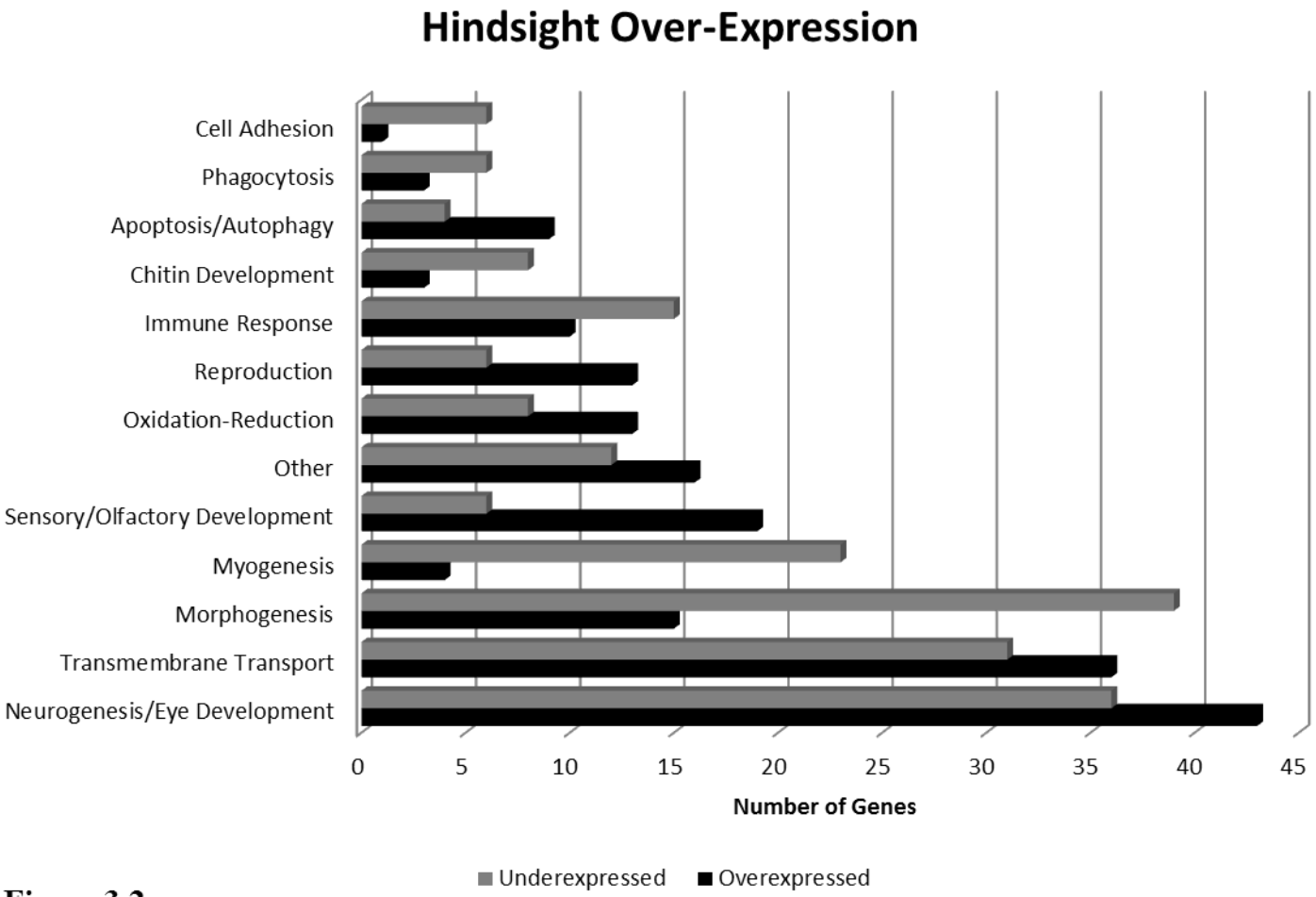


Figure 3.2.

A graphical representation of the areas of development affected by HNT over-expression, when compared to the control, from the Microarray Analysis. The grey bars indicate the number of genes under-expressed and the black bars represents the number of genes overexpressed. The genes used for this graphical representation are based on currently known genes that demonstrated at least a 2-fold change in expression, along with a 95% confidence rate.

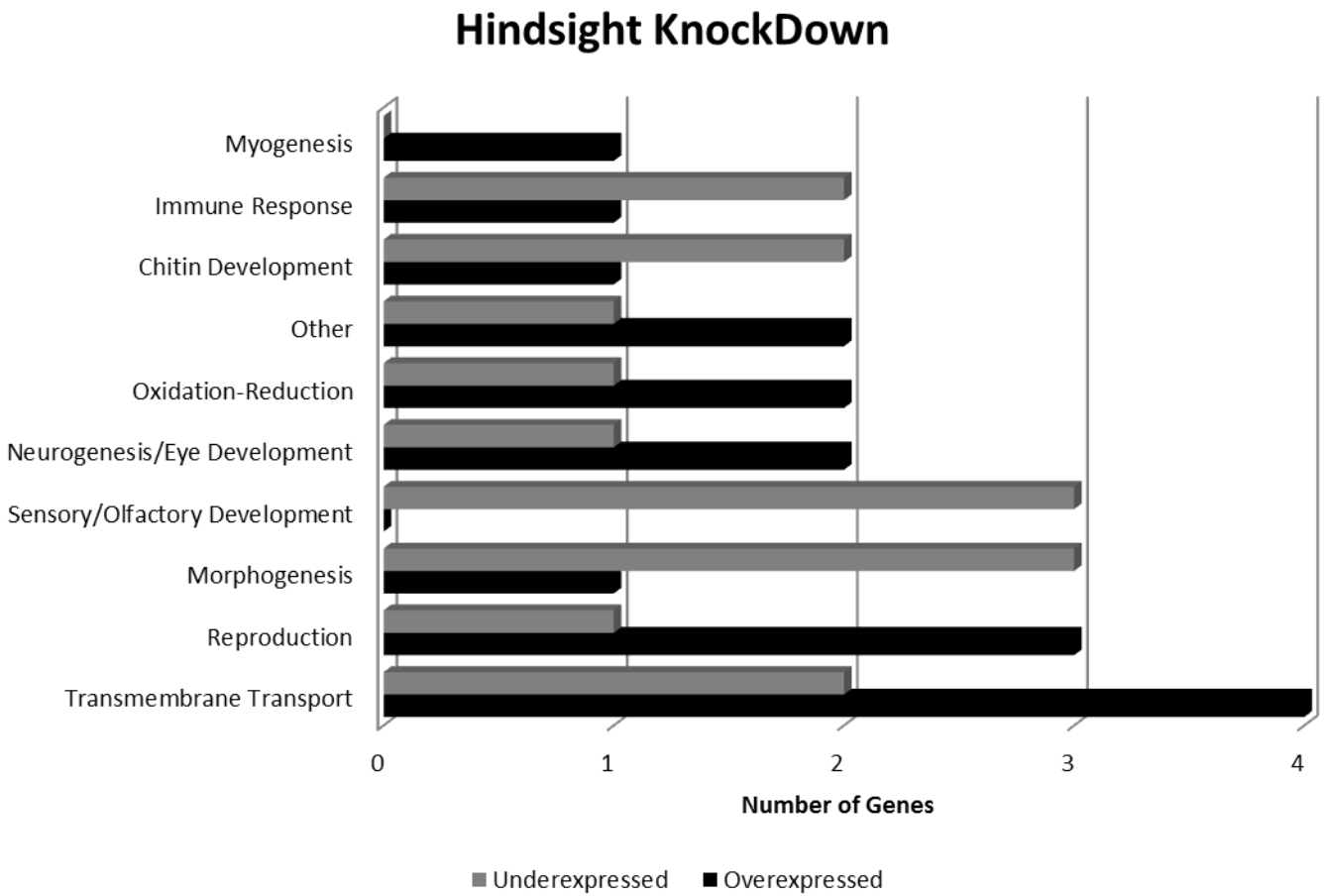


Figure 3.3.

A graphical representation of the areas of development affected by HNT knockdown, when compared to the control, from the Microarray Analysis. The grey bars indicate the number of genes under-expressed and the black bars represents the number of genes overexpressed. The genes used for this graphical representation are based on currently known genes that demonstrated at least a 2-fold change in expression, along with a 95% confidence rate.

Table 3.2

The number of *yellow* and *white* gene copies is compared between the Control and HNT over-expression that was used in the microarray data. Females of the y w and +w; UAS-GFP-HNT were crossed with +w; daGAL4 males. The daGAL4 carries a y/+ and contains one copy of [w^+] (white) in the w^{1118} on the driver. The y and w, in the stock notation indicates that the stock is mutant for that gene, while the + notation in the stock indicates that the stock is not mutant for that gene. The Microarray linear expression values also compares the *yellow* and *white* gene copies between the Control and the HNT over-expression.

Genetic Cross	**Number of *yellow* and *white* gene Copies**	**Microarray Linear Expression Values**
Control		
y w **X** *+ w; daGAL4*	*yellow*: *y*/+ = 1X (copy)	*yellow:* 9.0
	white: w^{1118}; 1X[w^+] = 1X (copy)	*white:*10.4
HNT over-expression		
+ w; UAS-GFP-HNT **X** *+ w; daGAL4*	*yellow*: +/+ = 2X (copy)	*yellow:*10.5
	white: w^{1118}; 2X[w^+] = 2X (copy)	*white*: 12.1

3.2.1 Confirmation of Hindsight expression in experimental models (HNT over-expression versus RNAi depletion)

The substantial difference between the number of genes affected by the HNT over-expression compared to the RNAi depleted line suggested that the UAS-HNT-RNAi2A; UAS-HNT-RNAi2B line may not have provided a strong enough depletion of HNT. To confirm this hypothesis, the expression of HNT in these lines was re-examined using the microarray analysis data. Figure 3.4 displays a graph comparing the microarray linear expression of HNT in the control against the over-expression and RNAi depleted reporter lines. The over-expression line had significantly over-expressed HNT, while the depleted reporter line appeared not to be strong enough to deplete HNT; since the HNT depleted linear expression value was not significantly different from the control. Therefore, further investigation into the potential targets of HNT was only carried out using the HNT over-expression microarray data.

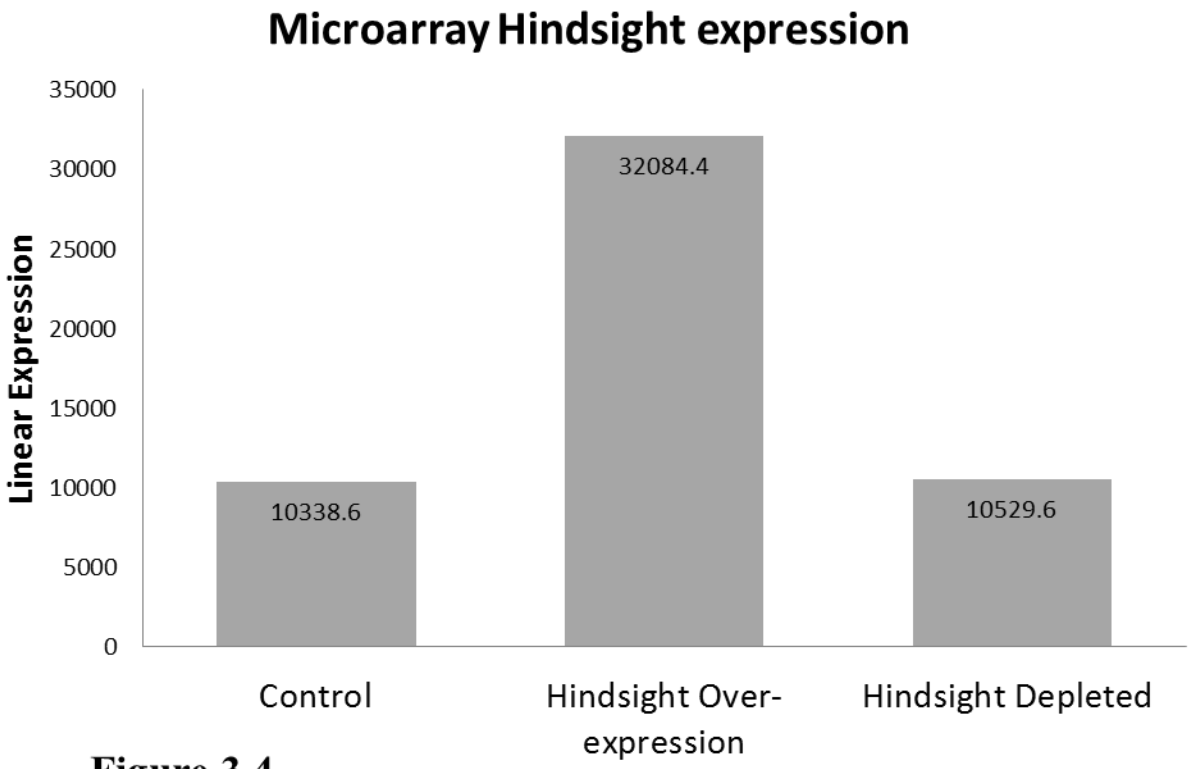


Figure 3.4

A comparison of the linear expression levels of the HNT cDNA transcript from the Microarray analysis between the control, HNT over-expression and HNT depleted, by RNAi, embryos.

3.3 Association of Hindsight expression with Muscle Development

In a cell line that has characteristics similar to *Drosophila* adult muscle progenitor cells, HNT was documented to be a target of Notch in a genome-wide response to Notch activation, after 30 minutes in these cell lines (Krejci et al., 2009). HNT's potential involvement in muscle development was supported by the microarray analysis data, as indicated by the number of muscle identity genes down-regulated by HNT over-expression, shown in Table 3.3.

From the list of candidate genes in Table 3.3, *Pox meso* was selected for further investigation using fluorescent *in-situ* hybridization (FISH) stain, which was done by Ronit Wilk from the Krause Lab at the University of Toronto. FISH staining revealed the wild-type expression pattern of *Pox meso*, which is that it's usually seen along the ventral side, head and tail end of the embryo. The *Pox meso* expression along the ventral side potentially shows its expression in muscle progenitor cells. As indicated in the microarray data, *Pox meso* was down-regulated in a 21.9 fold change in expression, in the presence of HNT over-expression (Table 3.3). Similar to this result, the *in-situ* of the control compared to HNT over-expression embryos showed that *Pox meso* expression was almost completely absent in HNT over-expression embryos (Figure 3.5).

Table 3.3

Known muscle identity genes in the list of differentially expressed genes on HNT over-expression (Appendix B). These genes have a known role in muscle development during embryogenesis

Fbgn_ID (Flybase ID)	CG	Name(symbol)	Protein function	Up/Down expression	Fold Change	Description [ref]
Myogenesis						
FBgn0003129	CG9610	Pox meso (Poxm)	Transcription factor	Down	21.856	Regulates the development of larval body wall muscles and a muscle identity function (Duan et al., 2007)
FBgn0000606	CG2328	even skipped (eve)	Transcription factor	Down	2.387	Regulates segment polarity and in selecting muscle identity in muscle founder cells (Dobi, Metzger, & Baylies, 2011; Liu, Qian, Han, Wu, & Bodmer, 2008)
FBgn0003975	CG3830	vestigal (vg)	Presumptive transcription factor	Down	2.295	Required in ventral longitudinal muscles to induce formation of stable intermusclar attachments and is a muscle identity gene (Deng, Bell, & Simmonds, 2010)
FBgn0002941	CG6534	slouch/S59 (slou)	Transcription factor	Down	2.181	Expression in muscle founder cells responsible for the origin of specific musculature of each segment (Cox & Baylies, 2005)
FBgn0002922	CG10250	nautilus (nau)	Transcription factor	Down	3.070	Defines the subset of mesodermal muscle founder cells and a differentiation role in mature fibers (Wei, Rong, & Paterson, 2007)

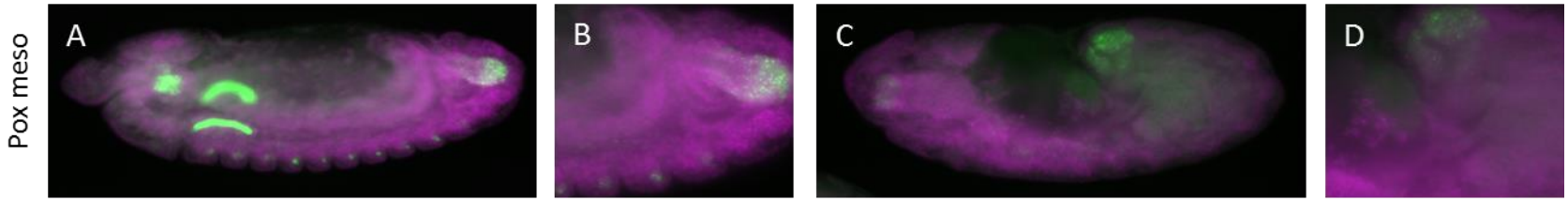


Figure 3.5

Fluorescent *in-situ* hybridization of the embryonic transcription of the gene *Pox meso* as seen in the control (A,B), yw, and the HNT over-expression (C,D), daGAL4>UAS-GFP-HNT, embryos. A cropped area of the *Pox* meso gene expression is shown next to the expression in the entire embryo for the control (B) and the HNT over-expression (D). The green fluorescence represents the gene expression of *Pox meso,* and the DAPI is pseudo-colored purple. The Fluorescent *in-situ* hybridizations were kindly done by Ronit Wilk from the Krause Lab at the University of Toronto.

3.3.1 The regulation of muscle formation by *Hindsight*

To investigate the effect of HNT on muscle development TRITC-Phalloidin, which labels filamentous actin (F-actin) in the embryo (Warn & Magrath, 1983), was used to examine muscle morphology. F-actin expression was examined in embryos of the following genotypes: control (*yw*), HNT over-expression (daGAL4>UAS-GFP-HNT), HNT null (hnt^{XE81}), and Notch null ($Notch^{55ell}$), embryos, as shown in Figure 3.6. Control embryos exhibited organized muscle filaments along the lateral side of the embryo (Figure 3.6A), as represented by the organized F-actin expression, whereas embryos with HNT over-expression showed a disorganized arrangement of the F-actin filaments, indicative of disorganized muscle filaments (Figure 3.6B). The HNT null mutants displayed a characteristic phenotype of a failure in GBR, as indicated by the embryo having arrested in development (Yip et al., 1997); however, the HNT null also displayed organized muscle filaments, similar to the control, and unlike the disorganized muscle filaments in the HNT over-expression (Figure 3.6C). The organized muscle pattern seen in the HNT null suggested that the complete loss of HNT expression has no severe effect on muscle development. The Notch null in this study could be considered as a positive control for muscle formation failure because previous research by Baker and Schubiger showed that embryos without Notch function had too many muscle founder cells and failed to properly differentiate somatic muscle, suggesting that Notch is needed for muscle development (Baker & Schubiger, 1996). Indeed, this experiment showed that the Notch null demonstrated a disorganized muscle filament expression, similar to the HNT over-expression (Figure 3.6D).

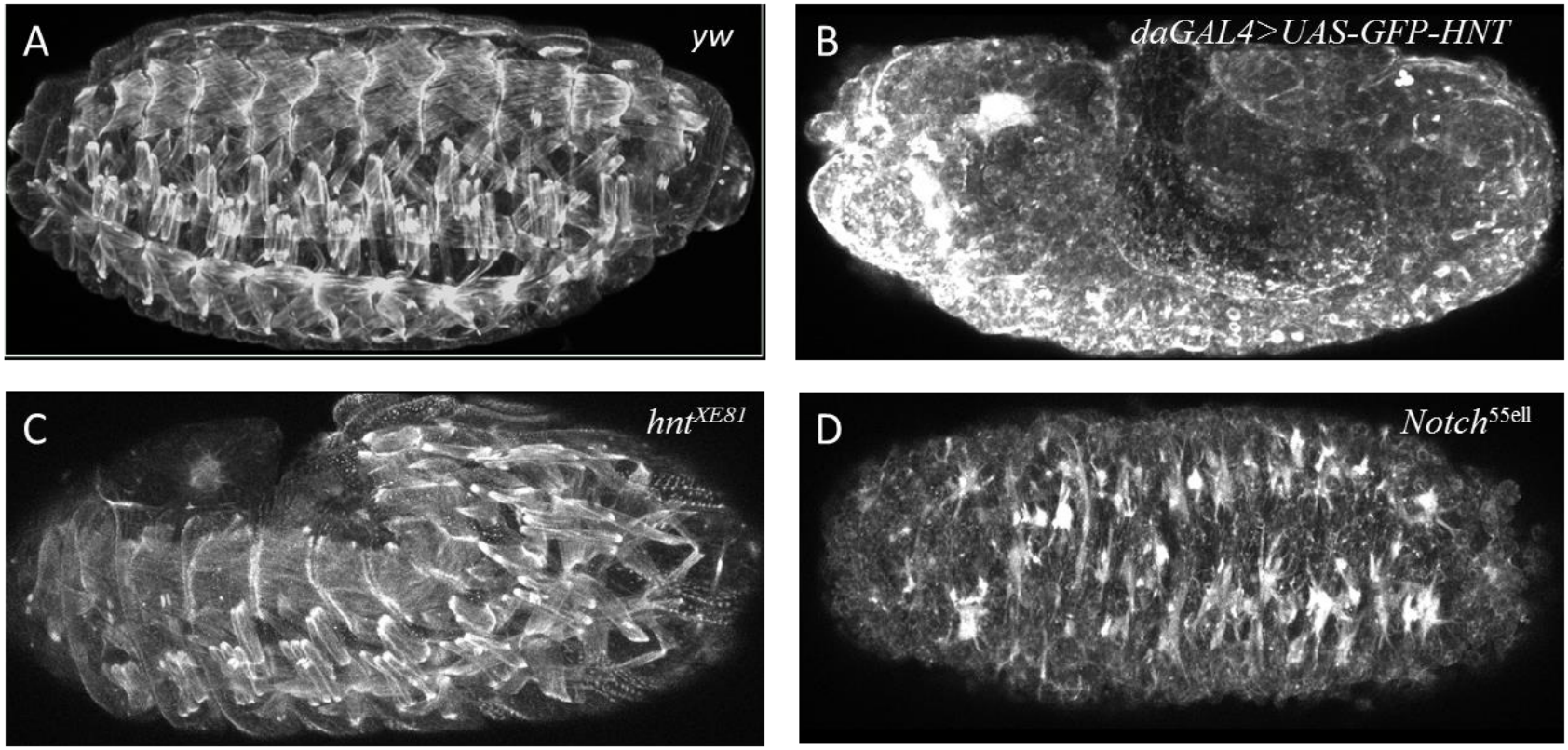


Figure 3.6
TRITC-Phalloidin stained embryos representing F-actin distribution of control (A), HNT over-expression (B), the HNT null (C), and the Notch null (D).

3.3.2 The regulation of muscle strand development by *Hindsight*

To further study the effects of HNT over-expression on muscle development, a D*mefGAL4*>UAS*moesinCherry* stock was used to outline muscle fibres in live embryos. Dmef-GAL4 drives expression of GAL4 in mesodermal precursors that represent muscle fibres (Sandmann et al., 2006). As shown in Figure 3.7, when the Dmef expression in the control was compared to HNT over-expression, the muscle strands in the HNT over-expression cross appeared disorganized and fragmented, while the Dmef expression demonstrated normal organized muscle strands in the control. These results support the finding that muscle fibre development can be disrupted by HNT over-expression.

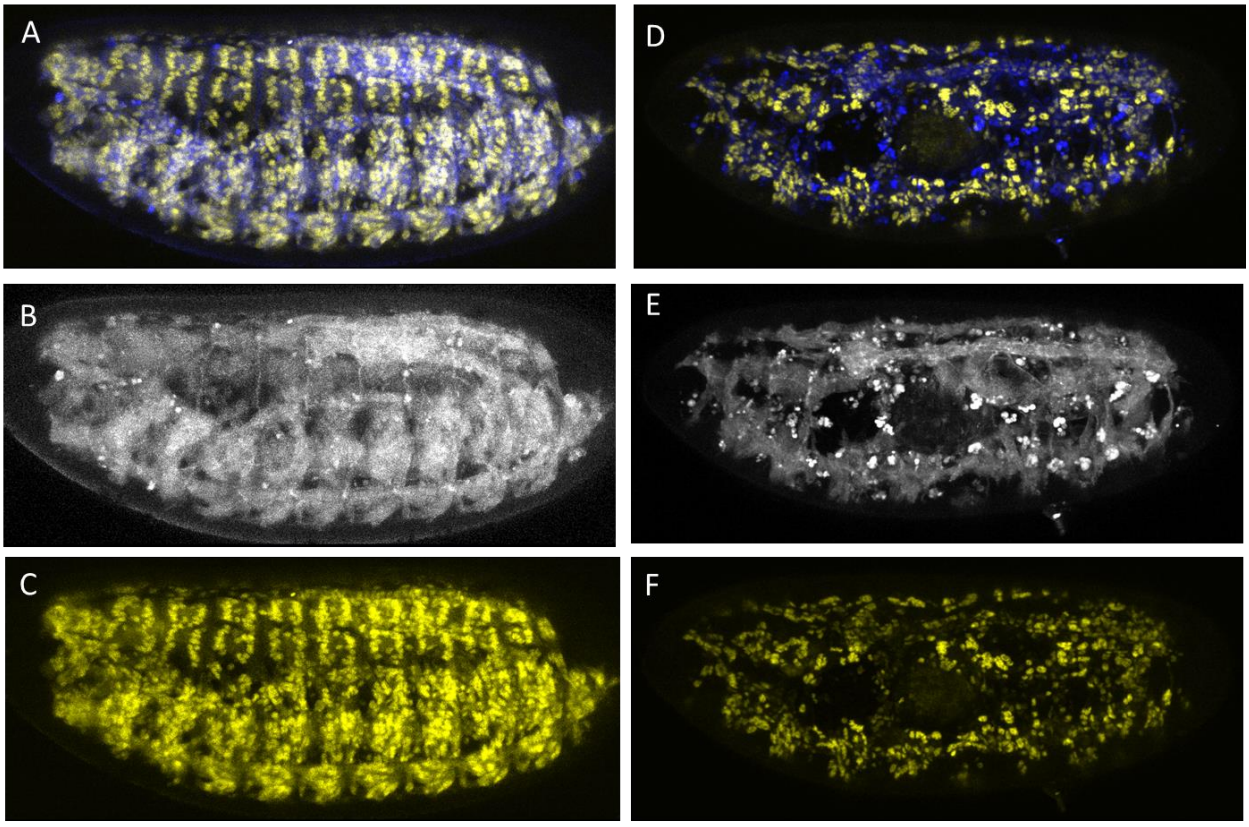


Figure 3.7

Confocal live imaging expression of the DmefGAL4>UASmoesinCherry/TM3,Sb stock, representing muscle strands in grey (B and E), when crossed with the UAS-GFP^{nls} , as seen in yellow (C). The combined expression of the DmefGAL4>UASmoesinCherry/TM3,Sb and the UAS-GFP^{nls} (A, blue represents the moesinCherry expression, yellow representing the UAS-GFP^{nls}) represents the control expression, where the muscle strands are not disrupted. When the DmefGAL4>UASmCherry/TM3,Sb stock is crossed with HNT over-expression (F), in yellow, line UAS-GFP-HNT, the combined expression (D, blue represents the moesinCherry expression, yellow represents HNT expression) shows the affect of over-expressing HNT on muscle strands (E).

3.3.3 Investigation of the sensitivity of muscle development to HNT over-expression during development

To investigate the effects of inducing HNT expression on fully developed muscle fibres, the D*mefGAL4*>UAS*moesinCherry* stock was crossed to the reporter line UAS-GFP-HNT;tub-GAL80^{ts}. The reporter line carries tub-GAL80^{ts}, a temperature sensitive repressor of GAL4 (described in the Materials & Methods). This technique allows the induction of HNT expression following muscle specification and differentiation, which allows the question of HNT's role in muscle maintenance to be addressed.

The effect of HNT over-expression on embryonic muscle strands was examined by inducing HNT expression in fully formed embryonic muscle strands and in larvae muscle strands. Embryos aged between 0-16 hours following an overnight collection at 25^{o}C, were shifted to 29^{o}C for 4 hours. The effect of the 4 hour temperature shift (HNT induction) is illustrated in Figure 3.8 D-F. Confocal live imaging showed that the embryos exhibited strong HNT expression, as demonstrated in Figure 3.8 F, confirming HNT expression. The embryos that were temperature shifted for 4 hours were compared to embryos aged 0-16 hours that were also temperature shifted to 29^{o}C, but for 24 hours (Figure 3.8 A-C). The embryos shifted for 24 hours demonstrate the effects of early induction of HNT expression, which acts as a control for the GAL80^{ts} function, since we know that HNT can affect muscle fibres at the beginning of muscle development. The moesinCherry expression of the muscle fibres, in embryos shifted for 4 hours, was more or less the same as what was seen in the control embryo (Figure 3.7 A-C), suggesting that the 4-hour induction of HNT may not have a significant effect on the muscle fibres. In addition, using the same embryos as in Figure 3.8, the embryos were allowed to develop into 1st in-star larvae at 25^{o}C, at which point they were temperature shifted to 29^{o}C for

48 hours. The resulting larvae remained viable and motile, suggesting that induction of HNT by DmefGAL4 did not disrupt somatic muscle function during larval stages (Data not shown). Overall, these results suggest that HNT does not play a role in muscle maintenance, but does perhaps have a role in specification or differentiation of embryonic muscles.

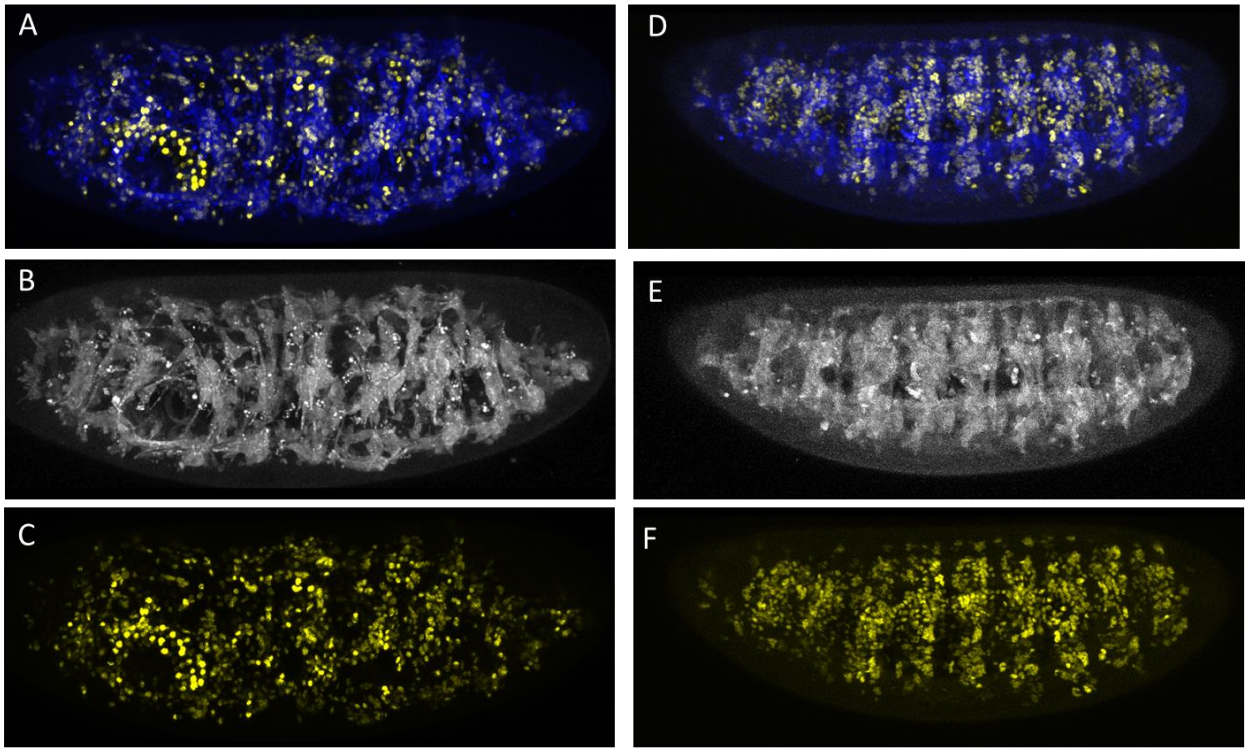


Figure 3.8

Confocal live imaging of the DmefGAL4>UASmoesinCherry/TM3,Sb stock when crossed with a temperature sensitive HNT over-expression line: UASGFPHNT;tub-GAL80^{ts}. Embryos were aged between 0-16 hours at 25^{o}C, and then temperature shifted at 29^{o}C for 24 hours (A-C) and 4 hours (D-F). Embryo expression after 24 hours (A, moesinCherry expression in blue and HNT expression in yellow), represent the effects of HNT over-expression (C) on muscle strands, in grey, (B) at the beginning of muscle development. Embryo expression after 4 hours (A, moesinCherry expression in blue and HNT expression in yellow) represent the effects of HNT over-expression (F) on muscle strands, in grey, (E) after they were already developed, for 4 hours.

3.3.4 The Hindsight expression in Muscle founder cells

The microarray analysis showed that a number of muscle identity genes, present in muscle founder cells that are required for the specification of muscle types, were down-regulated following HNT over-expression. These included genes *even-skipped* (*eve*), *nautilus* (*nau*), *slouch* (*slou*), *vestigial* (*vg*), and *Pox meso* (*Poxm*). These data suggest that HNT could be affecting muscle development by disrupting the specification of muscle founder cells. To investigate this possibility, an anti-HNT antibody stain was performed on embryos of the muscle founder marker driver RP298-GAL4, driving expression of UAS-GFP^{nls}. The aim of this experiment was to determine if HNT is expressed in muscle founder cells, and in part to address the question as to whether HNT could function autonomously in these cells. Figure 3.9 A-C displays embryos at stages 13-14 of development, while Figure 3.9 D-C represents later stage 16 embryos. Earlier staged embryos demonstrated potential co-localization between the RP298 marked and HNT expression cells, which was not seen in the later staged embryos (Figure 3.9 C). The absence of co-localization in the stage 16 embryos, however, may be attributed to the apparent lack of robust nuclear localization of the GFP^{nls} in muscles, making interpretation difficult. Ideally, we would want to look at muscle identity gene expression in the RP298>UAS-GFP-HNT, to reaffirm HNT's potential down-regulation of identity genes in muscle founder cells. However, the localization of HNT in the muscle founder cells in the early stages of the embryo could still suggest that HNT can affect muscle development by regulating gene expression the muscle founder cells.

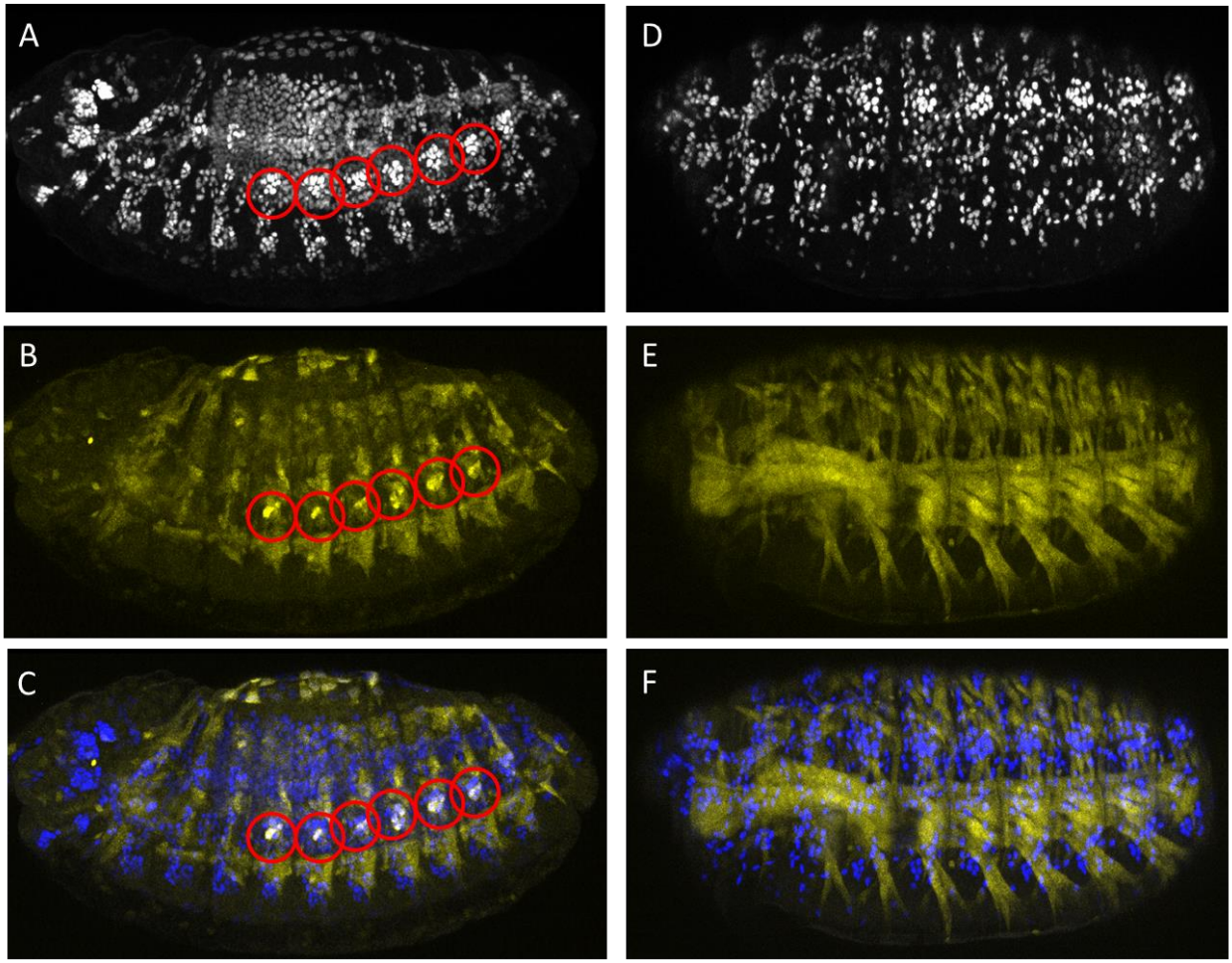


Figure 3.9

HNT antibody stain of the RP298-GAL4 muscle founder driver crossed with UAS-GFP^{nls}. Early staged embryos (A-C), between stages 11-12, were HNT antibody stained, in grey, (A) against the RP298-GAL4 muscle founder GFP expression, in yellow, (B). The combined expression (C) demonstrates potential areas of co-localization between HNT, in blue, and muscle founder expression, in yellow. The potential areas of co-localization are outlined in red. At later stage embryos (D-F), stage 14 and greater, HNT antibody stain, in grey, (D) against the RP298-GAL4 muscle founder GFP expression, in yellow (E). The combined expression (F) does not appear to demonstrate strong areas of co-localization between HNT, in blue, and muscle founder expression, in yellow. Fixed embryos were devitellized using heptane/ethanol as described in the Materials & Methods to preserve GFP fluorescence.

3.3.5 The effect of inducing Hindsight expression in Muscle founder cells

Results from the above experiments implied that HNT might regulate muscle development by a previously unknown role in the specification of muscle founder cells. To test this hypothesis, the effect of over-expressing HNT in muscle founder cells on muscle fibers was investigated. Figure 3.10 shows phalloidin stained embryos carrying an RP298 driver and UAS-GFP-HNT reporter (Figure 3.10 D-F); compared to control embryos (Figure 3.10 A-C) at embryonic stages 12-13. Over-expressing HNT in the muscle founder cells using the RP298 driver, decreased the amount of F-actin filaments (Figure 3.10 D), when compared to the control. At later embryonic stages, the phenotype of HNT overexpressing embryos (Figure 3.11 D-F) was significantly different from that of control embryos (Figure 3.11 A-C). In the control, there was organized and non-striated muscle and actin filament formation; however, in the HNT over-expression embryos the actin filaments were disorganized, and nuclear GFP expression again was not well localized to the nuclear compartment. From these results it can be suggested that over expressing HNT may be affecting muscle development by acting on muscle founder cells expressing identity genes, despite it not being necessary for muscle development as seen with the HNT null (Figure 3.6 C).

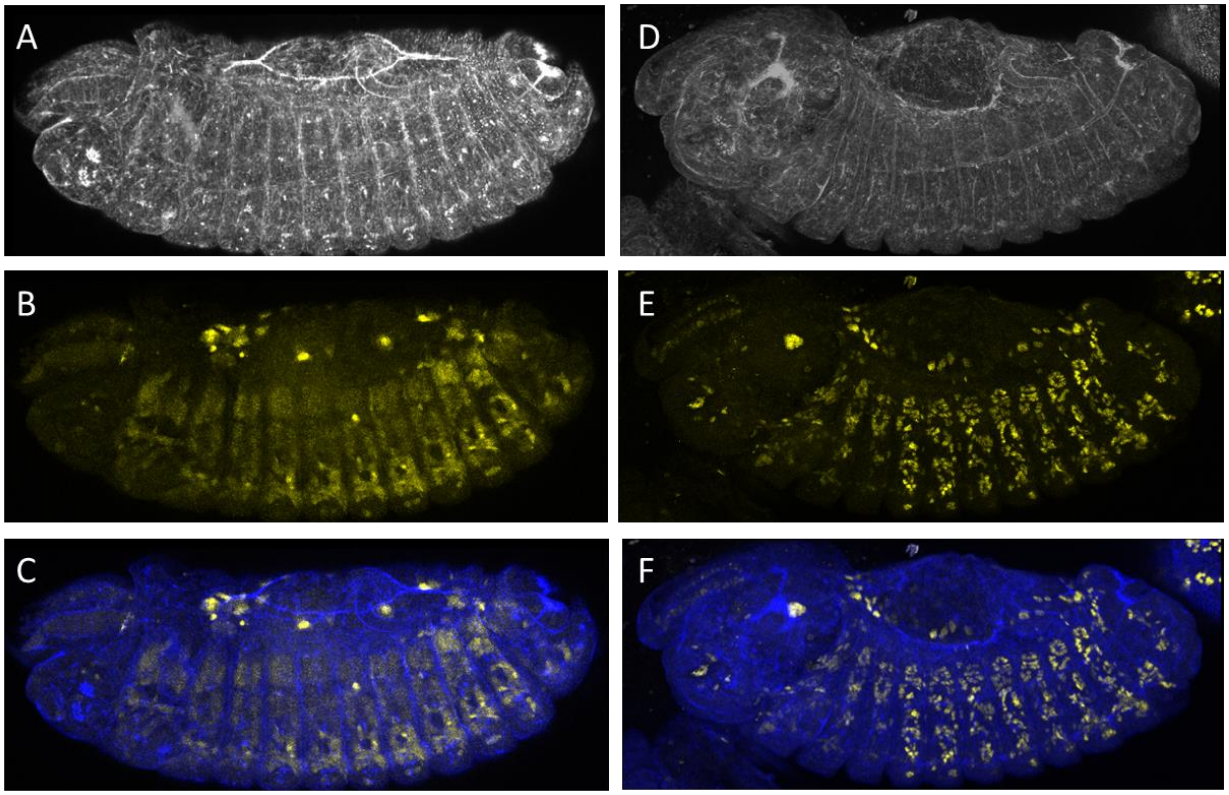


Figure 3.10

A TRITC-Phalloidin stain, representing F-actin expression, of embryos between stages 12-13. The expression of the control (A-C) is compared to the HNT over-expression (D-F) embryos. The phalloidin stain, in grey, (A) of the RP298-GAL4 driving GFP expression, in yellow, (B), and their combined expression (C), with blue representing the phalloidin stain and yellow representing the GFP expression), in the control is compared to the phalloidin stain, in grey, (D) of the RP298-GAL4 driving HNT GFP over-expression, in yellow, (E), and their combined expression (F, blue representing the phalloidin stain and yellow representing the GFP expression). Fixed embryos were devitellized using heptane/ethanol as described in the Materials & Methods to preserve GFP fluorescence.

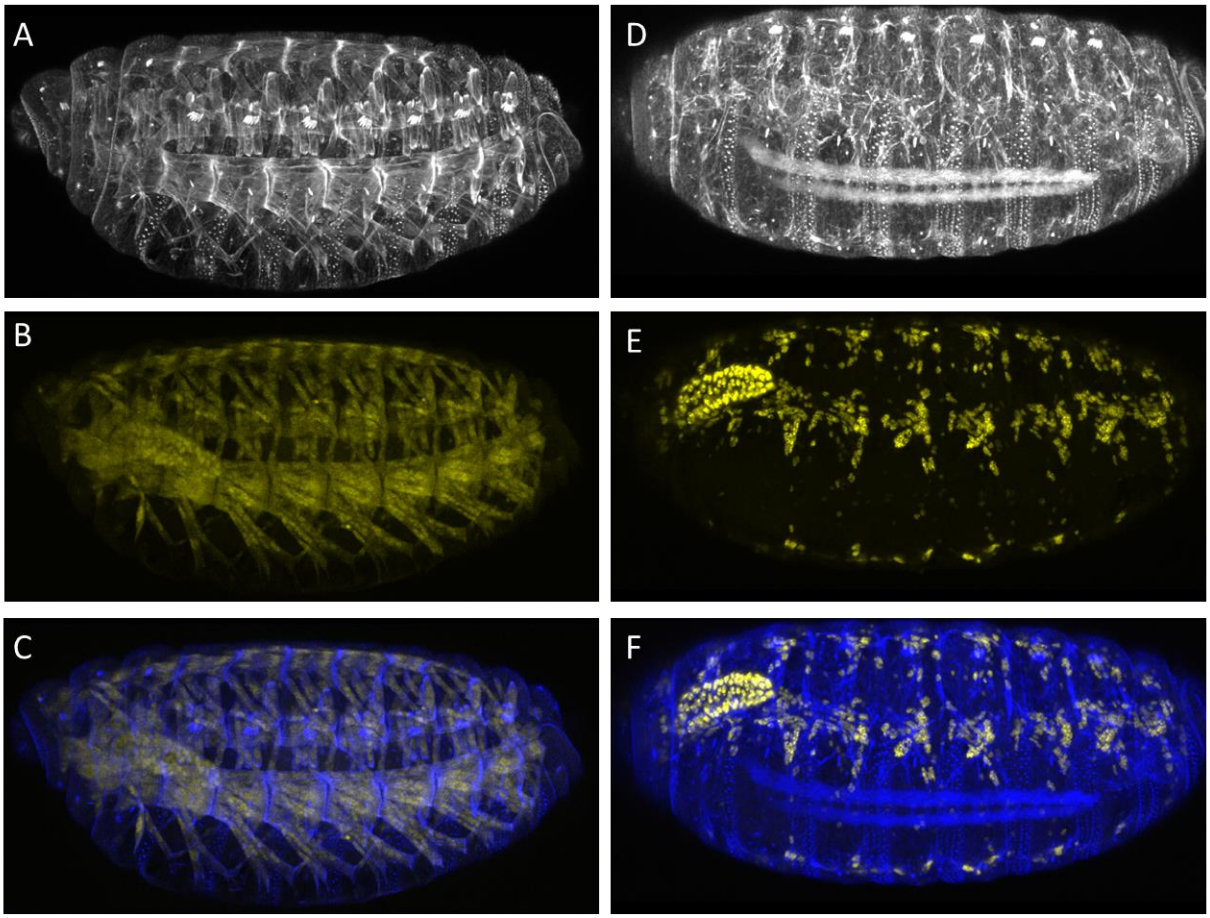


Figure 3.11

A TRITC-Phalloidin stain, representing F-actin expression, of embryos at a stage greater than 14. The expression of the control (A-C) is compared to the HNT over-expression (D-F) embryos. The phalloidin stain, in grey, (A) of the RP298-GAL4 driving GFP expression, in yellow, (B), and their combined expression (C, blue representing the phalloidin stain and yellow representing the GFP expression), in the control is compared to the phalloidin stain, in grey, (D) of the RP298-GAL4 driving HNT GFP over-expression, in yellow, (E), and their combined expression (F, blue representing the phalloidin stain and yellow representing the GFP expression). Fixed embryos were devitellized using heptane/ethanol as described in the Materials & Methods to preserve GFP fluorescence

3.3.6 Summary: the roles of *Hindsight* in muscle development

The data suggests that over-expressing HNT can affect myogenesis during the early stages of embryogenesis, despite the fact that HNT is not necessary for muscle maintenance. The mode of HNT action may involve down-regulating identity genes in the muscle founder cells, especially since those genes were down-regulated in the microarray analysis of HNT over-expression embryos. However, the precise nature of how over-expressing HNT can affect muscle development in the muscle founder cells has yet to be determined.

3.4 The association of *Hindsight* with Neuron development, and Notch signaling

A recent study by Buffin and Gho shows that HNT is expressed in sensory organ precursor cells (SOP), which are precursor cells for peripheral nervous system (PNS) and microchaete bristle development (Buffin & Gho, 2010). Microarray analysis of HNT over-expression embryos also supports the idea that HNT may affect neurogenesis, given the large number of neurogenesis related genes that were over- and under-represented in the presence of HNT over-expression (Table 3.4). All of the genes selected for FISH had at least a 2-fold change in expression in the presence of HNT over-expression, and were selected based on their involvement in neural development. Figure 3.12 compares that the FISH levels of *shaven*, otherwise known as D-Pax2, *scute*, *scabrous* and *Nplp1* between the control and the HNT over-expression embryos.

Table 3.4

Known muscle identity genes in the list of differentially expressed genes on HNT over-expression (Appendix B). These genes have a known role in neuron development during embryogenesis

Fbgn_ID (Flybase ID)	CG	Name(symbol)	Protein function	Up/Down-expression	Fold Change	Description [ref]
Neural						
FBgn0000216	CG3096	Bearded (Brd)	Counteracts neurogenic genes	Up	5.573	Activated by proneural genes as a direct target of Notch and antagonizes Notch signalling by directly competing with Delta (E. C. Lai, Bodner, Kavaler, Freschi, & Posakony, 2000)
FBgn0003326	CG17579	scabrous (sca)	Lateral inhibition	Up	2.637	Plays role in restriction of neural precursor fate in cells which defines the pattern of Notch signalling (Li, Fetchko, Lai, & Baker, 2003)
FBgn0004170	CG3827	scute (sc)	Transcription factor	Up	4.055	Target of Notch signalling and a proneural gene (Stagg, Guardiola, & Crews, 2011)
FBgn0035092	CG3441	Neuropeptide-like precursor 1 (Nplp1)	Neuropeptide hormone activity	Up	3.060	A marker for subtype-specific terminal differentiation gene in neurons (Overend et al., 2012)
FBgn0005561	CG11049	shaven/DPax2 (sv)	Transcription factor	Up	2.262	Direct Notch target for the proper differentiation of PNS define external sensory organ development and likely antagonist of Notch signalling (Charlton-Perkins et al., 2011)
FBgn0003651	CG11502	seven up (svp)	Transcription factor	Down	2.087	Acts as a switching factor in the temporal cascade for embryonic neuroblasts to generate different cell types (Benito-Sipos et al., 2011)
FBgn0004644	CG4637	hedgehog (hh)	Growth factor	Down	2.614	Growth factor signalling system is necessary for the initiation of proliferation of neural stem cells/neuroblast (Nfonsam, Cano, Mudge, Schilkey, & Curtiss, 2012)
FBgn0003130	CG8246	Pox neuro (Poxn)	Transcription factor	Down	2.098	Involved in development of larval poly-inverted external sensory organs and in specification of neuro identity (Awasaki & Kimura, 2001)

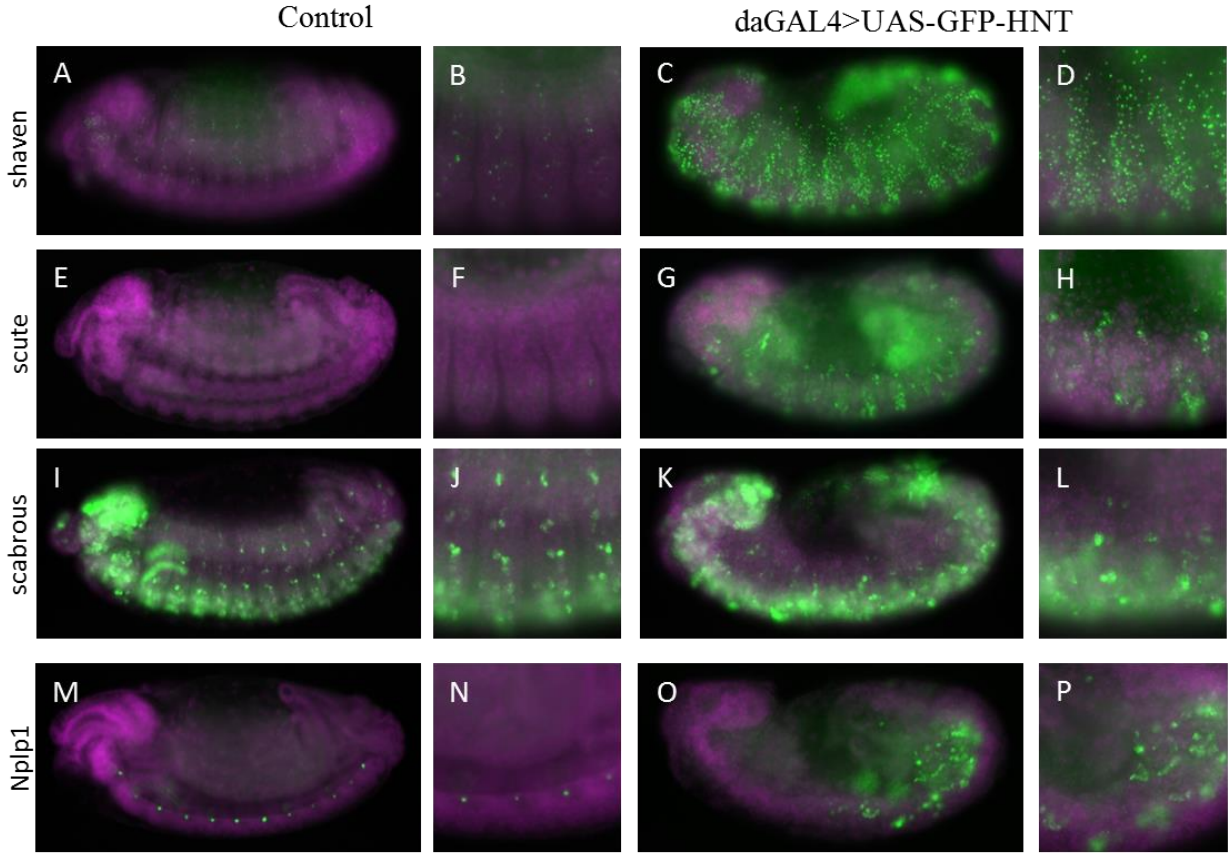


Figure 3.12

Fluorescent *in-situ* hybridization of the embryonic transcription levels of the genes *shaven* (A-D), *scute* (E-H), *scabrous* (I-L) and *Nplp1* (M-P), as seen in the control (A,B,E,F,I,J,M,N), yw, and the HNT over-expression (C,D,G,H,K,L,O,P), daGAL4>UAS-GFP-HNT, embryos. A cropped area of the gene expression is shown next to the expression in the entire embryo for the control (B,F,J,N) and the HNT over-expression (D,H,L,P). The green fluorescence represents the gene expression, and the DAPI is pseudo-colored purple. The Fluorescent *in-situ* hybridizations were kindly done by Ronit Wilk from the Krause Lab at the University of Toronto.

3.4.1 *Shaven/D-Pax2*

From the microarray data (Table 3.4) and the FISH analysis (Figure 3.12), one of the candidate genes that had increased expression in response to HNT over-expression was *shaven*/D-Pax2. D-Pax2 encodes a transcription factor, and is suggested to function as an antagonist of Notch signaling, while Notch has been noted to function as an inhibitor of D-Pax2 expression in the PNS (Cau & Blader, 2009). The microarray data implies that D-Pax2 could be a transcriptional target of HNT, since over expressing HNT appears to up-regulate the expression of D-Pax2. To validate the up-regulation seen in the FISH analysis, antibody staining was performed on control and HNT over-expression embryos.

3.4.2 The relationship between Hindsight and D-Pax2 expression in wild type embryos

To investigate HNT and D-Pax2 expression in wild type embryos, the relationship between these two proteins was examined by a double antibody stain with anti-HNT and anti-D-Pax2 at different embryonic stages: an early stage, stage 11, a middle stage, stage 12, and a late stage, stages 13-14 (Figure 3.13) (Campos-Ortega & Hartenstein, 1997).

Figure 3.13 A-C shows the early staged embryos with D-Pax2 expression (0.6±0.89 cells/per view), HNT expression (3.6±2.07 cells/per view), and the co-localized expression of the two proteins (23.2±1.79 cells/per view). At the early stage, almost every D-Pax2 expressing cell contained HNT expression. Figure 3.13 D-F displays middle staged embryos expressing D-Pax2 (6.71±4.11 cells/per view), HNT (9.43±4.72 cells/per view), and co-localized expression (43.57±9.43 cells/per view). In comparison to early staged embryos (Figure 3.13 A-C), middle staged embryos have more cells that express D-Pax2 or/and HNT, and there was also an increase

in the proportion of single-stained D-Pax2 cells to double–stained D-Pax2 and HNT cells. Figure 3.13 G-I shows the later staged embryos expressing D-Pax2 (34.7±7.33 cells/per view), HNT (61±6.10 cells/per view), and co-localization (24.17±6.97 cells/per view), at this stage of development, when compared to those at the middle stage, the number of D-Pax2 or HNT expressing cells increased, while the number of the cells with co-localization between these two proteins decreased.

Figure 3.14 compares the cell count representing HNT expression of the control embryos at the early, middle, and late stages ($p < 0.0001$ one-way ANOVA). The graph shows a steady increase in HNT expression from early to middle, but a large spike of HNT at the later stage.

Overall, there is a general trend whereby HNT and D-Pax2 expression appears to co-localize in early and middle, but not in later staged embryos. In later staged embryos, the expression of the two proteins appears to be found in neighbouring cells in the PNS. HNT appears to be expressed within the neurons, whereas D-Pax2 appears to be expressed in accessory cells. Given D-Pax2's role in neural development, specifically in the PNS, we also wanted to test if over-expressing HNT can effect neural development.

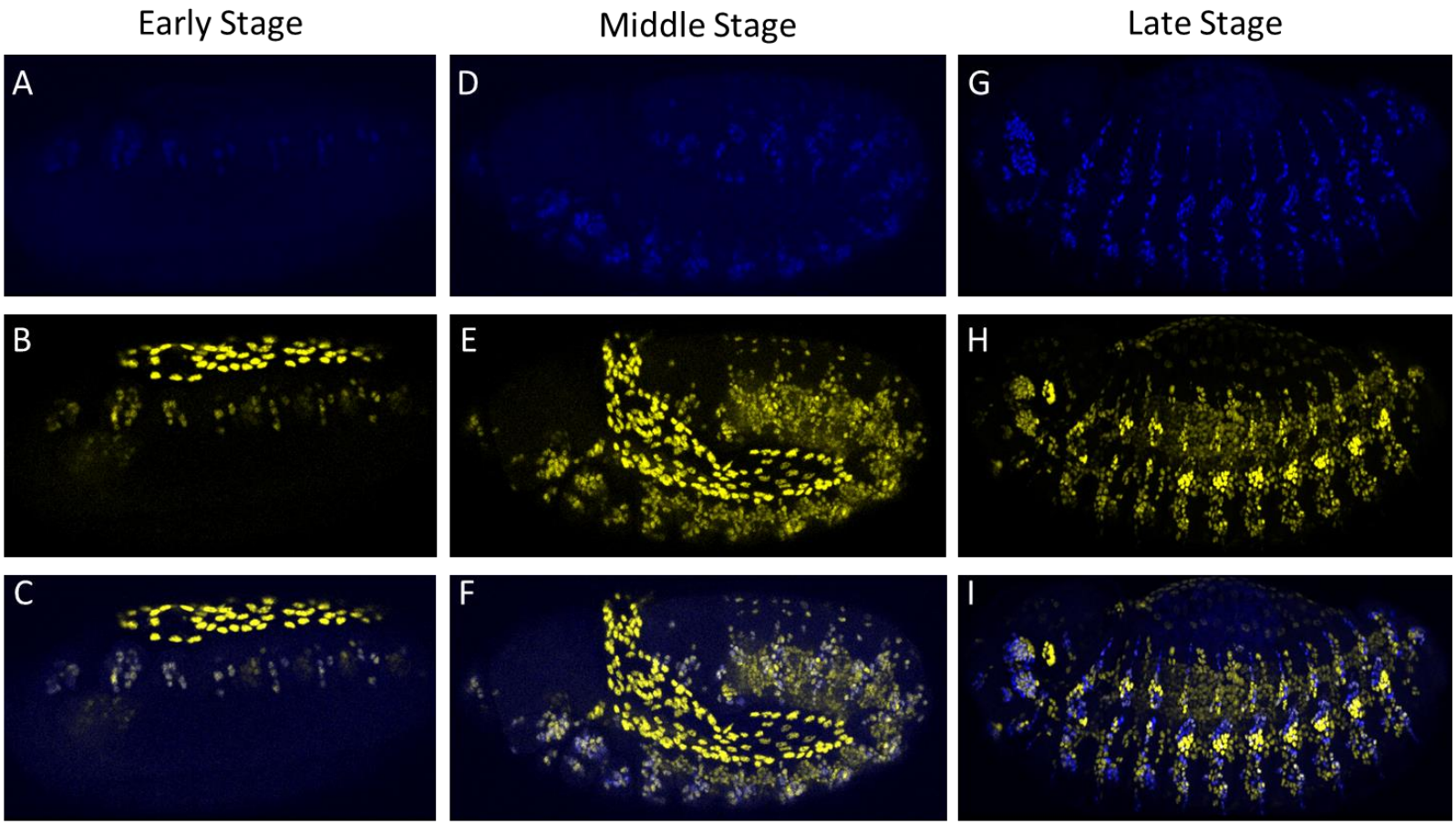


Figure 3.13

Double antibody staining with Anti-D-Pax2 and Anti-HNT of the control embryos, yw at the early stage (A-C), stage 10-11, the middle stage (D-F), stage 12, and the late stage (G-I), stage 13-14. The D-Pax2 expression, in blue, in the early stage (A), is compared to the middle (D) and late stages (G). The HNT expression, in yellow, at the early stage (B) is also compared to the middle (E) and late stages (H). The combined expression of the two antibodies during the early stage (C) is compared to the middle (F) and late (I) stages.

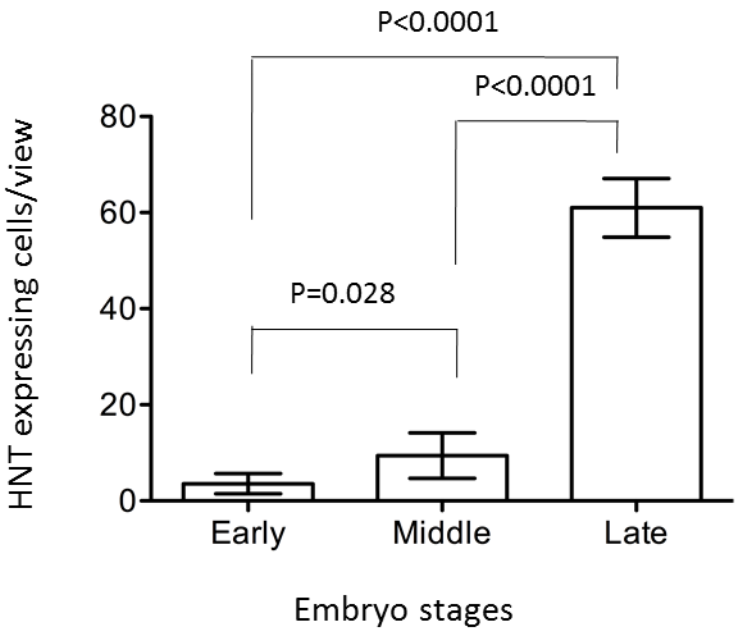


Figure 3.14 Hindsight expressing cells in the control embryos at different developmental stages

The sections of the control, yw, embryos were antibody stained with both anti-HNT and anti-D-Pax2 antibodies. The number of HNT expressing cells was counted in selected microscopic views (20X magnification), as described in the Materials and Methods, of the embryos at different stages: early, stage 11, (n=6); middle, stage 12, (n=7); and late, stage 13-14, (n=6). The changes of the cell numbers were statistically analyzed with the stage/time factor (one-way ANOVA).

3.4.3 The analysis of neurogenesis defects associated with HNT over-expression

To determine the effect of HNT over-expression in the embryonic nervous system, a 22C10 stain was used to outline the peripheral and central nervous systems in developing embryos. 22C10 is an monoclonal antibody that is a widely used as a neuronal marker to visualize neuronal morphology and axonal projections (Hummel, Krukkert, Roos, Davis, & Klambt, 2000). Figure 3.15 compares of the nervous system of HNT over-expression embryos (Figure 3.15B) to that of the control - *yw* (Figure 3.15A). In comparison to the control, the HNT over-expression embryos display a neurogenic phenotype, which could be the specification of neuronal cells at the expense of epidermal cells. This phenotype is similar, but not exact, to the Notch null ($Notch^{55ell}$), which displays an expected neurogenic mutant phenotype: a hypertrophy of neural cells at the expense of epidermal cells (Figure 3.15D) (Cabrera, 1990).

The HNT null, hnt^{XE81}, on the other hand, did not display a neurogenic phenotype similar to the HNT over-expression and Notch null embryos, instead there appeared to be fewer neural cells (Figure 3.15C). Unfortunately, since these embryos were not staged, it is difficult to say whether without HNT expression there is a reduction of neural cells or whether these cells just have not fully developed. However, HNT null embryos do have a reduction in the number of chordotonal (Ch) organs, which are components of the PNS. In wild type embryos there are usually 5-8 found in each abdominal hemisegment (Okabe & Okano, 1997), the HNT null appears to have only 3-4, which could be indicative of a role of HNT in neural development.

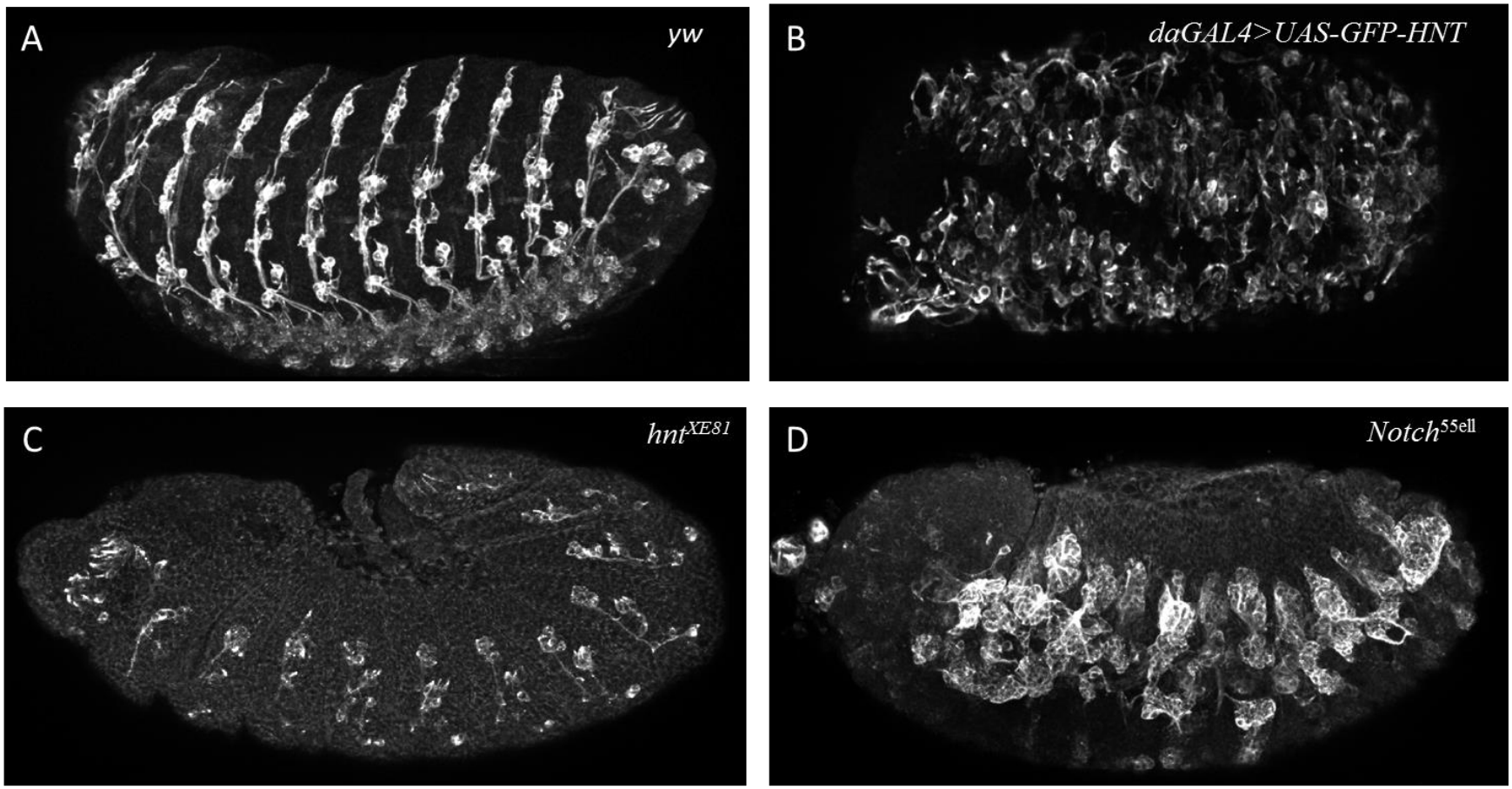


Figure 3.15
22C10 stained embryos representing F-actin distribution of control (A), HNT over-expression (B), the HNT null (C), and the Notch null (D).

3.4.4 The co-localization of D-Pax2 and Hindsight in different experimental models

Despite the complementary pattern observed between HNT and D-Pax2 at later stages of embryonic development, the microarray data showed that increased HNT expression also increased D-Pax2 expression. This suggests that HNT may function to co-regulate D-Pax2 during neural development. This up-regulation could involve the Notch signaling pathway, which is well known to be required for the differentiation of neuroblasts (Artavanis-Tsakonas et al., 1990; Artavanis-Tsakonas et al., 1999). This is an compelling model since previously published studies, such as those on adult muscle progenitors, have reporter that HNT is a direct transcriptional target of Notch (Krejci et al., 2009). If this is also the case in neural progenitors, then Notch null mutants would expect to have reduced HNT expression, and if the effect of HNT expression on D-Pax2 was dependent on Notch signaling, than Notch null mutants should also have reduced HNT and D-Pax2 expression.

To investigate whether or not the up-regulation of D-Pax2 following the over-expression of HNT involves the Notch signaling pathway, anti-HNT and anti-D-Pax2 double staining was examined in the control (Figure 3.16 A-C), HNT over-expression (Figure 3.16 D-F), and Notch null (Figure 3.16 G-I) embryos. In comparison to the control, HNT over-expression embryos (Figure 3.16 D-F) had an increased number of cells with co-localized HNT and D-Pax2 expression, as well as an increase in the number of cells expressing D-Pax2 without HNT expression. Notch null (*Notch*^{55ell}) mutant embryos (Figure 3.16 G-I) were found to have excessive HNT expression, but displayed only barely detectable levels of D-Pax2 expression. This suggested that Notch could be required to inhibit HNT expression, but not D-Pax2 expression, and Notch signaling is required for the maintenance of D-Pax2 expression. In

addition, the relationship between HNT and D-Pax2 does not appear to involve Notch signaling, as evident by the lack of HNT inhibition in the Notch null mutants, and the increased D-Pax2 expression in HNT over-expression mutants.

The inhibitory effects of Notch on HNT expression were reaffirmed by an HNT antibody stain on Notch null (*Notch*^{55ell}) and Delta mutants (Delta-GAL4/TM6) (Figure 3.17). The over expression of HNT on the Notch null (Figure 3.17 B) resembles the pattern seen with the 22C10 stain on the Notch null (Figure 3.15D), suggesting that the neural hypertrophy is constituent with the over-expression of HNT in neural cells. The signaling pathway by which Notch inhibits HNT in neural cells is potentially through the Delta ligand, since the HNT antibody stain on Delta mutants (Figure 3.17C) resembles the over-expression of HNT in the Notch null.

The number of cells with co-localized HNT and D-Pax2 was also quantitatively compared between the control, HNT over-expression (daGAL4> UAS-GFP-HNT), and the Notch null (*Notch*^{55ell}). As shown in Figure 3.18, the HNT over-expressing embryos had a greater number of co-localized cells (148±9.43 per view) than the control (43.6±9.43 per view) and the Notch null (0); please note that the amount of D-Pax2 expression observed in the Notch null could be attributed to the late stage of the embryo, and the barely detectable number of D-Pax2 expressing cells could not be properly counted and was denoted as being 0 for comparison purposes ($p < 0.0001$, Control vs. UAS-GFP-HNT, Student t-test).This result further reaffirms the idea that D-Pax2 may still be an indirect or direct target of HNT, and the over-expression of D-Pax2 in the HNT over-expression reporter line seen in Figure 3.16 does not require Notch signaling pathway.

This result appears to contradict previous studies that showed HNT is transcriptionally activated by Notch, in the muscle progenitor cells (Krejci et al., 2009); however, this could be

due to the fact that neural development is a different developmental system. This suggests that during muscle development Notch may be needed to activate HNT expression, while in neural development, Notch may or may not be needed to inhibit HNT expression.

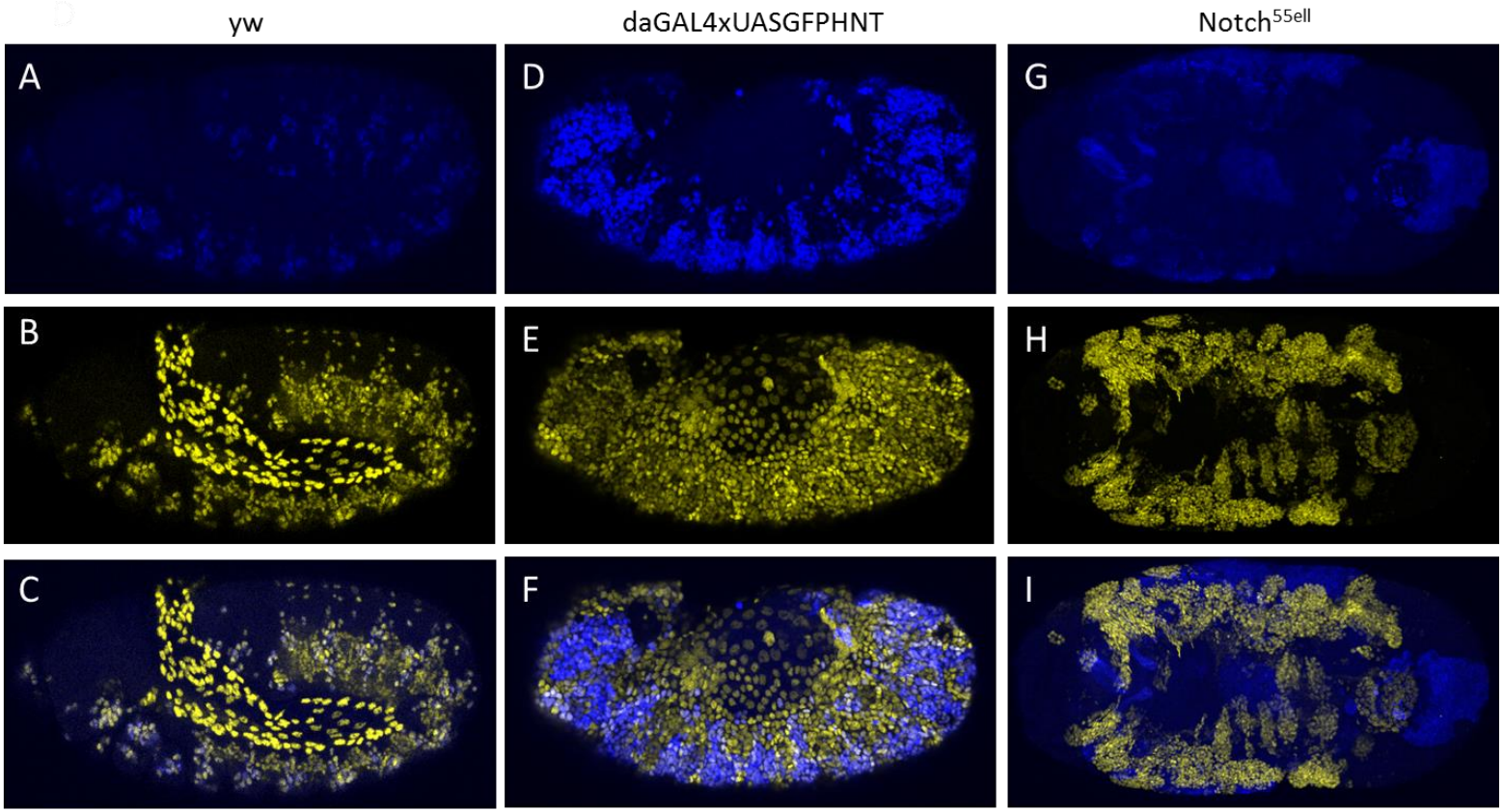


Figure 3.16

Double antibody staining with Anti-D-Pax2 and Anti-HNT on control (A-C), yw, HNT over-expression (D-F), daGAL4>UAS-GFP-HNT, and Notch null (G-I), Notch^{55ell} embryos. The D-Pax2 expression, in blue, compares the control (A) to the D-Pax2 expression in the HNT over-expression (D) and the Notch null (G). The HNT expression, in yellow, compares the control (B) to the HNT expression of the HNT over-expression (D) and the Notch null (H). The combined expression of the two antibodies is also seen in the control (C), the HNT over-expression (F), and the Notch null (I) embryos.

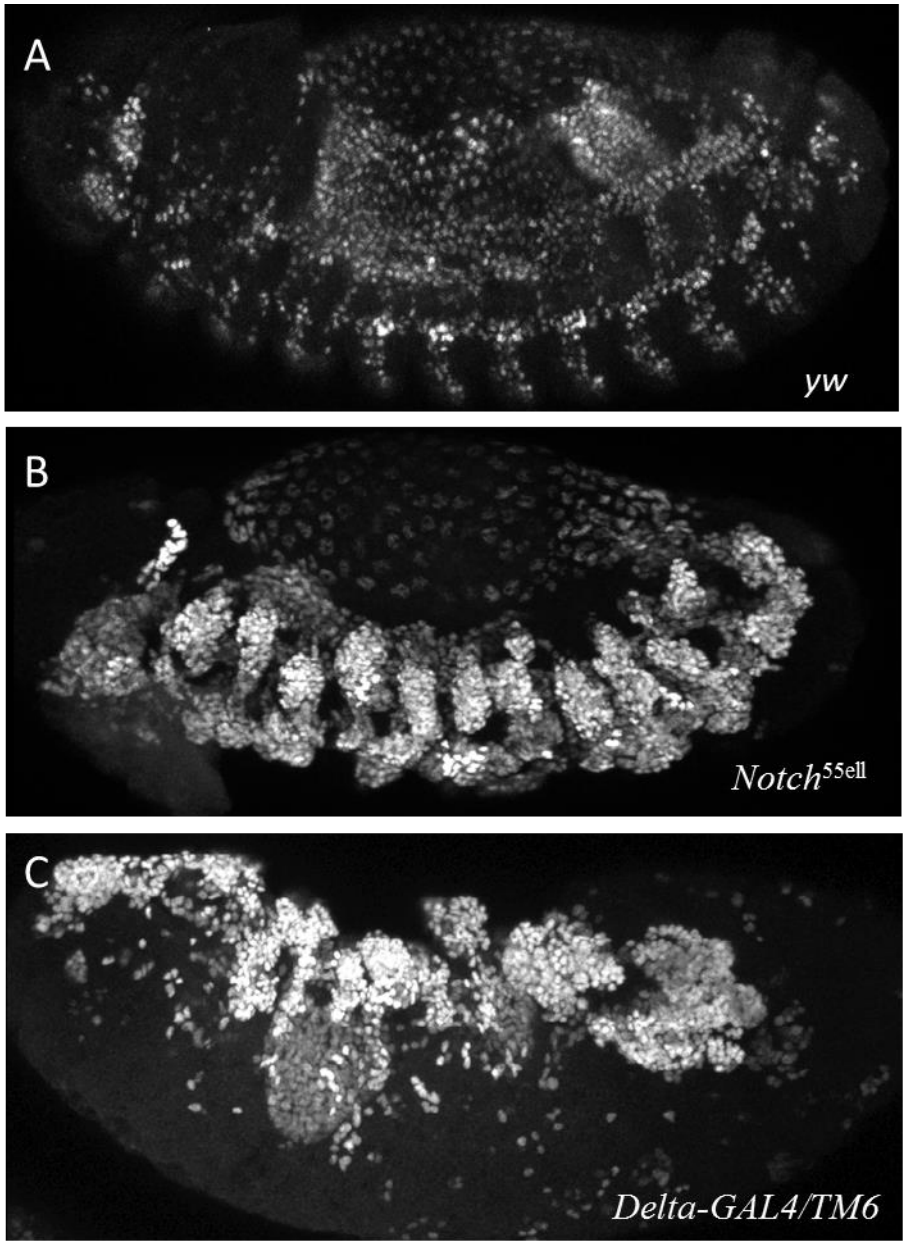


Figure 3.17
Hindsight antibody stained embryos comparing the control (A), to the Notch null, (B) and Delta null mutant (C)

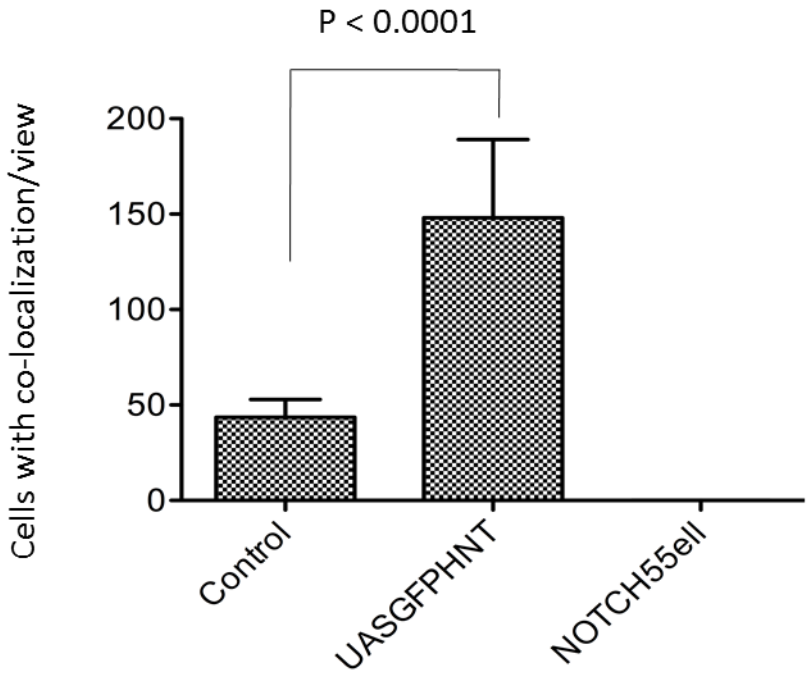


Figure 3.18 Regulation of HNT/D-Pax2 co-localization in embryos of HNT over-expression and Notch null

The sections of the embryos were antibody stained with both anti-HNT and anti-D-Pax2 antibodies. The number of HNT/P-Pax2 co-localizing cells was counted in selected microscopic views (20X magnification), as described in the Materials and Methods, of each sample. Control, yw, embryos at the middle stage, stage 12, (n=7); UASGFPHNT embryos represent the HNT over-expression phenotype, one stage, (n =7); and $NOTCH^{55ell}$ embryos represent the Notch null, one stage, (n=5). $p < 0.0001$ (Control vs. UASGFPHNT, t-test)

3.5 D-Pax2 expression may be dependent on the level of HNT expression

3.5.1 D-Pax2 expression is not robustly increased using the *hnt* reporter line *EP55*

Double immunostaining of HNT and D-Pax2 on HNT over-expressing embryos did reveal a dramatic up-regulation of D-Pax2, but this effect was not observed in all embryos (therefore D-Pax2 over-expression was not 100% in daGAL4>UAS-GFP-HNT embryos). To address this issue, this experiment was repeated using the *hnt* reporter line EP55, which is associated with a less severe phenotype when expressed in the pupal eye and is associated with lower levels of HNT expression. Using EP55 to over express HNT in the embryo with the daGAL4 driver did not result in a dramatic up-regulation of D-Pax2 (Figure 3.19).

Although there was no immediate obvious change in D-Pax2 expression in daGAL4>EP55 embryos, some embryos did appear to show some mild differences. For this reason, a statistical analysis of D-Pax2/HNT co-localization and D-Pax2 expression was performed. As shown in Figure 3.20 A, the number of D-Pax2/HNT co-localized expressing cells compared the control (early stage: 23.2±1.79 cells/per view, middle stage 43.57±9.43 cells/per view, and late stage 24.17±6.97 cells/per view) to the EP55 cell count (early stage: 24.3±2.31 cells/per view, the middle stage: 41.75±2.75 cells/per view, and the late stage: 45.5±16.3 cells/per view). When compared to the control, statistical analysis of, which HNT and D-Pax2 were co-localized, cells indicated that there was not a significant difference between EP55 and the control at an early to middle stage ($p=0.4625$ and $p=0.7173$), but at a later stage there was a significant difference ($p=0.0199$). This suggests that despite there not being a significant phenotypic difference in HNT/D-Pax2 co-localized expressing cells between the control and

EP55 embryos, EP55 embryos were able to increase the number of co-localized cells at later staged embryos.

Figure 3.20 B compared the amount of D-Pax2 expressing cells in the EP55 embryos at the early (5.33±1.53 cells/per view), the middle (13.5±3.41 cells/per view), and the late (58.75±8.42 cells/per view) stages, to the control. In comparison, the statistical analysis suggested that D-Pax2 expression had significantly increased, in EP55 embryos compared to the control, in all stages of development ($p<0.05$, two-way ANOVA).

Taken together, this data indicated that even though EP55 did not result in dramatic D-Pax2 over-expression (as seen in the UAS-GFP-HNT reporter line), there was an increase in the number of cells co-expressing HNT and D-Pax2 at later embryonic stages, in addition to an increase in the number of cells expressing D-Pax2 throughout all embryonic developmental stages.

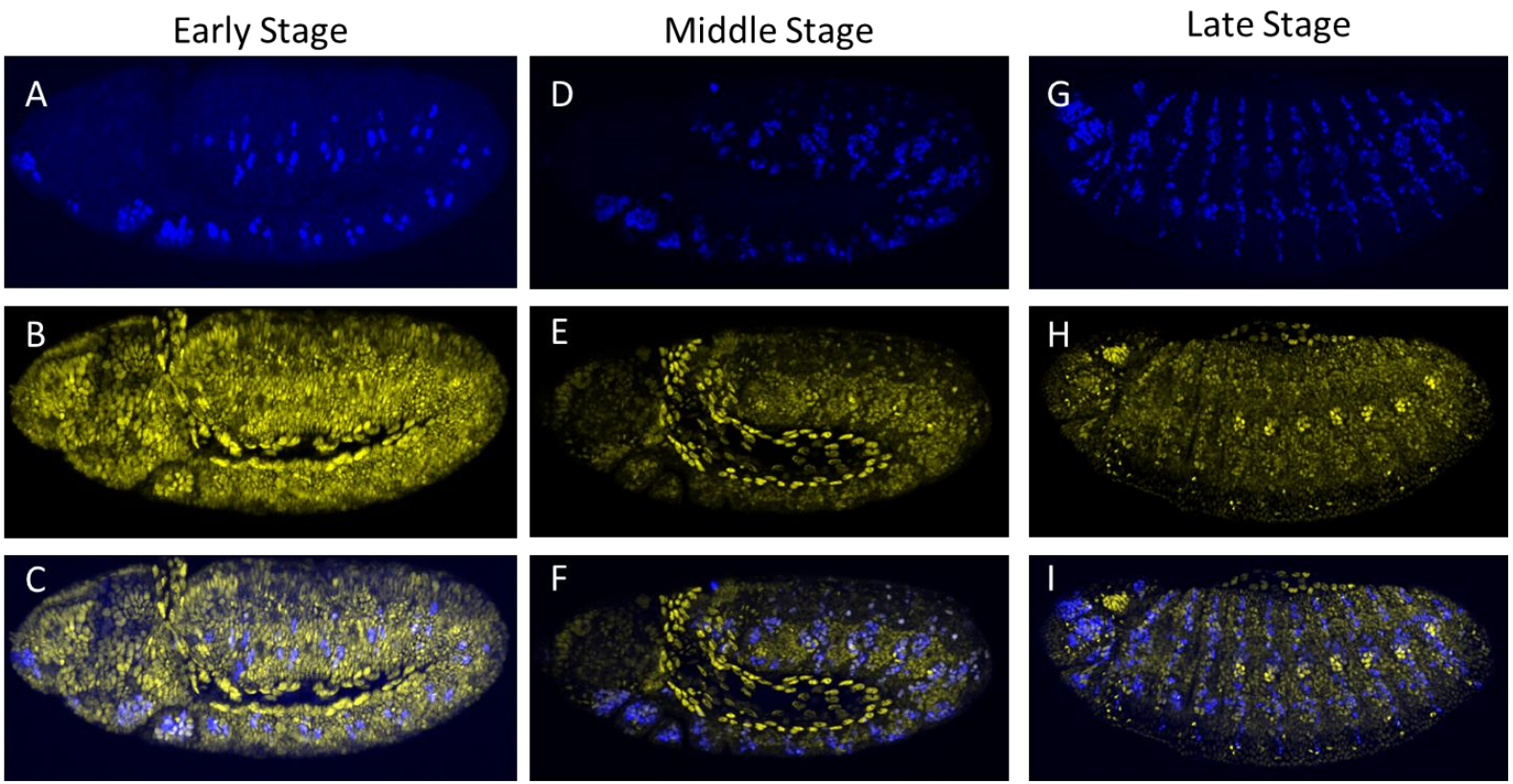


Figure 3.19

Double antibody staining with Anti-D-Pax2 and Anti-HNT of HNT over-expression embryos using the EP55 reporter line crossed with daGAL4 of embryos at the early stage (A-C), stage 10-11, the middle stage (D-F), stage 12, and the late stage (G-I), stage 13-14. The D-Pax2 expression, in blue, in the early stage (A), is compared to the middle (D) and late stages (G). The HNT expression, in yellow, at the early stage (B) is also compared to the middle (E) and late stages (H). The combined expression of the two antibodies during the early stage (C) is compared to the middle (F) and late (I) stages.

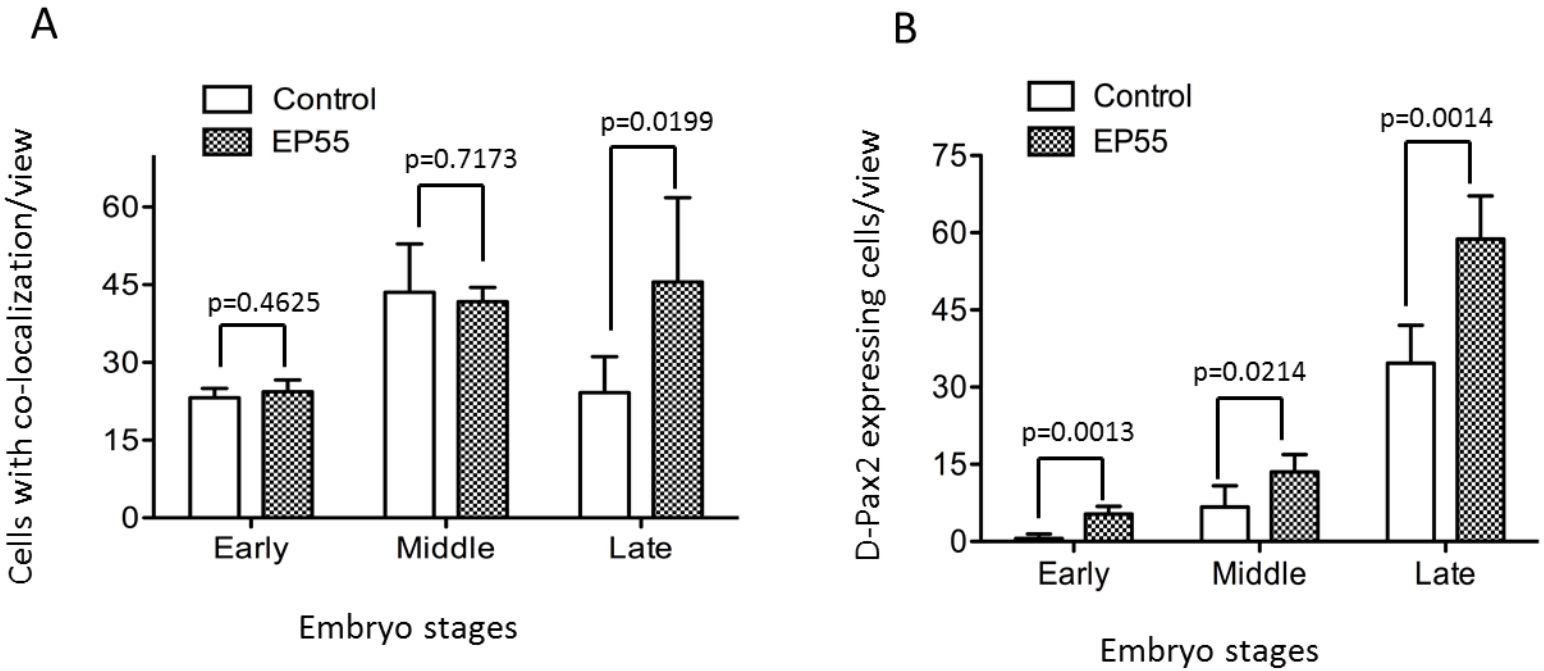


Figure 3.20 HNT and/or D-Pax2 expression in control embryos versus EP55, HNT over-expression embryos
The sections of the embryos were antibody stained with both anti-HNT and anti-D-Pax2 antibodies. The number of HNT/P-Pax2 co-localizing or D-Pax2 expressing cells was counted in selected microscopic views (20X magnification), as described in the Materials and Methods, of the embryos (Control vs. EP55) at different stages: early, stage 11, (Control: n=6; EP55: n=3); middle, stage 12, (Control: n=7; EP55: n=4); and late, stage 13-14, (Control: n=6; EP55: n=4). The difference of the cell numbers between these two groups were statistically analyzed using Students t-test. **(A)** The cells expressing co-localization of HNT and D-Pax2 at the early, middle and late stages between the Control and EP55 $P = 0.0441$ (Control vs. EP55, 2-way ANOVA). **(B)** The cells expressing only D-Pax2 at the early, middle and late stages between the Control and EP55 $P < 0.0001$ (Control vs. EP55, 2-way ANOVA)

3.5.2 Hindsight over-expression via the *UAS-GFP-HNT* reporter is greater than the *EP55* reporter

Even though EP55 was able to induce a mild but significant effect on D-Pax2 expression, the strong D-Pax2 expression in the UAS-GFP-HNT reporter line was not seen. Despite both reporters being HNT over-expression lines, it is possible that the difference between the two reporter lines might be the cause behind the significant difference in D-Pax2 expression. To test this hypothesis, the HNT expression levels of EP55 and UAS-GFP-HNT was compared under identical confocal settings that allowed the HNT expression between these two constructs to be directly compared with anti-HNT immunostaining.

Figure 3.21 demonstrates the difference between HNT expression of these two reporter lines, using the same driver daGAL4. The data showed that despite randomly choosing the embryos from a larger sample pool, the reporter line UAS-GFP-HNT displayed much stronger HNT expression than the EP55 reporter line, suggesting that there might be a threshold level of HNT expression that needs to be met to induce the strong over-expression of D-Pax2, as seen with the UAS-GFP-HNT reporter line. Especially since daGAL4>EP55 embryos, which from Figure 3.21, has lower HNT expression than daGAL4>UAS-GFP-HNT embryos, and was unable to produce the same strong D-Pax2 expression.

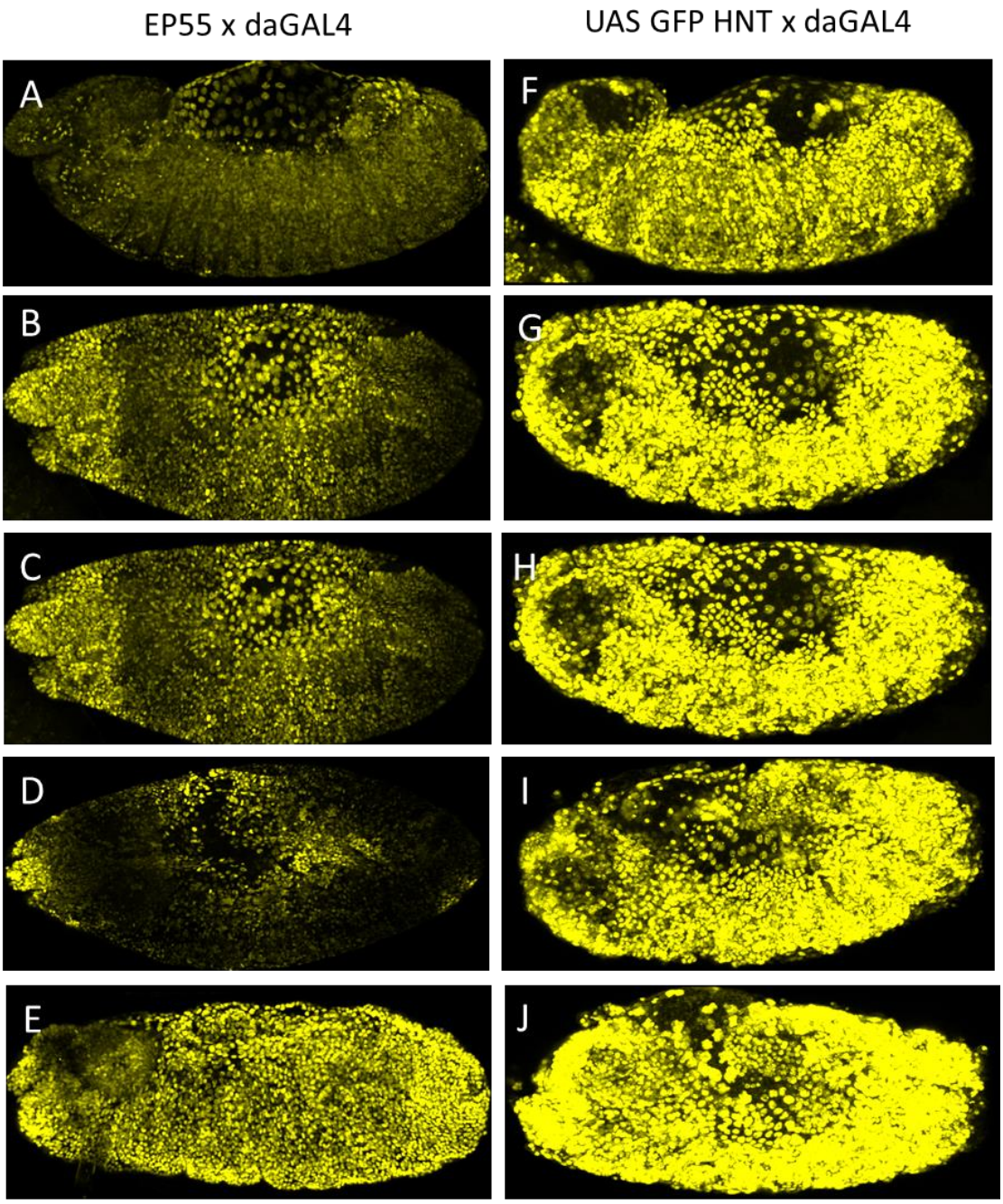


Figure 3.21

Under identical confocal settings, HNT expression between EP55 and UAS-GFP-HNT can be directly compared with anti-HNT immunostaining. A-E compares the HNT fluorescent expression of the EP55 reporter line, to the UAS-GFP-HNT reporter line (F-J), when crossed with the daGAL4 driver.

3.5.3 Increasing Hindsight expression in *EP55* embryos is unable to give strong D-Pax2 expression

The greater level of HNT over-expression when using the UAS-GFP-HNT line suggests that there could be a threshold level of HNT that needs to be met in order to elicit strong D-Pax2 expression. To investigate this threshold idea, levels of HNT expression were modulated by increasing and decreasing the temperature the genetic crosses were incubated at, to determine if it will have an impact on D-Pax2 expression. First, we attempted to over-induce the endogenous HNT in the EP55 embryos by temperature shifting it to 29^{o}C. As shown in Figure 3.22, even with the temperature shift on EP55, the same level of D-Pax2 over-expression as the UAS-GFP-HNT reporter line was not phenotypically seen.

In addition, when comparing the number of HNT/D-Pax2 co-localizing (48.86±8.63 cells/per view) and D-Pax2 expressing (29.86±5.75 cells/per view) cells in the temperature shifted EP55 line to the co-localizing (148±9.43 cells/per view) and D-Pax2 expressing cells (61±14.25 cells/per view) in the UAS-GFP-HNT line, the statistical analysis showed that the co-localized and D-Pax2 cell counts in UAS-GFP-HNT embryos were still significantly higher ($p<0.05$) (Figure 3.23). Demonstrating that just by increasing the temperature the genetic cross is incubated at is unable to increase HNT expression enough in EP55 embryos to provide the strong level of D-Pax2 expression.

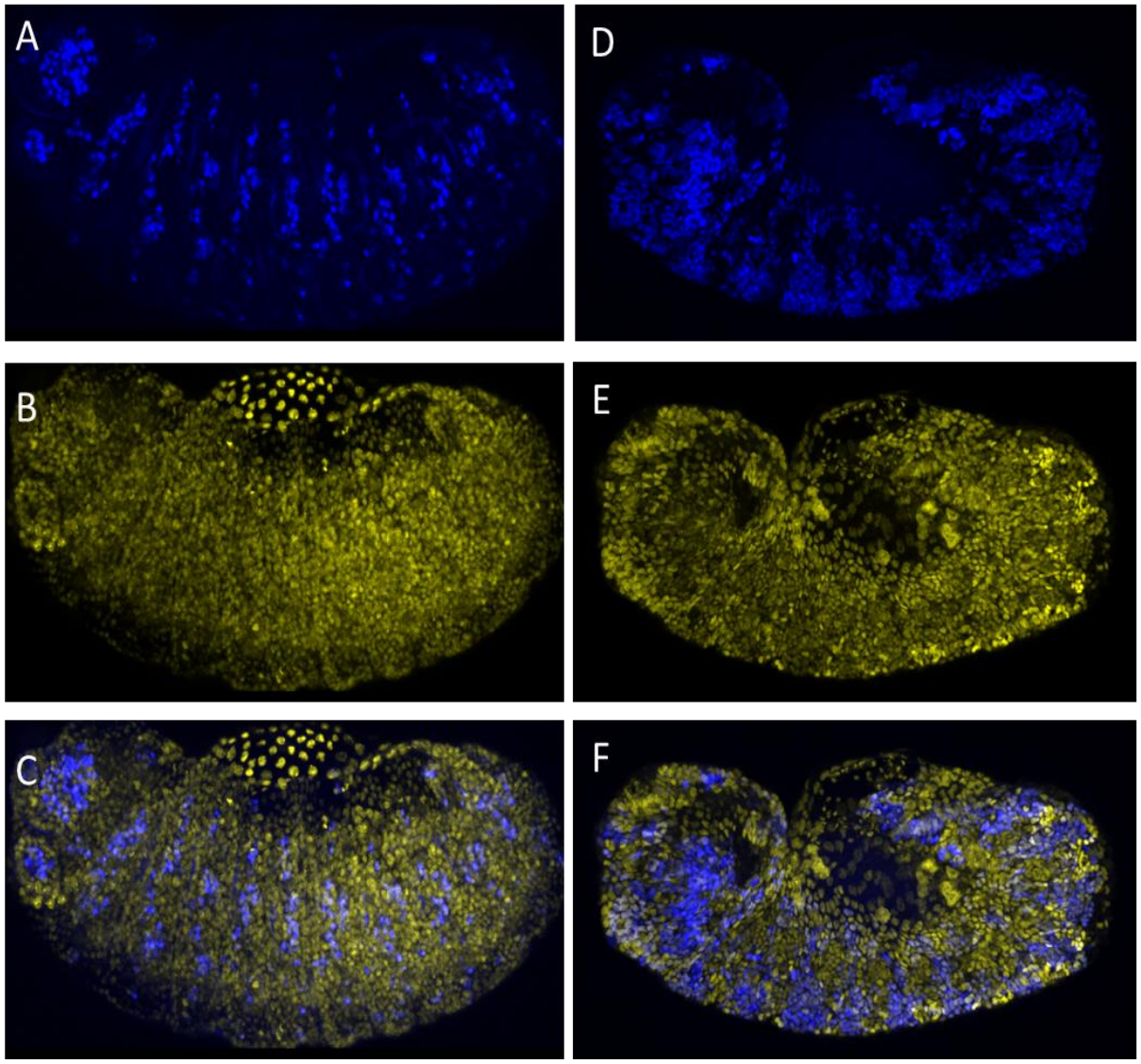


Figure 3.22
Double antibody staining with Anti-D-Pax2 and Anti-HNT compares HNT over-expression embryos using the EP55 reporter line, temperature shifted to 29°C (A-C) to the UAS-GFP-HNT reporter line (D-F), crossed with daGAL4. Due to the severity of the HNT over-expression, the embryos arrested in development, leaving only one recognizable stage. The D-Pax2 expression, in blue, of the EP55 embryos (A), is compared to the UAS-GFP-HNT (D) embryos. The HNT expression, in yellow, of the EP55 embryos (B) is also compared to the UAS-GFP-HNT (E) embryos. The combined expression of the two antibodies of the H9 (C) is compared to the UAS-GFP-HNT (F) embryos.

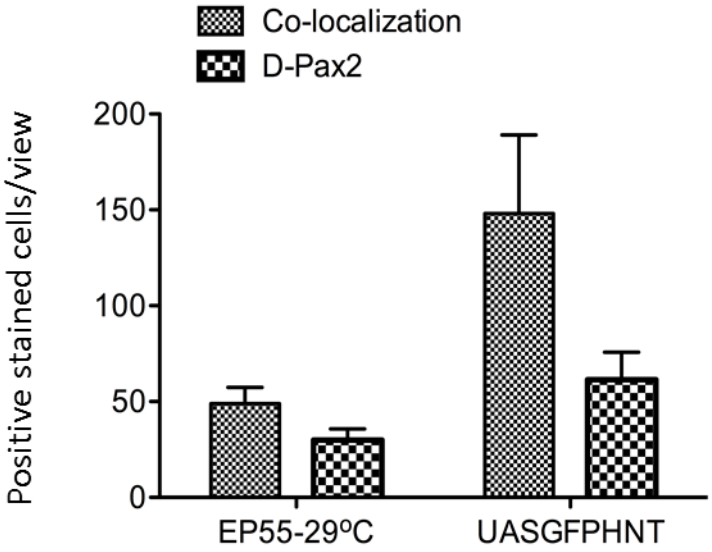


Figure 3.23 Regulation of HNT and/or D-Pax2 expression in the embryos by different levels of HNT over-expression

The sections of the embryos were antibody stained with both anti-HNT and anti-D-Pax2 antibodies. The number of HNT/P-Pax2 co-localizing or D-Pax2 expressing cells was counted in selected microscopic views (20X magnification), as described in the Materials and Methods, of the EP55 at 29ºC and UASGFPHNT embryos at the one stage (EP55-29ºC: n=7; and UASGFPHNT: n=7). The difference of the cell numbers between these two groups were statistically analyzed using Students t-test. HNT/D-Pax2 co-localization: $p < 0.0001$. D-Pax2: $p = 0.0002$.

3.5.4 Reducing Hindsight expression in the *UAS-GFP-HNT* line has little effect on D-Pax2 expression

In addition, we also tried to reduce HNT expression in the UAS-GFP-HNT reporter line by temperature shifting it to 18^{o}C. Figure 3.24 indicates that at the later development stage there is still a strong D-Pax2 over-expression. However, when the HNT/D-Pax2 co-localizing cell counts (early stage: 10±4.58 cells/per view; middle stage: 28.7±5.51 cells/per view; and late stage: 96±37.75 cells/per view) of the UAS-GFP-HNT at 18^{o}C, as shown in Figure 3.25 A, were compared to the EP55 at 25^{o}C (early stage: 24.3±2.31 cells/per view, the middle stage: 41.75±2.75 cells/per view, and the late stage: 45.5±16.3 cells/per view) there was a significant difference between the two groups at the early stage ($p=0.0084$), and at the later stage ($p=0.0428$), with more expression in UAS-GFP-HNT than EP55, but no significant difference was found at the middle stage ($p=0.3684$).

In addition, when comparing the D-Pax2 expression (early stage: 14±1.73 cells/per view; middle stage: 52.3±9.5 cells/per view; and late stage: 56.6±7.79 cells/per view) of the UAS-GFP-HNT at 18^{o}C, as shown in Figure 3.25 B, to those of EP55 at 25^{o}C, at both the early and middle stages, the UAS-GFP-HNT line still has significantly higher expression of D-Pax2 than in the EP55 ($p=0.0029$ and $p=0.0006$, respectively); but at the later stage there was no significant difference between the two groups ($p=0.07031$). These results suggest that temperature shifting the UAS-GFP-HNT to 18^{o}C can reduce the HNT expression enough to have a noticeable effect on cells just expressing D-Pax2, but not on cells expressing both HNT and D-Pax2.

Overall, trying to modulate temperature increases or decreases on HNT expression was not sufficient enough to affect the threshold needed to induce strong D-Pax2 expression levels in embryos. This suggests that the large amount of HNT expression produced by the

daGAL4>UAS-GFP-HNT embryos causes the strong D-Pax2 expression seen in those embryos, and perhaps it's the GFP-HNT construct of the UAS-GFP-HNT reporter line that causes the strong D-Pax2 expression.

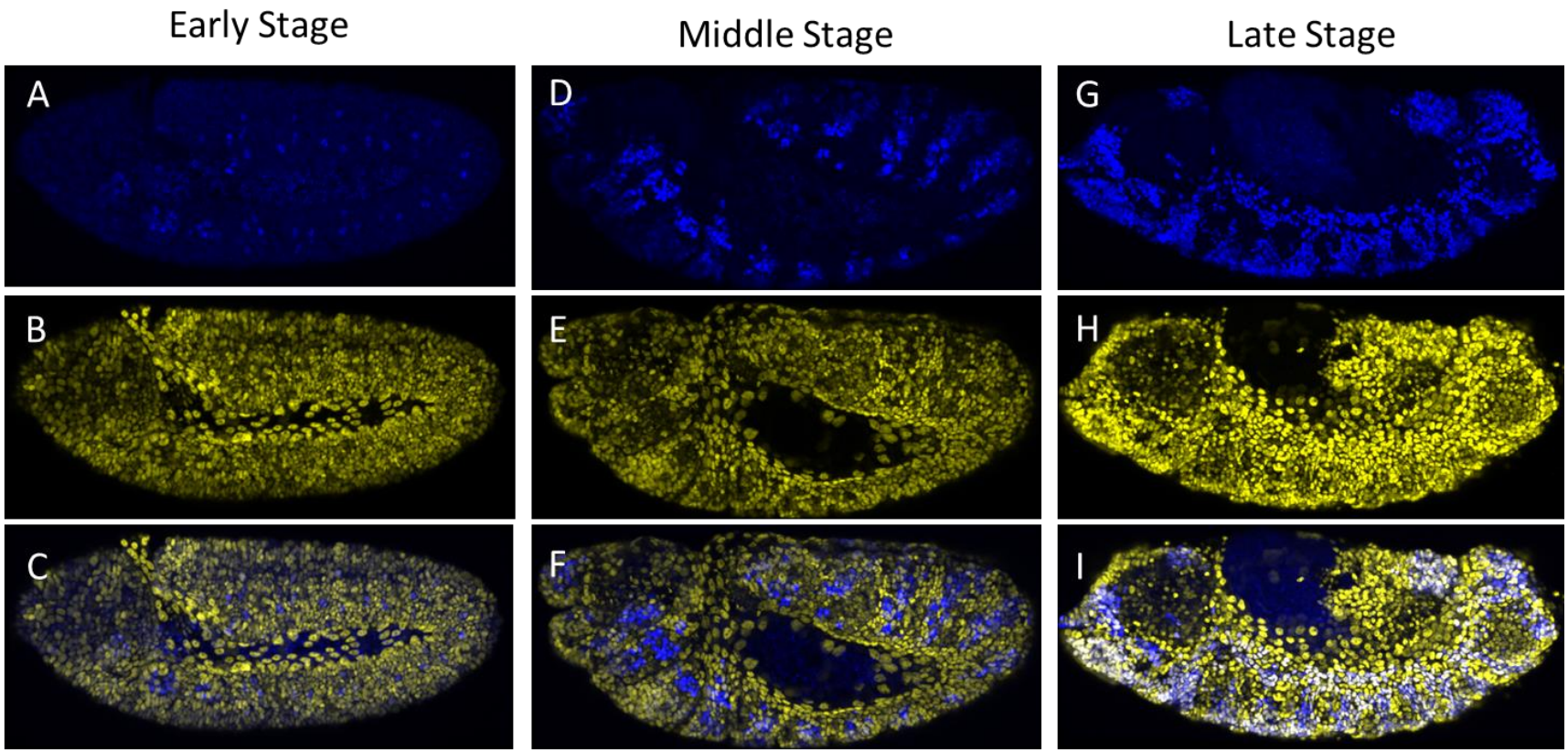


Figure 3.24

Double antibody staining with Anti-D-Pax2 and Anti-HNT of HNT over-expression embryos using the UAS-GFP-HNT reporter line crossed with daGAL4, that was temperature shifted to 18°C, of embryos at the early stage (A-C), stage 10-11, the middle stage (D-F), stage 12, and the late stage (G-I), stage 13-14. The D-Pax2 expression, in blue, in the early stage (A), is compared to the middle (D) and late stages (G). The HNT expression, in yellow, at the early stage (B) is also compared to the middle (E) and late stages (H). The combined expression of the two antibodies during the early stage (C) is compared to the middle (F) and late (I) stages.

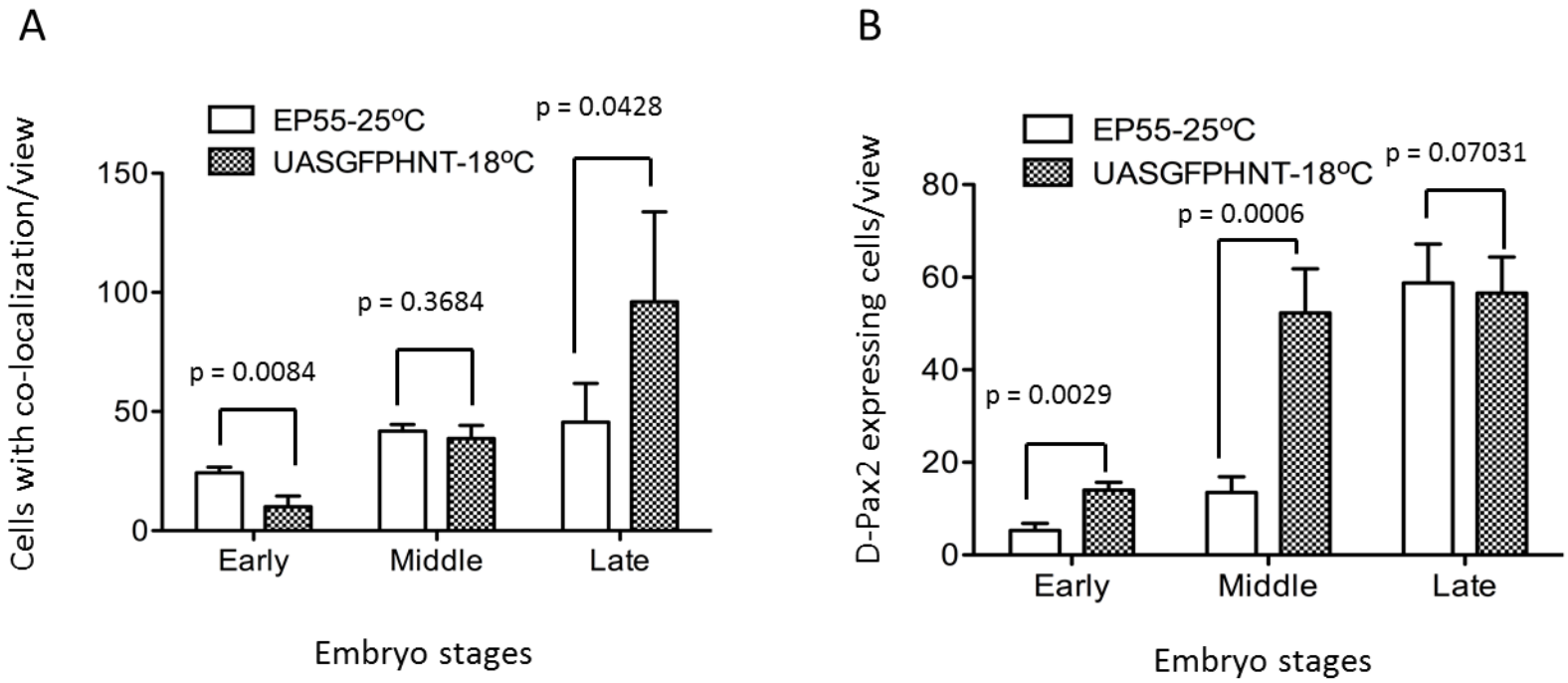


Figure 3.25 HNT and/or D-Pax2 expression in the embryos by modulating different levels of HNT expression
The sections of the embryos were antibody stained with both anti-HNT and anti-D-Pax2 antibodies. The number of HNT/P-Pax2 co-localizing or D-Pax2 expressing cells was counted in selected microscopic views (20X magnification), as described in the Materials and Methods, of the embryos (UASGFPHNT-18ºC vs. EP55-25ºC) at different stages: early, stage 11, (UASGFPHNT-18ºC: n=3; EP55-25ºC: n=3); middle, stage 12, (UASGFPHNT-18ºC: n=3; EP55-25ºC: n=4); and late, stages 13=14 (UASGFPHNT-18ºC: n=5; EP55-25ºC: n=4). The difference of the cell numbers between these two groups were statistically analyzed using Students t-test. **(A)** The cells expressing co-localization of HNT and D-Pax2 at the early, middle and late stages between the Control and EP55 $P = 0.3219$ (UASGFPHNT vs. EP55, 2-way ANOVA). **(B)** The cells expressing only D-Pax2 at the early, middle and late stages between the Control and EP55 $P < 0.0001$ (UASGFPHNT vs. EP55, 2-way ANOVA)

3.5.5 The UAS-GFP-HNT construct is not the cause of the strong D-Pax2 expression

The UAS-GFP-HNT reporter line expresses a GFP-HNT-fusion protein, which could stabilize the HNT protein, resulting in the strong D-Pax2 expression. HNT could be an unstable protein, and fusing the GFP molecule to the HNT protein could be somehow stabilizing HNT, thus allowing for increased D-Pax2 expression.

To study whether or not the construct contributes to the strong D-Pax2 expression, a double antibody stain of HNT and D-Pax2 was done on UAS-GFP-HNT^{J18} embryos. UAS-GFP-HNT^{J18} has the exact same GFP-fusion construct as the UAS-GFP-HNT, the only difference in the UAS-GFP-HNT^{J18} reporter line is that the UAS-GFP-HNT construct was jumped (by Dr. Bruce Reed) to a different site of the HNT genome via a genetic P-element mobilization scheme, producing a less severe phenotype. The double antibody stain on UAS-GFP-HNT^{J18} embryos, as indicated in Figure 3.26, demonstrates that UAS-GFP-HNT^{J18} does not have same D-Pax2 expression seen in the UAS-GFP-HNT embryos, suggesting that the construct itself does not attribute to the strong D-Pax2 expression.

Figure 3.27 A compares the numbers of the HNT/P-Pax2 co-localizing cells between EP55 (41.75±2.75 cells/per view) and UAS-GFP-HNT (148±9.43 cells/per view) to the UAS-GFP-HNT^{J18} embryos (39.2±4.49 cells/per view), which suggested that there was not statistically difference between EP55 and UAS-GFP-HNT^{J18} ($p=0.3559$). However, when the D-Pax2 expression of EP55 (13.5±3.41 cells/per view) or UAS-GFP-HNT (61±14.25 cells/per view) was compared to UAS-GFP-HNT^{J18} (21.4±5.73 cells/per view), as shown in Figure 3.27 B, there was barely a significant difference between EP55 and UAS-GFP-HNT^{J18} ($p=0.0463$).

Overall, Figure 3.27 suggested there little to no significant difference in the level of expression caused between EP55 and UAS-GFP-HNT^{J18}. There was a significant difference, however, when comparing the co-localized ($p<0.05$) and D-Pax2 ($p<0.05$) expressing cells of the UAS-GFP-HNT line to EP55 and UAS-GFP-HNT^{J18}. The UAS-GFP-HNT reporter line has significantly more co-localized and D-Pax2 expressing cells than in EP55 and UAS-GFP-HNT^{J18}, reinforcing the idea that the construct itself is not the cause of the strong D-Pax2 expression seen in the UAS-GFP-HNT reporter line, and it could still be the high level of HNT expression.

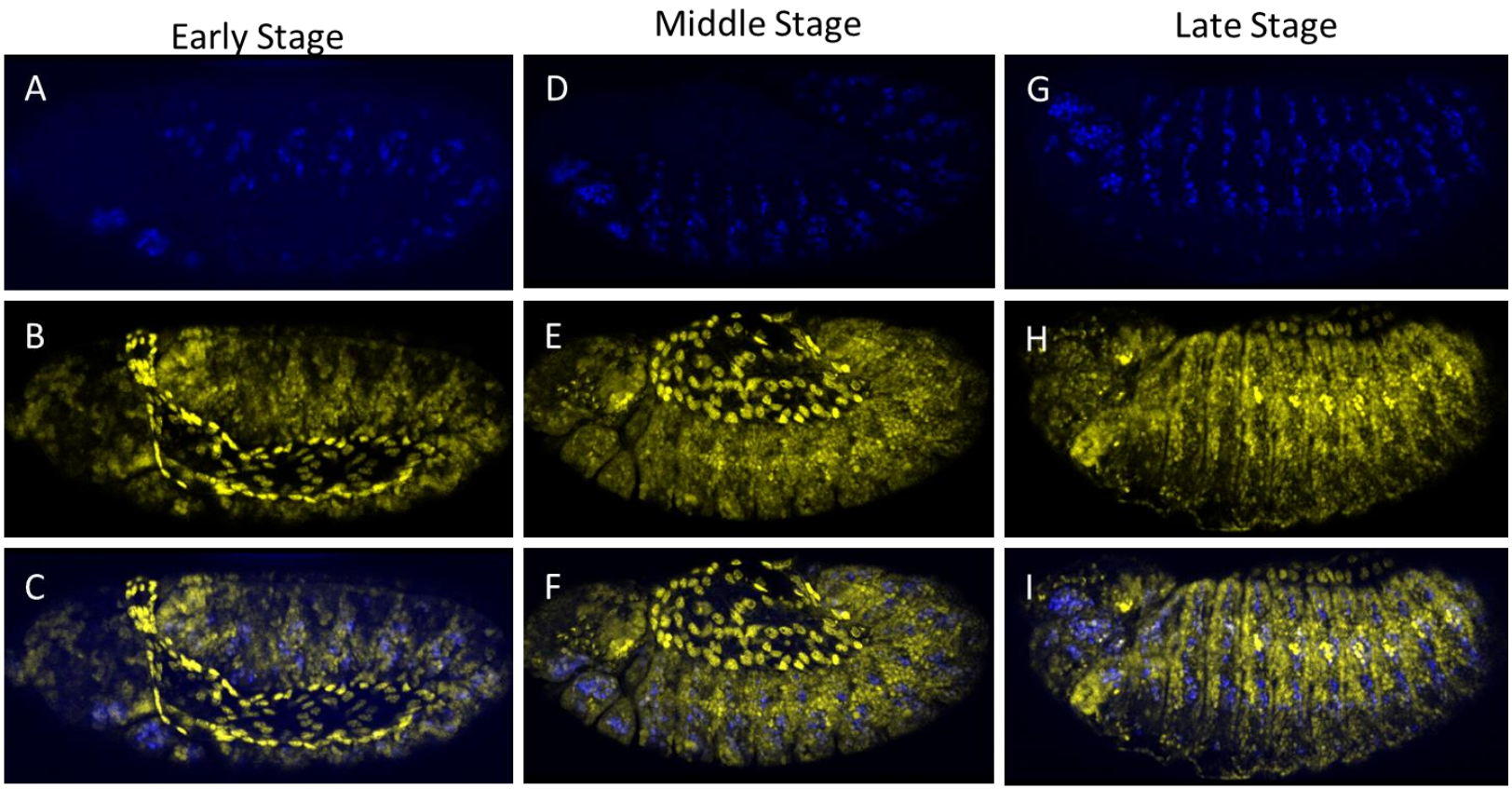


Figure 3.26

Double antibody staining with Anti-D-Pax2 and Anti-HNT of HNT over-expression embryos using the UAS-GFP-HNT^{J18} reporter line crossed with daGAL4 of embryos at the early stage (A-C), stage 10-11, the middle stage (D-F), stage 12, and the late stage (G-I), stage 13-14. The D-Pax2 expression, in blue, in the early stage (A), is compared to the middle (D) and late stages (G). The HNT expression, in yellow, at the early stage (B) is also compared to the middle (E) and late stages (H). The combined expression of the two antibodies during the early stage (C) is compared to the middle (F) and late (I) stages.

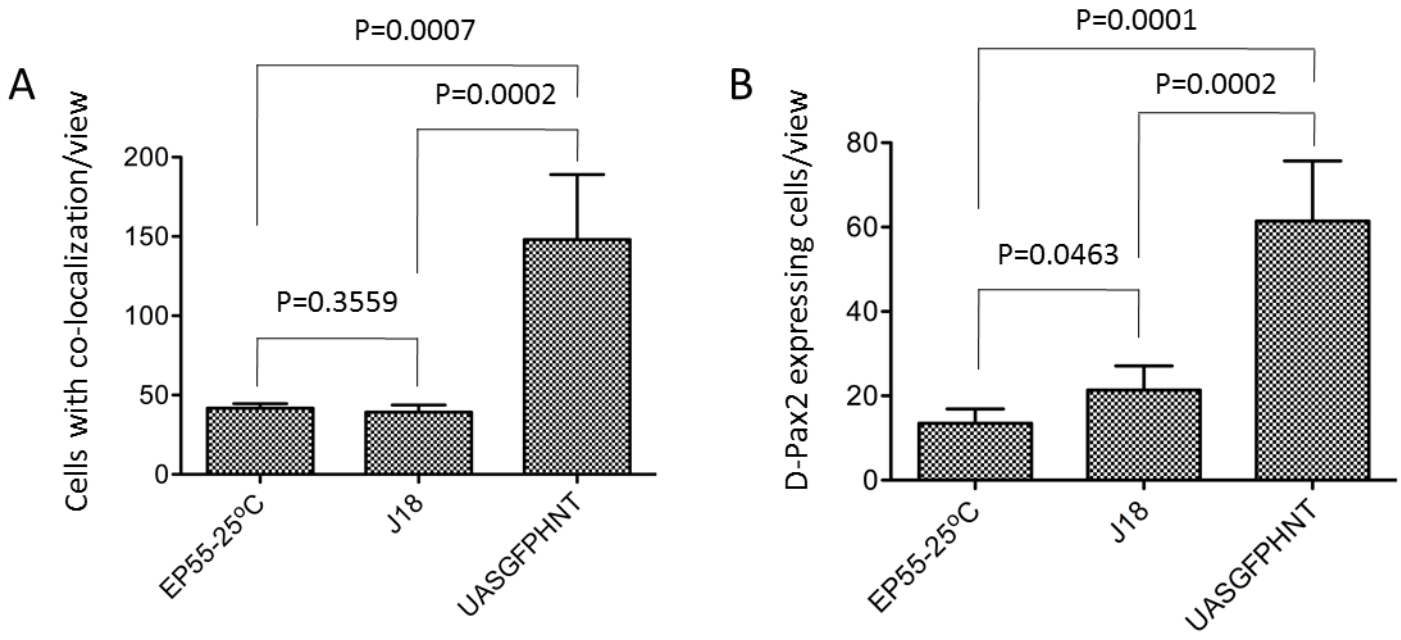


Figure 3.27 Regulation of HNT and/or D-Pax2 expression in the embryos in different HNT over-expression stocks

The sections of the embryos were antibody stained with both anti-HNT and anti-D-Pax2 antibodies. The number of HNT/P-Pax2 co-localizing or D-Pax2 expressing cells was counted in selected microscopic views (20X magnification), as described in the Materials and Methods, of the EP55 embryos at 25°C and UASGFPHNT^{J18} at the middle stage were compared to the cells of the UASGFPHNT at only one stage (EP55 at 25°C: n=4; UASGFPHNT^{J18}: n=5; and UASGFPHNT 25°C cross: n=7). The difference of the number of cells between these groups were statistically analyzed using Students t-test. **(A)** The number of cells expressing both HNT and D-Pax2. **(B)** The cells expressing only D-Pax2.

3.6 Summary: The role of *Hindsight* in Neuron development

Microarray analysis of HNT over-expression embryos has also suggested a role for HNT in neural development, and one of the ways HNT could be affecting neural development though the regulation of D-Pax2. Overall, there is a general trend for HNT and D-Pax2 expression in control embryos whereby they appear to co-localize in early and middle, but not in later staged embryos. The separation of cells expressing HNT and D-Pax2 at the later stages of embryogenesis appears not to involve Notch signaling, as suggested by the over expression of HNT and the lack of D-Pax2 expression in Notch null mutants; which demonstrates that Notch may be needed to inhibit HNT but activate D-Pax2 expression. Furthermore, the strong D-Pax2 expression seen in UAS-GFP-HNT embryos could be due to a threshold effect where a high level of HNT expression is needed to induce the dramatic D-Pax2 expression. A model for the normal function of HNT might be as a negative regulator of D-Pax2 expression, but when HNT is inappropriately over-expressed, HNT could function as an activator of D-Pax2 expression.

Chapter 4. Discussion

Microarray analysis has shown that the HNT RNAi depleted reporter line was unable to successfully deplete HNT expression, this could be due to the ineffectiveness of the technique on *Drosophila* embryos, or it could also be due to the degree of RNAi depletion of the reporter line suggesting that the UAS-HNT-RNAi2A; UAS-HNT-RNAi2B reporter line is not strong enough to fully deplete HNT expression. In addition, the microarray analysis of HNT over-expression embryos was able to transcriptionally affect many gene targets. Given the physical appearance of the HNT over-expression embryos, this could be an indication that development was greatly perturbed by over expression HNT, which could have disrupted some of the core signaling pathways, such as Notch signaling, thus causing the significant number of microarray targets affected by HNT over-expression.

4.1 Muscle Development during embryogenesis

4.1.1 Down-regulation of muscle identity genes by *Hindsight*

This study showed that HNT may not be required for the proper development of muscle fibres, evidenced by the lack of significant muscle defects, represented by F-actin, in the HNT null mutant; however, over expressing HNT may affect muscle development by acting on the muscle founder cells. This hypothesis is supported by the microarray data which showed that over expressing HNT can down-regulate the expression of a number of muscle identity genes, including *even skipped* (*eve*), *nautilus* (*nau*), *vestigial* (*vg*), *slouch* (*slou*), and *Pox meso* (*poxm*). Muscle identity genes are usually activated in muscle founder cells, which derive all individual

larval muscles (Tixier et al., 2010). One potential mechanism by which HNT over-expression could down-regulate muscle identity gene expression is through the Notch signalling pathway. HNT has been documented to be a target of Notch signaling, and in addition, other research has shown that HNT can also regulate Notch signaling, such as in cone cells of the pupal eye imaginal disc (Pickup et al., 2002; Sun & Deng, 2007).

Notch and Delta expression are strongly expressed in subsets of mesodermal cells during early muscle differentiation, and Notch signaling is required by mesoderm cells to establish the proper ratio of muscle founders by lateral inhibition (Corbin et al., 1991; Kooh, Fehon, & Muskavitch, 1993). Mutations in the Notch-Delta signalling pathway have been found to affect that ratio of muscle founder cells to fusion competent myoblasts. Notch and Delta loss of function mutants display muscle founder hypertrophy, where the number of founder cells is increased, and the fusion-competent myoblasts are reduced (Bate, 1990; Corbin et al., 1991; Stute, Schimmelpfeng, Renkawitz-Pohl, Palmer, & Holz, 2004). However, when an activated form of Notch is expressed in the mesoderm, muscle founder cell hypotrophy is observed. Activated Notch protein has been found to strongly inhibit myoblast fusion and can repress transcription of putative muscle founder determinants (Baker & Schubiger, 1996).

The hypotrophy of muscle founder cells can result in the down-regulation of the muscle identity genes; a phenotype that is similar to that of HNT over-expression in this study. Krejci et al. also reported that myoblast phenotypes associated with HNT over-expression are similar to those associated with excessive activated Notch (Krejci et al., 2009). This suggests that over-expressing HNT could be activating the Notch signaling in muscle founder cells, which could subsequently down-regulate muscle identity gene expression.

One potential mechanism by which HNT could activate Notch is by up-regulating Delta expression. In the cone cells of the *Drosophila* larval eye disc, induction by the R1/R6 photoreceptor precursors requires the integration of the Notch-Delta signalling pathway (Pickup, Ming, & Lipshitz, 2009). HNT is required in the R1/R6 precursor cells to elevate Delta ligand concentration to a high-enough level that is sufficient to activate the Notch receptor in the adjacent cell (Pickup et al., 2009). Thus, if HNT can up-regulate Delta in the photoreceptor precursor cells, over-expressing HNT could potentially elevate Delta past a threshold, resulting in an over-activation of Notch signaling in muscle founder cells. However, further research into how HNT and Notch-Delta could interact in the muscle precursors is required.

4.1.2 Down-regulating muscle identity genes by *Hindsight* through *Jelly Belly*

An alternative mechanism by which HNT down-regulates muscle identity genes is through *Jelly belly* (*Jeb*) signalling. *Jeb* encodes a protein that is produced from somatic mesodermal cells and taken up by the visceral muscle cells of the *Drosophila* midgut (Weiss, Suyama, Lee, & Scott, 2001). The microarray results in this study also showed that over-expressing HNT was able to up-regulate *Jeb* expression 2.619 fold, compared to the control.

During gastrulation, mesodermal cells are subdivided into two main types of musculature: the somatic and visceral muscles (Hosono, Takaira, Matsuda, & Saigo, 2003). *Drosophila* midgut visceral muscles arise by the fusion of founder cells and fusion-competent myoblasts, similar to the formation of the somatic muscles (San Martin, Ruiz-Gómez, Landgraf, & Bate, 2001). Mutations in *Jeb* cause a loss of visceral midgut muscles, resulting in a phenotype whereby the visceral mesoderm consists only of fusion-competent myoblasts and is devoid of muscle founder cells (Stute et al., 2004); suggesting that the process of founder cell

determination in the visceral mesoderm depends on *Jeb* signalling. Moreover, it has been demonstrated that somatic mesoderm determination of the fusion-competent myoblasts, also depends on *Jeb* (Stute et al., 2004). In that sense, *Jeb* signalling may be involved in crosstalk between the somatic and visceral mesoderm, which could be a mechanism by which over-expressing HNT is able to down-regulate muscle identity genes in the somatic muscle founder cells and affect muscle development. However, further investigation needs to examine how HNT and the *Jeb* signaling pathway are interacting before coming to more definite conclusions.

4.2 Neuron development during embryogenesis

The microarray result, confirmed by FISH and immunohistochemical staining, indicates that HNT over-expression can lead to an up-regulation of D-Pax2. In wild type development, HNT and D-Pax2 are initially co-localized in the embryonic SOPs. Throughout the subsequent development of the embryonic PNS, HNT and D-Pax2 are not substantially co-localized but show complementary expression patterns with HNT being expressed with in the neuronal lineage whereas D-Pax2 expression is associated with various accessory cells.

Given these observations it is compelling to suggest that HNT and D-Pax2 display complex regulatory interactions. For example, high levels of HNT expression are capable of dramatically up-regulating D-Pax2, but the pattern of expression in later stage embryos would suggest that the normal role of HNT does not involve D-Pax2 up-regulation, but rather down-regulation.

In addition, 22C10 staining of the HNT null mutant suggested that HNT may be required for some aspect of neural development, at least in regards to chordotonal (Ch) development. HNT's involvement in neural development is also supported by two independently conducted

genome wide screens, each of which reported strong HNT expression in SOPs of the larval wing imaginal disc and the pupal notum (Buffin & Gho, 2010; Reeves & Posakony, 2005).

HNT's involvement in neural development could also involve the Notch signaling pathway. Anti-HNT and Anti-D-Pax2 double antibody staining of the Notch mutant embryos demonstrated a large amount of HNT expression, and since the over-expression of HNT resembles the 22C10 stain pattern in the Notch null, as indicated by the neurogenic clusters, neuronal hypertrophy seen with the 22C10 stain can also be a reflection of an over-expression of HNT in neural cells. This could suggest that the Notch signaling pathway could be needed to inhibit HNT expression during neural development, or HNT could function as an antagonist of Notch signaling. However, Notch signaling is not needed for the interaction between HNT and D-Pax2.

Overexpression of HNT using the UAS-GFP-HNT reporter line was able to significantly increase the amount of cells expressing D-Pax2. However, how the UAS-GFP-HNT reporter line manages to increase the levels of D-Pax2 expression is still unknown, given that modulating HNT expression levels does not increase the D-Pax2 expression in EP55 embryos to the level of the UAS-GFP-HNT embryos, nor is the GFP HNT fusion protein involved in increasing the D-Pax2 expression levels.

In addition, the effects seen by the HNT over-expression embryo could just be the result of the massive amount of HNT over-expression. At the same time, the interaction between HNT and D-Pax2 may not be an artifact of the massive HNT over-expression, which could cause HNT to behave as an activator, where it would normally function as a repressor.

4.2.1 How *Hindsight* could be affecting neural development

Sensory organ development in the peripheral nervous system (PNS) and in microchaete bristles is initiated by restricting the expression of proneural genes to define a proneural cluster (PNC). The cluster consists of cells that have the potential to development into SOP cells, since they all express the basic-helix-loop-helix transcription factors encoded by the achaete-scute complex (Cabrera, Martinez-Arias, & Bate, 1987; Cubas, de Celis, Campuzano, & Modolell, 1991; Romani, Campuzano, & Modolell, 1987; Skeath & Carroll, 1991). SOP cells are then specified within each PNC by lateral inhibition mediated by Notch signalling (Cabrera, 1990; Hartenstein & Posakony, 1990; Simpson, 1990). Therefore, neural patterning depends on two opposing forces, the proneural bHLH genes driving neural determination, and Notch signalling opposing them in certain cells.

The division of SOP into external sense (es) organ cell types is mediated by the genes Notch-Delta, Numb, and Hairless (Schweisguth & Posakony, 1994). Notch and Delta are required in the es organs for the directional inhibitory effect of Notch signaling, in a process known as lineage decisions, between es organ cell types, while Numb and Hairless provide resistance to, or antagonize, the inhibition. This interaction is so important that the complete loss of Notch or Delta causes all the progeny cells to adopt the neuron fate (Hartenstein & Posakony, 1990; Parks & Muskavitch, 1993), while the loss of Numb or Hairless results in all four cells developing into socket cells (Bang, Hartenstein, & Posakony, 1991; Rhyu, Jan, & Jan, 1994).

D-Pax2 is a key player in the differentiation of es organ cell types, in the bristles (Fu, Duan, Frei, & Noll, 1998). During es organ development, D-Pax2 protein is present in the SOP a few hours after it is selected from the PNC. Shortly after it is detectable, the SOP divides and D-Pax2 is present in all of the cells of the es organ lineage throughout the divisions (Kavaler, Fu,

Duan, Noll, & Posakony, 1999). The early expression of D-Pax2 in the SOP lineage is initiated by the activity of proneural proteins, such as *Achaete* and *Scute*, which are also required for the specification of SOP es organs, in peripheral nervous system and bristle development (Villares & Cabrera, 1987).

Immunostaining of Notch mutant embryos demonstrates abundant HNT expression, and in the absence of Notch signaling HNT expression is not prevented in neurogenic tissues. This suggests that HNT may be expressed in the PNC, of the embryonic PNS, before being confined by Notch into individual SOP cells. Furthermore, in the absence of HNT expression there appears to be a defect in PNS development, suggesting that HNT may be required in the SOP for the differentiation of es and/or Ch organs. Especially since the differentiation of es organs requires inhibitory effects of Notch, which suggests that Notch may be needed to repress HNT expression in one of the es organs, for the differentiation of either the SOP to pIIa and pIIb, or even the differentiation of pIIa and pIIb to their respective cells. Overexpressing HNT may then prevent the directional inhibitory effects of Notch, in lineage decisions, which can prevent the differentiation of SOP into some of the es organ cells. However, identification of the type of es cells produced in the presence of HNT over-expression is needed before it can be concluded what the role HNT plays in neural development.

4.2.2 How *Hindsight* may be effecting D-Pax2 expression

Overexpressing HNT was shown to largely increase the number of cells expressing both D-Pax2 and HNT, along with cells just expressing D-Pax2. This suggests that HNT is present in proneural cells, but when HNT expression is initiated in the proneural cells is unknown; therefore, over-expressing HNT could potentially increase the expression of proneural genes,

such as *scute* (*sc*). Interestingly, increased *sc* expression was also seen in the microarray analysis of HNT over-expression embryos and confirmed by FISH. *sc* is a member of the achaete-scute complex (Cabrera et al., 1987; Cubas et al., 1991; Romani et al., 1987; Skeath & Carroll, 1991), and up-regulating *sc* could increase the number of proneural cells driving neural determination, which could reduce SOP specification as mediated by Notch signaling pathway through lateral inhibition (Simpson, 1997). Decreasing lateral inhibition could lead more cells being defined as SOP's, instead of being inhibited by Notch and becoming epithelial cells. Furthermore, increasing the number of SOP cells could also increase the amount of D-Pax2 expressing cells, which is regulated by proneural proteins in the SOP. This notion is possibly since ectopic expression of *sc* has been found to lead to the early activation of D-Pax2 expression (Kavaler et al., 1999). Therefore, over expressing HNT could be affecting proneural gene expression, which could then affect D-Pax2 expression, and thus increase the amount of co-localization of D-Pax2 and HNT.

An alternative mechanism by which the over-expression of HNT could affect neural development and D-Pax2 expression is through *Bearded* (*Brd*). *Brd* is involved in sensory organ development and was found to be up-regulated by the HNT over-expression in the microarray analysis. Brd antagonizes Notch signaling pathway in cell fate decisions during adult sensory organ development (E. C. Lai et al., 2000). Therefore, if HNT over-expression up-regulates *Brd*, *Brd* could then down-regulate the Notch signalling pathway, which could either increase unspecified SOP cells and/or force the es organs to differentiate into sensory neurons (Hartenstein & Posakony, 1990; Parks & Muskavitch, 1993). A down-regulation of Notch signaling could account for the large number of cells co-expressing HNT and/or D-Pax2, since D-Pax2 is expressed in all es organs, and HNT is expressed in SOP cells (Buffin & Gho, 2010;

Reeves & Posakony, 2005). Down-regulating Notch could also explain the observation of cells just expressing D-Pax, since D-Pax2 expression in those cells could be a product of other asymmetric divisions not dependent on Notch, such as Numb and Hairless, which could also allow some differentiation of es organs (Schweisguth & Posakony, 1994). However, an examination of the type of neural cells in the HNT over-expression mutant needs to be analyzed before determining the precise relationship between HNT and D-Pax2.

4.3 Conclusion

In conclusion, over-expressing HNT could be affecting embryonic muscle development by over activating the Notch signaling in muscle founder cells, which could down-regulate the expression of muscle identity genes. Alternatively, HNT could be down-regulating *Jeb* signalling, which is involved in founder cell determination in the visceral mesoderm, and given the potential crosstalk between the somatic and visceral mesoderm, HNT could also be down-regulating somatic muscle identity genes through *Jeb* signaling.

In addition, HNT may also be involved in the development of neurons, since Notch signaling may be required to inhibit HNT expression in SOP cells, which could suggest a role for HNT in the differentiation of SOPs. Furthermore, overexpressing HNT can up-regulate proneural gene expression, which could increase D-Pax2 expression by increasing the amount of neuron cells, and/or alternatively, overexpressing HNT could also up-regulate *Brd*, which antagonizes the Notch signalling pathway, and that could prevent SOP cells from differentiating into es organs and remain as SOP cells, and increase the expression of D-Pax2.

Ultimately, however, how representative over-expressing HNT is of normal HNT expression in embryonic muscle and neural development would need to be determined.

Chapter 5. Future directions

5.1 Further directions with Microarray Data

With such a large amount of data collected from the microarray analysis, another logical step would be to investigate what effects HNT may have on other developmental systems. For example, in the presence of HNT over-expression, a number of genes related to morphogenesis were under-expressed, while a number of genes related to sensory and olfactory development were over-expressed. The role of HNT in morphogenesis is expected since it is known to down-regulate the JNK pathway in the amnioserosa, which is required for the successful completion of GBR and DC (Reed et al., 2001; Yip et al., 1997). However, the functions of HNT for sensory and olfactory development have not yet been investigated, and could be an avenue of investigation for the future studies.

5.2 Muscle development

The presence of HNT in muscle progenitor cells suggests a role for HNT in muscle differentiation. However, due to the broad screen conducted with the microarray analysis, it is difficult to pinpoint out exactly how over-expressing HNT can affect muscle development through the muscle progenitor cells. One way to determine how over-expressing HNT can affect muscle development is by staging the embryos and antibody staining for different muscle progenitors and differentiated muscles. Staging the embryos on a per hour or even half an hour basis, and then antibody staining them for different identity genes and differentiated muscles can determine the how over-expressing HNT may be affecting muscle founder cells at different embryonic stages.

Furthermore, investigation into potential interaction of HNT with the *jelly belly* signalling pathway can reveal if any form of crosstalk between the developing visceral muscles can affect the development of the somatic muscles.

5.3 Neuron development

The expression of HNT in SOP suggests a role for HNT in neural development; however, the UAS-GFP-HNT over-expression reporter line produces a very severe developmental mutation that prevents the precise dissection of HNT activities. The EP55 over-expression reporter line was able to induce a less severe phenotype, than the UAS-GFP-HNT line, and had significantly more HNT and D-Pax2 co-localizing and D-Pax2 expressing cells, than the control. The EP55 line could then be used to identify the potential role HNT in the differentiation of SOP into es organs, since the EP55 embryos wouldn't be arrested in development, and staining for the types of es organs could provide information on SOP differentiation, if any. Furthermore, es organ staining in the HNT null or knockout mutants may also help determine what could be differentiated from a lack of HNT expression.

To determine the differences between the UAS-GFP-HNT and EP55 reporter lines, which have a significant difference in D-Pax2 expression; these two reporter lines can be genetically sequenced and compared. Sequencing the UAS-GFP-HNT line can also provide information on what part of the fourteen zinc fingered gene is disrupted by the construct, and if the construct is disrupting any potential binding or enhancer sites that can affect D-Pax2 expression. In addition, to confirm whether or not D-Pax2 is a direct or indirect target of HNT, any potential HNT binding sites on the D-Pax2 gene could be investigated. In line with that investigation, potential

HNT binding sites could also be determined for proneural genes, such as *scute* and *Bearded*, to see if HNT is directly affecting their expression, which can then affect D-Pax2 expression.

As mentioned in the discussion, there is the possibility that over expressing HNT may cause it to behave as an activator, instead of a repressor. One way to test this would be to turn HNT from a repressor into an activator by creating a VP16-HNT fusion protein. This technique allows detection of dominant defects associated with the miss-expression of genes that are normally negatively regulated by a given transcription factor (Wildonger & Mann, 2005).

References

Artavanis-Tsakonas, S., Delidakis, C., Fehon, R., Hartley, D., Herndon, V., Johansen, K., . . . et al. (1990). Notch and the molecular genetics of neuroblast segregation in Drosophila. *Mol Reprod Dev, 27*(1), 23-27. doi: 10.1002/mrd.1080270107

Artavanis-Tsakonas, S., Rand, M. D., & Lake, R. J. (1999). Notch signaling: cell fate control and signal integration in development. *Science, 284*(5415), 770-776.

Awasaki, T., & Kimura, K. (2001). Multiple function of poxn gene in larval PNS development and in adult appendage formation of Drosophila. *Dev Genes Evol, 211*(1), 20-29.

Baker, R., & Schubiger, G. (1996). Autonomous and nonautonomous Notch functions for embryonic muscle and epidermis development in Drosophila. *Development, 122*(2), 617-626.

Bang, A. G., Hartenstein, V., & Posakony, J. W. (1991). Hairless is required for the development of adult sensory organ precursor cells in Drosophila. *Development, 111*(1), 89-104.

Bate, M. (1990). The embryonic development of larval muscles in Drosophila. *Development, 110*(3), 791-804.

Bate, M., Rushton, E., & Frasch, M. (1993). A dual requirement for neurogenic genes in Drosophila myogenesis. *Dev Suppl*, 149-161.

Benito-Sipos, J., Ulvklo, C., Gabilondo, H., Baumgardt, M., Angel, A., Torroja, L., & Thor, S. (2011). Seven up acts as a temporal factor during two different stages of neuroblast 5-6 development. *Development, 138*(24), 5311-5320. doi: 10.1242/dev.070946

Borkowski, O. M., Brown, N. H., & Bate, M. (1995). Anterior-posterior subdivision and the diversification of the mesoderm in Drosophila. *Development, 121*(12), 4183-4193.

Bray, S. (1998). Notch signalling in Drosophila: three ways to use a pathway. *Semin Cell Dev Biol, 9*(6), 591-597. doi: 10.1006/scdb.1998.0262

Bray, S. J. (2006). Notch signalling: a simple pathway becomes complex. *Nat Rev Mol Cell Biol, 7*(9), 678-689. doi: 10.1038/nrm2009

Brewster, R., & Bodmer, R. (1995). Origin and specification of type II sensory neurons in Drosophila. *Development, 121*(9), 2923-2936.

Buffin, E., & Gho, M. (2010). Laser microdissection of sensory organ precursor cells of Drosophila microchaetes. *PLoS One, 5*(2), e9285. doi: 10.1371/journal.pone.0009285

Cabrera, C. V. (1990). Lateral inhibition and cell fate during neurogenesis in Drosophila: the interactions between scute, Notch and Delta. *Development, 110*(1), 733-742.

Cabrera, C. V., Martinez-Arias, A., & Bate, M. (1987). The expression of three members of the achaete-scute gene complex correlates with neuroblast segregation in Drosophila. *Cell, 50*(3), 425-433.

Campos-Ortega, J.A., & Hartenstein, V. (1997). *The embryonic development of Drosophila melanogaster*: Springer.

Campuzano, S., & Modolell, J. (1992). Patterning of the Drosophila nervous system: the achaete-scute gene complex. *Trends Genet, 8*(6), 202-208.

Carmena, A., Bate, M., & Jimenez, F. (1995). Lethal of scute, a proneural gene, participates in the specification of muscle progenitors during Drosophila embryogenesis. *Genes Dev, 9*(19), 2373-2383.

Carmena, A., & Baylies, M. (2006). Development of the larval somatic musculature. *Muscle Development in Drosophila*, 79-91.

Cau, E., & Blader, P. (2009). Notch activity in the nervous system: to switch or not switch? *Neural Dev, 4*, 36. doi: 10.1186/1749-8104-4-36

Charlton-Perkins, M., Whitaker, S. L., Fei, Y., Xie, B., Li-Kroeger, D., Gebelein, B., & Cook, T. (2011). Prospero and Pax2 combinatorially control neural cell fate decisions by modulating Ras- and Notch-dependent signaling. *Neural Dev, 6*, 20. doi: 10.1186/1749-8104-6-20

Corbin, V., Michelson, A. M., Abmayr, S. M., Neel, V., Alcamo, E., Maniatis, T., & Young, M. W. (1991). A role for the Drosophila neurogenic genes in mesoderm differentiation. *Cell, 67*(2), 311-323.

Cox, V. T., & Baylies, M. K. (2005). Specification of individual Slouch muscle progenitors in Drosophila requires sequential Wingless signaling. *Development, 132*(4), 713-724. doi: 10.1242/dev.01610

Cubas, P., de Celis, J. F., Campuzano, S., & Modolell, J. (1991). Proneural clusters of achaete-scute expression and the generation of sensory organs in the Drosophila imaginal wing disc. *Genes Dev, 5*(6), 996-1008.

Deng, H., Bell, J. B., & Simmonds, A. J. (2010). Vestigial is required during late-stage muscle differentiation in Drosophila melanogaster embryos. *Mol Biol Cell, 21*(19), 3304-3316. doi: 10.1091/mbc.E10-04-0364

Dobi, K. C., Metzger, T., & Baylies, M. K. (2011). Characterization of early steps in muscle morphogenesis in a Drosophila primary culture system. *Fly (Austin), 5*(2), 68-75.

Dohrmann, C., Azpiazu, N., & Frasch, M. (1990). A new Drosophila homeo box gene is expressed in mesodermal precursor cells of distinct muscles during embryogenesis. *Genes Dev, 4*(12A), 2098-2111.

Duan, H., Zhang, C., Chen, J., Sink, H., Frei, E., & Noll, M. (2007). A key role of Pox meso in somatic myogenesis of Drosophila. *Development, 134*(22), 3985-3997. doi: 10.1242/dev.008821

Duffy, J. B. (2002). GAL4 system in Drosophila: a fly geneticist's Swiss army knife. *Genesis, 34*(1-2), 1-15. doi: 10.1002/gene.10150

Frank, L. H., & Rushlow, C. (1996). A group of genes required for maintenance of the amnioserosa tissue in Drosophila. *Development, 122*(5), 1343-1352.

Fu, W., Duan, H., Frei, E., & Noll, M. (1998). shaven and sparkling are mutations in separate enhancers of the Drosophila Pax2 homolog. *Development, 125*(15), 2943-2950.

Hartenstein, V. (1993). *Atlas of Drosophila development*: Cold Spring Harbor Laboratory Press.

Hartenstein, V., & Posakony, J. W. (1990). A dual function of the Notch gene in Drosophila sensillum development. *Dev Biol, 142*(1), 13-30.

Hosono, C., Takaira, K., Matsuda, R., & Saigo, K. (2003). Functional subdivision of trunk visceral mesoderm parasegments in Drosophila is required for gut and trachea development. *Development, 130*(3), 439-449.

Hummel, T., Krukkert, K., Roos, J., Davis, G., & Klambt, C. (2000). Drosophila Futsch/22C10 is a MAP1B-like protein required for dendritic and axonal development. *Neuron, 26*(2), 357-370.

Irvine, K. D., & Wieschaus, E. (1994). fringe, a Boundary-specific signaling molecule, mediates interactions between dorsal and ventral cells during Drosophila wing development. *Cell, 79*(4), 595-606.

Jarman, A. P., Grau, Y., Jan, L. Y., & Jan, Y. N. (1993). atonal is a proneural gene that directs chordotonal organ formation in the Drosophila peripheral nervous system. *Cell, 73*(7), 1307-1321.

Kavaler, J., Fu, W., Duan, H., Noll, M., & Posakony, J. W. (1999). An essential role for the Drosophila Pax2 homolog in the differentiation of adult sensory organs. *Development, 126*(10), 2261-2272.

Kooh, P. J., Fehon, R. G., & Muskavitch, M. A. (1993). Implications of dynamic patterns of Delta and Notch expression for cellular interactions during Drosophila development. *Development, 117*(2), 493-507.

Kramer, J. M., & Staveley, B. E. (2003). GAL4 causes developmental defects and apoptosis when expressed in the developing eye of Drosophila melanogaster. *Genet Mol Res, 2*(1), 43-47.

Krejci, A., Bernard, F., Housden, B. E., Collins, S., & Bray, S. J. (2009). Direct response to Notch activation: signaling crosstalk and incoherent logic. *Sci Signal, 2*(55), ra1. doi: 10.1126/scisignal.2000140

Lai, E. C., Bodner, R., Kavaler, J., Freschi, G., & Posakony, J. W. (2000). Antagonism of notch signaling activity by members of a novel protein family encoded by the bearded and enhancer of split gene complexes. *Development, 127*(2), 291-306.

Lai, Eric C. (2004). Notch signaling: control of cell communication and cell fate. *Development, 131*(5), 965-973.

Lamka, M. L., & Lipshitz, H. D. (1999). Role of the amnioserosa in germ band retraction of the Drosophila melanogaster embryo. *Dev Biol, 214*(1), 102-112. doi: 10.1006/dbio.1999.9409

Lecuyer, E., Parthasarathy, N., & Krause, H. M. (2008). Fluorescent in situ hybridization protocols in Drosophila embryos and tissues. *Methods Mol Biol, 420*, 289-302. doi: 10.1007/978-1-59745-583-1_18

Li, Y., Fetchko, M., Lai, Z. C., & Baker, N. E. (2003). Scabrous and Gp150 are endosomal proteins that regulate Notch activity. *Development, 130*(13), 2819-2827.

Liu, J., Qian, L., Han, Z., Wu, X., & Bodmer, R. (2008). Spatial specificity of mesodermal even-skipped expression relies on multiple repressor sites. *Dev Biol, 313*(2), 876-886. doi: 10.1016/j.ydbio.2007.10.026

Melani, M., Simpson, K. J., Brugge, J. S., & Montell, D. (2008). Regulation of cell adhesion and collective cell migration by hindsight and its human homolog RREB1. *Curr Biol, 18*(7), 532-537. doi: 10.1016/j.cub.2008.03.024

Milon, B. C., Agyapong, A., Bautista, R., Costello, L. C., & Franklin, R. B. (2010). Ras responsive element binding protein-1 (RREB-1) down-regulates hZIP1 expression in prostate cancer cells. *Prostate, 70*(3), 288-296. doi: 10.1002/pros.21063

Narasimha, M., & Brown, NH. (2006). Confocal microscopy of Drosophila embryos. *Cell Biology: A Laboratory Handbook, 3*, 77-86.

Neumann, C. J., & Cohen, S. M. (1997). Long-range action of Wingless organizes the dorsal-ventral axis of the Drosophila wing. *Development, 124*(4), 871-880.

Nfonsam, L. E., Cano, C., Mudge, J., Schilkey, F. D., & Curtiss, J. (2012). Analysis of the transcriptomes downstream of Eyeless and the Hedgehog, Decapentaplegic and Notch signaling pathways in Drosophila melanogaster. *PLoS One, 7*(8), e44583. doi: 10.1371/journal.pone.0044583

Okabe, M., & Okano, H. (1997). Two-step induction of chordotonal organ precursors in Drosophila embryogenesis. *Development, 124*(5), 1045-1053.

Overend, G., Cabrero, P., Guo, A. X., Sebastian, S., Cundall, M., Armstrong, H., . . . Davies, S. A. (2012). The receptor guanylate cyclase Gyc76C and a peptide ligand, NPLP1-VQQ, modulate the innate immune IMD pathway in response to salt stress. *Peptides, 34*(1), 209-218. doi: 10.1016/j.peptides.2011.08.019

Parks, A. L., & Muskavitch, M. A. (1993). Delta function is required for bristle organ determination and morphogenesis in Drosophila. *Dev Biol, 157*(2), 484-496. doi: 10.1006/dbio.1993.1151

Pascucci, T., Perrino, J., Mahowald, A. P., & Waring, G. L. (1996). Eggshell assembly in Drosophila: processing and localization of vitelline membrane and chorion proteins. *Dev Biol, 177*(2), 590-598. doi: 10.1006/dbio.1996.0188

Patel, N.H. (1994). Antibody Probes. *Drosophila melanogaster: Practical uses in cell and molecular biology, 44*, 445.

Pi, H., & Chien, C. T. (2007). Getting the edge: neural precursor selection. *J Biomed Sci, 14*(4), 467-473. doi: 10.1007/s11373-007-9156-4

Pickup, A. T., Lamka, M. L., Sun, Q., Yip, M. L., & Lipshitz, H. D. (2002). Control of photoreceptor cell morphology, planar polarity and epithelial integrity during Drosophila eye development. *Development, 129*(9), 2247-2258.

Pickup, A. T., Ming, L., & Lipshitz, H. D. (2009). Hindsight modulates Delta expression during Drosophila cone cell induction. *Development, 136*(6), 975-982. doi: 10.1242/dev.027318

Reed, B. H., McMillan, S. C., & Chaudhary, R. (2009). The preparation of Drosophila embryos for live-imaging using the hanging drop protocol. *J Vis Exp*(25). doi: 10.3791/1206

Reed, B. H., Wilk, R., & Lipshitz, H. D. (2001). Downregulation of Jun kinase signaling in the amnioserosa is essential for dorsal closure of the Drosophila embryo. *Curr Biol, 11*(14), 1098-1108.

Reed, B. H., Wilk, R., Schock, F., & Lipshitz, H. D. (2004). Integrin-dependent apposition of Drosophila extraembryonic membranes promotes morphogenesis and prevents anoikis. *Curr Biol, 14*(5), 372-380. doi: 10.1016/j.cub.2004.02.029

Reeves, N., & Posakony, J. W. (2005). Genetic programs activated by proneural proteins in the developing Drosophila PNS. *Dev Cell, 8*(3), 413-425. doi: 10.1016/j.devcel.2005.01.020

Rhyu, M. S., Jan, L. Y., & Jan, Y. N. (1994). Asymmetric distribution of numb protein during division of the sensory organ precursor cell confers distinct fates to daughter cells. *Cell, 76*(3), 477-491.

Romani, S., Campuzano, S., & Modolell, J. (1987). The achaete-scute complex is expressed in neurogenic regions of Drosophila embryos. *EMBO J, 6*(7), 2085-2092.

San Martin, B., Ruiz-Gómez, M., Landgraf, M., & Bate, M. (2001). A distinct set of founders and fusion-competent myoblasts make visceral muscles in the Drosophila embryo. *Development, 128*(17), 3331-3338.

Sandmann, T., Jensen, L. J., Jakobsen, J. S., Karzynski, M. M., Eichenlaub, M. P., Bork, P., & Furlong, E. E. (2006). A temporal map of transcription factor activity: mef2 directly regulates target genes at all stages of muscle development. *Dev Cell, 10*(6), 797-807. doi: 10.1016/j.devcel.2006.04.009

Schock, F., & Perrimon, N. (2002). Cellular processes associated with germ band retraction in Drosophila. *Dev Biol, 248*(1), 29-39.

Schweisguth, F., & Posakony, J.W. (1994). Antagonistic activities of Suppressor of Hairless and Hairless control alternative cell fates in the Drosophila adult epidermis. *Development, 120*(6), 1433-1441.

Scuderi, A., & Letsou, A. (2005). Amnioserosa is required for dorsal closure in Drosophila. *Dev Dyn, 232*(3), 791-800. doi: 10.1002/dvdy.20306

Simpson, P. (1990). Notch and the choice of cell fate in Drosophila neuroepithelium. *Trends Genet, 6*(11), 343-345.

Simpson, P. (1997). Notch signalling in development: on equivalence groups and asymmetric developmental potential. *Curr Opin Genet Dev, 7*(4), 537-542.

Skeath, J. B., & Carroll, S. B. (1991). Regulation of achaete-scute gene expression and sensory organ pattern formation in the Drosophila wing. *Genes Dev, 5*(6), 984-995.

Stagg, S. B., Guardiola, A. R., & Crews, S. T. (2011). Dual role for Drosophila lethal of scute in CNS midline precursor formation and dopaminergic neuron and motoneuron cell fate. *Development, 138*(11), 2171-2183. doi: 10.1242/dev.056507

Stronach, B. E., & Perrimon, N. (2001). Investigation of leading edge formation at the interface of amnioserosa and dorsal ectoderm in the Drosophila embryo. *Development, 128*(15), 2905-2913.

Stute, C., Schimmelpfeng, K., Renkawitz-Pohl, R., Palmer, R. H., & Holz, A. (2004). Myoblast determination in the somatic and visceral mesoderm depends on Notch signalling as well as on milliways(mili(Alk)) as receptor for Jeb signalling. *Development, 131*(4), 743-754. doi: 10.1242/dev.00972

Sun, J., & Deng, W. M. (2007). Hindsight mediates the role of notch in suppressing hedgehog signaling and cell proliferation. *Dev Cell, 12*(3), 431-442. doi: 10.1016/j.devcel.2007.02.003

Suster, M. L., Seugnet, L., Bate, M., & Sokolowski, M. B. (2004). Refining GAL4-driven transgene expression in Drosophila with a GAL80 enhancer-trap. *Genesis, 39*(4), 240-245. doi: 10.1002/gene.20051

Tixier, V., Bataille, L., & Jagla, K. (2010). Diversification of muscle types: recent insights from Drosophila. *Exp Cell Res, 316*(18), 3019-3027. doi: 10.1016/j.yexcr.2010.07.013

VanHook, A., & Letsou, A. (2008). Head involution in Drosophila: genetic and morphogenetic connections to dorsal closure. *Dev Dyn, 237*(1), 28-38. doi: 10.1002/dvdy.21405

Villares, R., & Cabrera, C. V. (1987). The achaete-scute gene complex of D. melanogaster: conserved domains in a subset of genes required for neurogenesis and their homology to myc. *Cell, 50*(3), 415-424.

Warn, R. M., & Magrath, R. (1983). F-actin distribution during the cellularization of the Drosophila embryo visualized with FL-phalloidin. *Exp Cell Res, 143*(1), 103-114.

Wei, Q., Rong, Y., & Paterson, B. M. (2007). Stereotypic founder cell patterning and embryonic muscle formation in Drosophila require nautilus (MyoD) gene function. *Proc Natl Acad Sci U S A, 104*(13), 5461-5466. doi: 10.1073/pnas.0608739104

Weiss, J. B., Suyama, K. L., Lee, H. H., & Scott, M. P. (2001). Jelly belly: a Drosophila LDL receptor repeat-containing signal required for mesoderm migration and differentiation. *Cell, 107*(3), 387-398.

Wildonger, J., & Mann, R. S. (2005). Evidence that nervy, the Drosophila homolog of ETO/MTG8, promotes mechanosensory organ development by enhancing Notch signaling. *Dev Biol, 286*(2), 507-520. doi: 10.1016/j.ydbio.2005.08.026

Wilk, R., Reed, B. H., Tepass, U., & Lipshitz, H. D. (2000). The hindsight gene is required for epithelial maintenance and differentiation of the tracheal system in Drosophila. *Dev Biol, 219*(2), 183-196. doi: 10.1006/dbio.2000.9619

Yip, M. L., Lamka, M. L., & Lipshitz, H. D. (1997). Control of germ-band retraction in Drosophila by the zinc-finger protein HINDSIGHT. *Development, 124*(11), 2129-2141.

Zeidler, M. P., Tan, C., Bellaiche, Y., Cherry, S., Hader, S., Gayko, U., & Perrimon, N. (2004). Temperature-sensitive control of protein activity by conditionally splicing inteins. *Nat Biotechnol, 22*(7), 871-876. doi: 10.1038/nbt979

Appendix A. Genetic Lines

Stock Lines	Source
Driver	
w[*] P{w[+mW.hs]=GawB}NP3312 +Apoliner / FM7c	NP3312 from *Drosophila* Genetic Resource Center, Kyoto Institute of Technology; Recombinant made in BH Reed Lab
NP3312; [Dp(1,2)4FRDup](UAS-mCherry-GFP-DrAtg8a)	Dp from Dr. Helen Salz, Case Western Reserve University, Ohio; DrAtg8a from Dr. Harald Stenmark, Norwegian Radium Hospital, Oslo; Recombinant made in BH Reed Lab
w; (YET1); daGAL4	YET1 from Dr. Alan M. Michelson, Harvard Medical School; Recombinant made in BH Reed Lab
KrGAL4+UASGFPClc5/TM3	Recombinant made in BH Reed Lab
NP3312; Dp/+	Recombinant made in BH Reed Lab
w;Cherry;daGAL4+Spider/TM3,Ser	Spider from Dr. Antonio Jacinto, Instituto de Medicina Molecular, Portugal; Recombinant made in BH Reed Lab
DmefGAL4>UASmoesinCherry/TM3	Dr. Roger Jacobs, McMaster University
Delta-GAL4/TM6	*Bloomington Drosophila* Stock Center, Indiana University
RP298-GAL4	Dr. Aaron Johnson, University of Colorado
P{da-GAL4.w^{-}}3	*Bloomington Drosophila* Stock Center, Indiana University
Reporter Lines, Controls, and Loss of Function Alleles	
yw^{67}	*Bloomington Drosophila* Stock Center, Indiana University
UASGFPHNT	Dr. Howard Lipshitz, University of Toronto
UASGFPHNT;GAL80^{ts}	Dr. Howard Lipshitz, University of Toronto
UASHNTRNAi2A; UASHNTRNAi2B	Dr. Howard Lipshitz, University of Toronto
UAS Dicer; UAS HNTRNAi[2B]	Dr. Howard Lipshitz, University of Toronto
EP55	*Drosophila* Genetic Resource Center, Kyoto Institute of Technology
EP55; dpplacZ^{10638}/CYO	Recombinant made in BH Reed Lab
Notch^{55e11} P{neoFRT}19A/FM7c	*Bloomington Drosophila* Stock Center, Indiana University
hnt^{XE81}	Dr. Howard Lipshitz, University of Toronto
w^{1118}; P{UAS-GFP.nls}14	*Bloomington Drosophila* Stock Center, Indiana University

Appendix B. Microarray Analysis of Hindsight Over-expression embryos compared with the Control

Transcript FBtr ID	Gene ID	Official Symbol	Official Name	Control - linear value	Over expression - linear value	P value before FDR	P value after FDR
FBtr0070003	CG32825-RA	Or19b	Odorant receptor 19b	2561.851	7166.968	9.12x10^-7	0.000363
FBtr0070031	CG15323			82.756	340.03	7.39E-05	0.00373
FBtr0070032	CG9571-RA	fd19B	forkhead domain 19B	283.48	1073.041	0.000255	0.00707
FBtr0070036	CG12655-RA			521.428	1432.637	0.000519	0.0102
FBtr0070071	CG3757-RA	y	yellow	507.008	2360.99	0.000345	0.00812
FBtr0070073	CG3827-RA	sc	scute	409.018	1658.865	3.23E-05	0.00243
FBtr0070080	CG17778-RA			367.186	1617.892	0.00013	0.00514
FBtr0070100	CG13374-RA	pcl	pepsinogen-like	730.305	3062.925	1.61E-05	0.00178
FBtr0070101	CG32816-RB			2861.966	7164.915	0.00434	0.0334
FBtr0070139	CG12311-RA	tw	Protein O-mannosyltransferase 2	14534.024	6933.533	0.000774	0.0126
FBtr0070200	CG14626-RA			1390.227	625.27	0.0075	0.0471
FBtr0070238	CG11409-RB			3442.178	1256.41	0.0011	0.0148
FBtr0070271	CG14797			1056.052	475.746	0.000468	0.00959
FBtr0070328	CG4194-RA			7907.114	3882.99	0.00614	0.0411
FBtr0070385	CG3630-RA			1510.656	708.163	0.000264	0.00715
FBtr0070450	CG8310-RA	Vha36-3	Vacuolar H^+ ATPase subunit 36-3	1485.848	644.635	0.0022	0.0222
FBtr0070462	CG12496-RA			783.76	1583.7	0.000275	0.00722
FBtr0070490	CG2759-RA	w	white	1313.361	4304.997	0.000142	0.00537
FBtr0070531	CG16782-RA	Pig1	Pre-intermoult gene 1	743.947	247.179	0.000441	0.00921
FBtr0070547	CG3588			5755.557	2306.739	3.07E-05	0.00241
FBtr0070549	CG3588			707.375	207.16	0.00132	0.0164
FBtr0070558	CG3603-RA			1152.963	2663.342	0.000245	0.00694
FBtr0070575	CG2872-RB	AlstR	Allatostatin Receptor	92.596	358.611	0.000448	0.00929
FBtr0070631	CG2913-RA	yin		3293.004	1449.079	0.000816	0.0129
FBtr0070674	CG3556-RA			1250.879	2585.093	0.00548	0.0382
FBtr0070680	CG12212-RA	peb	pebbled	10338.607	32084.384	0.000495	0.00993
FBtr0070691	CG3052-RA	HLH4C	Helix loop helix protein 4C	837.183	413.947	0.00439	0.0335
FBtr0070720	CG32770			488.459	1003.656	0.0004	0.00874
FBtr0070755	CG3315-RA	TrxT	Thioredoxin T	50.464	123.644	0.00607	0.0408
FBtr0070777	CG15784-RA			552.388	7436.943	0.000235	0.00682
FBtr0070778	CG16752-RA	SPR	Sex peptide receptor	1221.939	485.677	0.00131	0.0163
FBtr0070805	CG4096			714.61	271.369	7.59E-05	0.00377

FBtr0070836	CG3097-RA			8529.57	3900.498	0.00461	0.0345
FBtr0070861	CG6041-RA			908.047	2290.561	0.00449	0.0338
FBtr0070866	CG5966-RA			3963.024	1861.028	0.00182	0.02
FBtr0070881	CG32750-RA			1923.211	799.998	0.00131	0.0163
FBtr0070888	CG4690-RA	Tsp5D	Tetraspanin 5D	1030.399	337.711	0.0029	0.0261
FBtr0070891	CG4766-RA			637.676	127.124	0.000139	0.00537
FBtr0070960	CG14439-RA			879.507	3701.006	8.18E-05	0.00388
FBtr0071078	CG15478-RA			280.49	128.896	5.88E-05	0.00324
FBtr0071106	CG1571-RA			182.186	88.61	0.000663	0.0115
FBtr0071170	CG1632-RA			3724.639	1389.816	0.000396	0.00869
FBtr0071178	CG15343-RA			471.684	1459.771	1.11x10^-6	0.000377
FBtr0071186	CG10759-RA	Or7a	Odorant receptor 7a	46.7	393.678	1.52x10^-6	0.00044
FBtr0071193	CG15335-RB	cyr	cypher	1006.372	401.73	4.06E-05	0.00275
FBtr0071201	CG15350-RA	Cp7Fb	Chorion protein b at 7F	85.997	32.724	1.98E-05	0.00196
FBtr0071202	CG15351-RA	Cp7Fc	Chorion protein c at 7F	158.242	74.368	0.00197	0.0209
FBtr0071203	CG1478-RA	Cp36	Chorion protein 36	75.448	33.272	0.00256	0.0243
FBtr0071213	CG11265-RE	Trf4-1		8558.762	33.544	1.66x10^-7	0.000204
FBtr0071243	CG32713-RA			200.889	466.089	0.000159	0.00557
FBtr0071244	CG11202-RA	org-1	optomotor-blind-related-gene-1	4906.405	2037.306	0.00259	0.0245
FBtr0071249	CG1787-RA	Hexo2	Hexosaminidase 2	4961.791	14251.948	1.19x10^-7	0.000203
FBtr0071310	CG15370-RA			3194.228	1170.536	0.00546	0.0381
FBtr0071311	CG15371-RA	Gr8a	Gustatory receptor 8a	268.337	42.34	0.000017	0.00182
FBtr0071335	CG12120-RA	t	tan	3576.465	1156.47	0.000971	0.0138
FBtr0071386	CG32698-RA			428.459	1242.946	1.85E-05	0.00189
FBtr0071390	CG9689-RA			2187.699	684.573	0.00547	0.0381
FBtr0071395	CG1986-RA			2051.627	498.775	0.00118	0.0154
FBtr0071397	CG15247-RA			290.019	89.025	0.00155	0.018
FBtr0071434	CG12644-RA			125.453	416.499	0.000109	0.00462
FBtr0071436	CG15311-RA			253.289	833.526	0.00134	0.0164
FBtr0071457	CG32680			2855.571	1273.203	0.00187	0.0203
FBtr0071463	CG32683-RA			37.064	80.3	0.00288	0.0259
FBtr0071480	CG32682			445.246	944.894	0.000265	0.00714
FBtr0071502	CG11556-RA	Rph	Rabphilin	294.427	602.363	0.000512	0.0101
FBtr0071516	CG9236			273.277	662.491	0.00236	0.0231
FBtr0071542	CG10531-RA	Cht9		340.299	2214.1	0.000345	0.00813
FBtr0071543	CG3986-RA	Cht4	Chitinase 4	55.301	1059.678	0.000037	0.00263

FBtr0071544	CG30293-RA	Cht12		37.807	193.374	0.000853	0.0131
FBtr0071557		otp		3138.35	1482.026	0.000439	0.0092
FBtr0071558		otp		311.968	140.739	0.00174	0.0194
FBtr0071560	CG9993-RA			709.212	246.686	1.37E-05	0.00166
FBtr0071561	CG17999-RA			542.426	179.916	4.45E-05	0.0029
FBtr0071566	CG15655			1166.742	351.263	0.00569	0.0391
FBtr0071579	CG9441-RC	Pu	Punch	7011.286	3179.657	0.00368	0.03
FBtr0071580	CG9441-RA	Pu	Punch	9871.097	4373.77	0.000186	0.00603
FBtr0071664	CG15675			651.617	2435.4	0.000285	0.00736
FBtr0071665	CG15675			616.383	2805.109	7.21E-05	0.00365
FBtr0071669	CG30263			174.27	623.403	0.00638	0.0421
FBtr0071675	CG17922-RA			448.785	1107.877	0.000585	0.0107
FBtr0071693	CG30283			2787.879	1317.951	3.81E-05	0.00266
FBtr0071740	CG4363-RA			99.363	301.698	0.00312	0.0271
FBtr0071741	CG13492			1884.795	4868.785	0.00619	0.0414
FBtr0071745	CG4402-RA	lox2	lysyl oxidase-like 2	136.084	48.568	9.81E-05	0.00433
FBtr0071768	CG30279-RA			152.033	485.926	3.98E-05	0.00272
FBtr0071777	CG3380-RA	Oatp58Dc	Organic anion transporting polypeptide 58Dc	3422.07	1459.041	0.00277	0.0256
FBtr0071786	CG11170-RB			1163.862	2413.657	0.00184	0.0201
FBtr0071798	CG13502			32.304	70.263	0.000743	0.0123
FBtr0071799	CG13502-RA			148.032	385.523	6.02E-05	0.00328
FBtr0071823	CG6044-RA			317.861	1131.064	3.53x10^-6	0.000737
FBtr0071825	CG6044			174.479	664.735	0.000046	0.0029
FBtr0071826	CG33200-RA	ventrally-expressed-protein-D		1510.599	4797.15	3.21x10^-6	0.000678
FBtr0071829		rad50		280.519	572.857	0.00348	0.0291
FBtr0071831	CG10384			507.553	229.009	0.00644	0.0424
FBtr0071858	CG33143-RC			307.595	628.355	0.00776	0.0481
FBtr0071886	CG30271			99.363	1163.325	2.33x10^-6	0.00053
FBtr0071887	CG30266			39.961	308.383	4.82x10^-7	0.000306
FBtr0071888	CG30274			146.963	560.018	1.97E-05	0.00196
FBtr0071889	CG30264			430.229	1321.269	7.99x10^-6	0.00127
FBtr0071925	CG30217			1636.394	737.34	0.0021	0.0216
FBtr0071926	CG30217			839.764	394.722	0.00293	0.0262
FBtr0071931	CG30195-RA			2125.541	791.658	0.00584	0.0398
FBtr0071934	CG4414-RA	Ugt58Fa		7562.125	3303.059	0.00128	0.0161

FBtr0071979	CG9876-RA			640.498	170.195	0.00375	0.0304
FBtr0071986	CG9895			590.025	193.042	0.00019	0.00613
FBtr0072024	CG9815-RA			467.678	120.813	0.000346	0.00813
FBtr0072049	CG9871-RA	RpL22-like	Ribosomal protein L22-like	135.12	312.446	0.000123	0.00497
FBtr0072057	CG13559-RA			531.635	179.077	0.00199	0.021
FBtr0072059	CG33150-RA	Gr59f	Gustatory receptor 59f	450.401	217.692	0.00108	0.0148
FBtr0072079	CG5428			4271.992	1446.046	0.00569	0.0391
FBtr0072081	CG11293-RA			199.438	91.656	0.00381	0.0306
FBtr0072094	CG18128-RA			1195.14	504.975	0.00186	0.0202
FBtr0072117	CG17632-RA	bw	brown	5184.529	1986.156	0.00289	0.0259
FBtr0072131	CG5597-RA			1355.88	3124.924	0.000309	0.00759
FBtr0072135	CG13562-RA			1142.279	394.918	0.00293	0.0262
FBtr0072150	CG3006-RA	Fmo-1	Flavin-containing monooxygenase 1	568.412	274.311	0.00263	0.0246
FBtr0072161	CG3121-RA			77.866	34.897	0.000221	0.0066
FBtr0072181	CG30174			245.782	66.846	0.00346	0.0291
FBtr0072182	CG30179			360.753	99.797	0.00221	0.0222
FBtr0072197	CG4324-RA			4446.73	2083.961	0.00185	0.0202
FBtr0072239	CG4797-RB			151.204	487.734	0.000868	0.0132
FBtr0072243	CG13561-RA			44.689	102.363	0.00034	0.00801
FBtr0072246	CG13564-RA			141.488	62.766	0.0042	0.0327
FBtr0072257	CG3328-RA			2890.999	1140.161	0.000472	0.00966
FBtr0072289	CG13578-RA			77.253	353.772	0.00072	0.0121
FBtr0072329		Mmp1		648.752	1378.955	5.53E-05	0.00314
FBtr0072370	CG9196-RA	spz6	spatzle 6	14377.297	6414.548	0.000784	0.0126
FBtr0072371	CG3880-RA			1687.142	816.818	0.00707	0.0454
FBtr0072419	CG2857-RA	Tpc2	Thiamine pyrophosphate carrier protein 2	90.038	269.288	0.000202	0.00628
FBtr0072427	CG2928-RA	Reg-5	Rhythmically expressed gene 5	6834.91	3193.374	0.000947	0.0138
FBtr0072441	CG4871-RB	ST6Gal	Sialyltransferase	71.101	245.246	0.000405	0.00883
FBtr0072442	CG4871-RA	ST6Gal	Sialyltransferase	103.052	271.692	0.00102	0.0142
FBtr0072443	CG3441-RA	Nplp1	Neuropeptide-like precursor 1	1158.546	3545.543	1.32x10^-6	0.000417
FBtr0072462	CG32475-RA	mthl8	methuselah-like 8	59.507	22.58	0.00142	0.017
FBtr0072501	CG32476-RA	mthl14	methuselah-like 14	666.324	1354.203	0.00103	0.0143
FBtr0072507	CG12313-RA	ttm2	tiny tim 2	57.639	126.99	0.00024	0.00693
FBtr0072561	CG3200-RA	Reg-2	Rhythmically expressed gene 2	1032.819	488.102	5.17x10^-6	0.000984
FBtr0072594	CG12191-RA	dpr20		170.57	383.253	0.000352	0.00824
FBtr0072625	CG13912-RA			4036.46	1870.019	0.00636	0.042

FBtr0072636	CG32335			759.402	3941.544	6.11x10^-6	0.00104
FBtr0072651	CG9194-RA			6907.21	2645.562	0.00567	0.039
FBtr0072659	CG9134-RB			4781.431	1656.229	0.00439	0.0335
FBtr0072660	CG9134-RA			752.798	239.432	0.00279	0.0257
FBtr0072765	CG7991			2245.562	1021.103	6.24E-05	0.00333
FBtr0072796	CG18173-RA			722.281	3667.313	5.16x10^-7	0.000316
FBtr0072801	CG13932			301.289	91.705	0.00448	0.0338
FBtr0072802	CG13931-RA			1236.696	566.552	0.000859	0.0131
FBtr0072836	CG12026-RB	Tmhs	Tetraspan membrane protein in hair cell stereocilia ortholog	3271.891	1500.601	0.000907	0.0135
FBtr0072837	CG12026-RA	Tmhs	Tetraspan membrane protein in hair cell stereocilia ortholog	211.507	67.777	0.00258	0.0245
FBtr0072869	CG1919-RA	Cpr62Bc	Cuticular protein 62Bc	3228.655	7617.714	0.00656	0.043
FBtr0072879	CG13806-RA			1926.808	706.004	0.0033	0.0281
FBtr0072886	CG13802-RA			54.427	128.37	0.00181	0.02
FBtr0072950	CG12002-RB	Pxn	Peroxidasin	91.063	36.522	0.000972	0.0138
FBtr0072951	CG12002-RA	Pxn	Peroxidasin	10956.995	4437.229	0.000036	0.00262
FBtr0072954	CG12002-RE	Pxn	Peroxidasin	9393.22	3728.96	0.0022	0.0222
FBtr0072979	CG2113-RA			32.756	68.99	0.00162	0.0186
FBtr0073051	CG14960-RA			10289.053	4116.817	0.00439	0.0335
FBtr0073052	CG12017-RA			9299.702	3881.251	0.00396	0.0315
FBtr0073062	CG10812-RA	dro5	drosomycin-5	4338.918	262.126	0.000141	0.00534
FBtr0073066	CG12013-RC	PHGPx		2073.082	4574.076	0.000304	0.0075
FBtr0073067	CG12013-RA	PHGPx		1887.601	3996.157	0.000554	0.0104
FBtr0073068	CG12013-RD	PHGPx		383.361	921.799	0.000233	0.0068
FBtr0073069	CG14961-RA			171.902	1323.761	0.000638	0.0112
FBtr0073073	CG10810-RA	Drs	Drosomycin	41.55	86.514	0.00687	0.0445
FBtr0073110	CG14964			3639.654	1364.352	0.000703	0.0119
FBtr0073155	CG1072-RA	Awh	Arrowhead	3260.316	1281.457	0.00167	0.0189
FBtr0073156	CG1072-RB	Awh	Arrowhead	5114.316	2242.171	0.000567	0.0105
FBtr0073157	CG1079-RA	Fie	Fire exit	981.203	2461.609	0.000797	0.0127
FBtr0073162	CR32265-RA	Eip63F-2	Ecdysone-induced protein 63F 2	85.409	41.763	0.00132	0.0164
FBtr0073172	CG12766-RA			215.798	502.258	0.00294	0.0262
FBtr0073181	CG14979			33.023	153.828	0.000726	0.0121
FBtr0073203	CG1136-RA			322.446	776.324	0.00128	0.0162
FBtr0073231	CG1273-RB			10818.368	5062.201	0.00192	0.0206
FBtr0073248	CG15009-RA	ImpL2	Ecdysone-inducible gene L2	200.908	76.492	0.000302	0.00749
FBtr0073260	CG15002-RB	mas	masquerade	13387.821	5938.179	0.00102	0.0142

FBtr0073278	CG14993-RA	Faa	Fumarylacetoacetase	9599.778	4128.156	0.0061	0.0409
FBtr0073299	CG11348-RA	nAcRβ-64B	nicotinic Acetylcholine Receptor beta 64B	3109.303	1452.907	0.00201	0.0211
FBtr0073324	CG32244			6202.398	2230.936	0.000388	0.0086
FBtr0073326	CG32242			5626.345	2150.611	0.000978	0.0139
FBtr0073328	CG13721-RA			64.443	554.901	0.000656	0.0115
FBtr0073378	CG15209-RA			1988.032	4324.001	5.87x10^-6	0.00102
FBtr0073389	CG16922			2200.691	827.96	0.00043	0.00914
FBtr0073390	CG11160-RA			1400.086	455.609	0.000354	0.00826
FBtr0073391	CG11160-RB			1419.543	394.279	0.000152	0.00548
FBtr0073393	CG18085-RA	sev	sevenless	541.659	240.025	0.008	0.0491
FBtr0073399	CG15204			310.956	774.827	0.00022	0.00659
FBtr0073400	CG1567-RA	C901		8503.922	3354.177	0.000414	0.00898
FBtr0073429	CG2061-RA			477.971	963.023	4.44E-05	0.0029
FBtr0073502	CG17656			68.243	366.528	0.000046	0.00289
FBtr0073511	CG11697-RA			60.446	327.935	0.00175	0.0195
FBtr0073543	CG1572-RA			4271.822	10907.067	0.00163	0.0186
FBtr0073555	CG9369-RA	m	miniature	7105.943	2405.892	0.00208	0.0215
FBtr0073594	CG2467-RA	pot	papillote	4218.193	1945.245	0.0028	0.0257
FBtr0073612	CG9355-RA	dy	dusky	4197.114	1341.702	0.000579	0.0106
FBtr0073623	CG9360-RA			38.182	98.988	0.000134	0.00527
FBtr0073647	CG15927-RA			2312.756	985.647	0.00469	0.0348
FBtr0073701		Pde9		1019.414	483.749	0.0011	0.0149
FBtr0073763	CG1633-RB	Jafrac1	thioredoxin peroxidase 1	2616.341	5566.122	0.00375	0.0304
FBtr0073769	CG1640-RB			5469.494	10939.566	1.59x10^-6	0.000445
FBtr0073781	CG15753			329.759	122.297	0.00772	0.048
FBtr0073913	CG32600-RA	dpr8		128.326	285.891	0.00215	0.0219
FBtr0073920	CG9400-RA			190.147	69.585	0.000397	0.00869
FBtr0073929	CG12540-RA			603.832	280.273	0.00253	0.0241
FBtr0073934	CG5321			1995.444	642.216	0.000935	0.0137
FBtr0073986	CG9522-RA			4400.407	1859.504	3.91E-05	0.0027
FBtr0074026	CG9095-RA			7851.453	3831.97	0.0041	0.0322
FBtr0074052	CG12708-RA			184.393	488.056	0.002	0.021
FBtr0074190	CG8962-RA	Paf-AHα	Platelet-activating factor acetylhydrolase alpha	9242.432	4025.08	0.000103	0.00441
FBtr0074191	CG8962-RB	Paf-AHα	Platelet-activating factor acetylhydrolase alpha	8783.576	4189.268	0.000222	0.00657
FBtr0074206	CG14948-RA	dpr18		310.376	1070.175	0.000289	0.00738
FBtr0074248	CG12507			2328.231	8661.102	8.71E-05	0.00409

FBtr0074251	CG32577-RA	disco-r	disco-related	3352.54	1526.685	0.00441	0.0335
FBtr0074273	CG4394-RC	Traf-like	TNF-receptor-associated factor-like	2027.711	4255.491	0.0012	0.0155
FBtr0074321	CG4653-RA			692.061	1738.188	0.000776	0.0126
FBtr0074349	CG13003-RA			546.378	1117.188	0.00074	0.0123
FBtr0074351	CG13004-RA			1150.782	411.447	0.00333	0.0283
FBtr0074357	CG9623-RB	if	inflated	5735.425	2759.664	0.00223	0.0223
FBtr0074361	CG9672-RA			207.285	529.083	0.00324	0.0278
FBtr0074419	CG12996			501.393	182.616	0.00132	0.0164
FBtr0074474	CG12986-RA			202.368	86.504	0.00463	0.0345
FBtr0074477	CG32556-RA	chas	chascon	7838.558	3693.222	0.00511	0.0366
FBtr0074479	CG12990-RA			142.878	301.275	0.000966	0.0139
FBtr0074499	CR32496-RA			142.861	464.453	2.22E-05	0.00208
FBtr0074524	CG7178-RG	wupA	wings up A	5878.465	2890.313	0.00217	0.022
FBtr0074553	CG6106-RA			421.726	156.74	0.00292	0.0262
FBtr0074566	CG32547			95.04	324.789	0.000171	0.00574
FBtr0074579	CG6023-RA			391.95	145.752	0.000516	0.0102
FBtr0074581	CG5993-RA	os	outstretched	1753.231	738.28	0.00211	0.0217
FBtr0074591	CG12611-RA	Andorra		82.432	37.686	0.00618	0.0413
FBtr0074603	CG6578-RA	phm	phantom	500.243	214.392	0.00187	0.0203
FBtr0074609	CG6816-RA	Cyp18a1	Cytochrome P450-18a1	5096.02	2266.239	0.00497	0.0362
FBtr0074610	CG6816-RB	Cyp18a1	Cytochrome P450-18a1	1373.913	490.477	0.00316	0.0273
FBtr0074627	CG15044-RA			310.384	762.95	0.00283	0.0258
FBtr0074628	CG15046-RA			344.623	130.401	0.00421	0.0328
FBtr0074629	CG6367-RA	psh	persephone	653.915	249.413	0.00136	0.0167
FBtr0074630	CG6361-RA			940.713	393.539	0.000188	0.00608
FBtr0074649	CG7378-RA			568.007	1800.989	0.000792	0.0126
FBtr0074662		CCKLR-17D3		225.795	1081.738	3.26E-05	0.00244
FBtr0074698	CG7537-RB	inx5		72.992	210.995	0.000321	0.00771
FBtr0074701	CG15883-RA	Obp18a	Odorant-binding protein 18a	1234.903	562.832	0.00535	0.0377
FBtr0074757	CG14225			798.915	303.459	0.000145	0.00537
FBtr0074790	CG14234-RA			69.981	309.358	5.06x10^-6	0.000985
FBtr0074824	CG17147			503.294	1041.72	0.00441	0.0335
FBtr0074827	CG13813			3272.791	7585.859	0.000185	0.00604
FBtr0074843	CG6663	Spn77Bb	Serpin 77Bb	33.318	236.32	1.98E-05	0.00195
FBtr0074862	CG13811			479.951	977.345	0.00087	0.0132
FBtr0074863	CG7323			150.703	502.758	0.000125	0.005
FBtr0074869	CG7385-RA	Ir76b	Ionotropic receptor 76b	109.742	825.328	1.54x10^-7	0.000202
FBtr0074876	CG8533			694.317	214.708	0.000164	0.00564

FBtr0074897	CG7978-RA	Ac76E	Adenylyl cyclase 76E	251.684	590.394	0.000703	0.0119
FBtr0074945	CG9372-RA			1477.967	680.399	0.00537	0.0378
FBtr0074980	CG9449			846.452	235.669	0.00276	0.0255
FBtr0074981	CG9449			8366.324	3101.859	0.00415	0.0324
FBtr0075004	CG9614-RC	pip	pipe	3408.365	1654.675	0.00419	0.0327
FBtr0075040	CG18136-RA			285.394	115.551	0.002	0.021
FBtr0075046	CG11619-RA			1161.409	429.31	0.0011	0.0148
FBtr0075047	CG32204			47.311	144.65	0.00572	0.0392
FBtr0075060	CG6865-RA			239.552	1717.402	3.18E-05	0.00242
FBtr0075127	CG7330-RA			2134.06	5000.382	0.00447	0.0338
FBtr0075129	CG7313-RA	CheA75a	Chemosensory protein A 75a	319.464	110.521	0.00799	0.049
FBtr0075130	CG4345-RA	grim		3768.839	8757.353	8.26x10^-6	0.00127
FBtr0075138	CG32194			158.745	76.969	0.000985	0.0139
FBtr0075153	CG5485-RA	Prestin		1834.105	5285.082	1.22E-05	0.00157
FBtr0075167	CG5582-RA	cln3		227.982	529.721	0.00434	0.0334
FBtr0075185	CG32183-RA	Ccn		310.102	1299.79	3.36E-05	0.00249
FBtr0075186	CG32183-RB	Ccn		439.728	1764.9	1.35E-05	0.00164
FBtr0075194	CG6034-RA			58.569	283.894	8.92x10^-6	0.00129
FBtr0075261	CG13028-RA			201.725	1382.923	5.59x10^-6	0.000997
FBtr0075270	CG14060			5960.592	2724.224	0.000589	0.0107
FBtr0075271	CG3799			6106.78	2702.273	0.00168	0.019
FBtr0075290	CG6642-RA	a10	antennal protein 10	28.52	89.27	0.00684	0.0444
FBtr0075300	CG11905-RB			9474.927	3841.684	2.97E-05	0.00236
FBtr0075305	CG11905-RF			8483.032	3654.441	0.000966	0.0139
FBtr0075316	CG13032-RA			57.696	941.35	8.59x10^-7	0.000351
FBtr0075321	CG9701-RA			1215.128	581.384	0.0041	0.0322
FBtr0075361	CG4098-RA			1051.603	387.256	0.000362	0.00838
FBtr0075378	CG33257-RA			229.096	98.849	0.0023	0.0227
FBtr0075384	CG4842-RA			470.593	210.535	0.00624	0.0415
FBtr0075388	CG4680-RA			955.656	3387.367	6.37x10^-7	0.000331
FBtr0075391	CG4314-RA	st	scarlet	2296.567	892.096	0.00148	0.0175
FBtr0075403	CG32158			2795.566	1141.129	0.00168	0.0189
FBtr0075405	CG32158			2859.788	1303.027	0.00238	0.0232
FBtr0075441	CG32156-RE	Mbs	Myosin binding subunit	5299.609	2380.371	0.00284	0.0258
FBtr0075490	CG5157-RA			208.027	1676.2	2.26E-05	0.00207
FBtr0075507	CG32151			73.297	159.683	0.000846	0.0131

FBtr0075533	CG12486-RA			37.41	93.002	0.00199	0.021
FBtr0075534	CG32150-RB			2420.867	8494.402	3.91E-05	0.00269
FBtr0075535	CG32150-RA			1316.49	7522.004	2.30x10^-7	0.000232
FBtr0075578	CG7297-RA	pgant8	polypeptide GalNAc transferase 8	835.923	309.21	0.00629	0.0418
FBtr0075589		comm3		372.002	778.544	0.00215	0.0219
FBtr0075609	CG7255			840.519	410.142	0.000719	0.0121
FBtr0075619	CG13466			41.428	151.301	0.000617	0.0111
FBtr0075621	CG3096-RA	Brd	Bearded	594.666	3314.608	1.51x10^-6	0.000452
FBtr0075623	CG3349			159.301	403.75	0.00092	0.0136
FBtr0075666	CG18581-RA			1617.362	555.093	0.0056	0.0387
FBtr0075682	CG32143			3714.168	1248.006	0.000421	0.00907
FBtr0075683	CG32143			197.67	54.702	0.00312	0.0271
FBtr0075694	CG17839			666.618	3737.146	8.08x10^-7	0.000346
FBtr0075695	CG17839-RB			555.345	2935.566	7.83x10^-7	0.000344
FBtr0075747	CG32139-RA	Sox21b		2862.609	1310.425	0.000486	0.00984
FBtr0075751	CG32136-RA	Tsp68C	Tetraspanin 68C	2451.149	977.224	0.0015	0.0176
FBtr0075754	CG13737-RA			5146.471	2149.223	0.00273	0.0253
FBtr0075757	CG32137-RA			3236.069	6717.609	7.92x10^-6	0.00127
FBtr0075761	CG8937-RC	Hsc70-1	Heat shock protein cognate 1	1128.05	359.337	0.00101	0.0142
FBtr0075779	CG8100-RA			630.599	112.454	3.73E-05	0.00262
FBtr0075797	CG17368			265.528	1065.287	0.00125	0.0159
FBtr0075798	CG8760			422.837	1733.161	0.00286	0.0259
FBtr0075799	CG32131			656.858	2454.366	0.00624	0.0416
FBtr0075800	CG32132-RA			876.721	2788.74	0.00665	0.0435
FBtr0075803	CG8757			49.913	272.204	0.00062	0.0111
FBtr0075817	CG10710-RA			3546.079	1200.103	0.000506	0.0101
FBtr0075820	CG10089-RD			239.442	1174.503	5.30x10^-6	0.000976
FBtr0075821	CG10089-RB			640.965	1603.077	0.00695	0.0449
FBtr0075843	CG10717-RB	ImpL1	Ecdysone-inducible gene L1	1480.863	407.924	6.05E-05	0.00328
FBtr0075850	CG14109-RA			3262.538	1245.426	0.00334	0.0284
FBtr0075866	CG14107-RA			3451.233	1592.325	3.08E-05	0.0024
FBtr0075868	CG14120-RA			428.098	3216.353	0.000159	0.00557
FBtr0075882		RpS12		1248.064	497.824	0.00112	0.015
FBtr0075888	CG14116			239.565	78.151	0.00317	0.0274

FBtr0075909	CG10605-RA	caup	caupolican	1682.105	729.725	0.0034	0.0287
FBtr0075936	CG10943-RA			27.411	269.298	0.000525	0.0102
FBtr0075977	CG10663			1322.879	595.054	0.00508	0.0365
FBtr0075985	CG14122-RA	Smyd4	SET and MYND domain protein 4	3979.059	1302.243	0.00355	0.0295
FBtr0076001	CG6906-RA	CAH2	Carbonic anhydrase 2	4562.911	17041.593	2.71x10^-7	0.000232
FBtr0076008	CG4328			1983.544	746.264	0.00135	0.0166
FBtr0076021	CG9760			373.708	155.998	0.000619	0.0111
FBtr0076039	CG7260-RA	byn	brachyenteron	2902.124	1076.679	0.00413	0.0324
FBtr0076043	CG7248-RA			227.369	978.17	0.000095	0.00429
FBtr0076047	CG6938			74.022	228.508	0.000711	0.012
FBtr0076082	CG32092			1011.187	462.586	0.00222	0.0223
FBtr0076097	CG7512			1424.103	3120.787	3.03x10^-6	0.000657
FBtr0076146	CG6097-RA	rt	rotated abdomen	10643.805	4495.386	0.00154	0.018
FBtr0076164	CG14141-RA			1061.943	477.81	0.000121	0.00495
FBtr0076181	CG6163-RA			160.249	67.795	0.000429	0.00915
FBtr0076221	CG6216-RB			1123.9	536.581	0.000333	0.00787
FBtr0076230	CG32073-RA			5273.101	1556.541	0.00362	0.0298
FBtr0076243	CG6327-RA			2517.773	13173.087	7.32x10^-7	0.000348
FBtr0076305	CG6611-RA	ect	ectodermal	10199.619	5037.673	0.00397	0.0316
FBtr0076314	CG32054-RA			951.438	4678.307	7.52x10^-7	0.000339
FBtr0076338	CG32050-RA			960.339	321.212	0.00709	0.0455
FBtr0076345	CG14163			175.647	409.454	0.00197	0.0209
FBtr0076346	CG12524			169.812	425.445	0.00509	0.0366
FBtr0076371	CG33273-RA	Ilp5	Insulin-like peptide 5	231.554	82.337	0.000489	0.00987
FBtr0076432	CG32042-RF			622.479	1917.505	1.34E-05	0.00165
FBtr0076469	CG32037-RA			610.692	262.2	0.0065	0.0427
FBtr0076510	CG5008-RA	GNBP3	Gram-negative bacteria binding protein 3	2440.153	1136.398	0.00633	0.0419
FBtr0076512	CG13313-RA			492.797	219.897	2.14E-05	0.00204
FBtr0076521	CG5093-RA	Doc3	Dorsocross3	2607.284	1075.753	0.00358	0.0296
FBtr0076525	CG4821-RD	Tequila		3728.78	1835.723	0.00487	0.0357
FBtr0076566		mfr		40.617	283.25	2.50x10^-7	0.000238
FBtr0076572	CG6519-RA	Cp15	Chorion protein 15	31.177	1056.717	4.98E-05	0.00298
FBtr0076576	CG6576-RA			169.865	72.241	0.00117	0.0154
FBtr0076580	CG32024-RA			26.717	63.077	0.000142	0.00536

FBtr0076586		TrpA1		45.681	4029.447	6.95x10^-7	0.00034
FBtr0076607	CG32356-RB	ImpE1	Ecdysone-inducible gene E1	1966.979	680.13	0.000534	0.0102
FBtr0076622	CG6776-RA			1679.721	9753.065	6.67x10^-7	0.000336
FBtr0076623	CG6781-RA	se	sepia	42.882	370.519	2.15x10^-6	0.00051
FBtr0076662	CG32354-RA			5383.025	1714.503	0.00016	0.00556
FBtr0076799	CG7526			5855.208	2051.938	0.008	0.0491
FBtr0076807	CG7496-RA	PGRP-SD		806.864	278.351	0.000438	0.00921
FBtr0076811	CG7399-RA	Hn	Henna	1935.313	820.904	0.000175	0.00585
FBtr0076826	CG14837			78.511	205.753	0.000848	0.0131
FBtr0076833	CG14826-RA			1174.501	558.081	0.00403	0.0319
FBtr0076874		pst		3806.502	7877.041	0.000221	0.00658
FBtr0076887		unc-13-4A		245.363	733.781	0.0021	0.0215
FBtr0076918	CG8620-RA			114.855	3402.659	1.11x10^-6	0.00037
FBtr0076931	CG8641-RA			390.211	1069.317	0.000142	0.00536
FBtr0076948	CG32392-RB			322.069	2872.605	2.74x10^-7	0.000224
FBtr0077031	CG13288			81.999	189.899	1.76x10^-7	0.000188
FBtr0077146	CG4814			115.635	244.105	0.000681	0.0117
FBtr0077152	CG10630-RA	blanks		548.599	1814.266	1.13E-05	0.00149
FBtr0077212	CG1644-RA	Cyp6t1		1054.618	502.78	1.13E-05	0.00149
FBtr0077242	CG1742-RB	Mgstl	Microsomal glutathione S-transferase-like	233.239	610.084	0.000484	0.00982
FBtr0077243	CG1742-RA	Mgstl	Microsomal glutathione S-transferase-like	3395.955	8563.939	5.28x10^-6	0.000983
FBtr0077259	CG1501-RA	unc	uncoordinated	393.775	1105.789	0.000886	0.0134
FBtr0077335	CG17058-RA	Peritrophin-A		791.06	308.06	0.00261	0.0246
FBtr0077338	CG1504			119.802	248.247	0.00049	0.00987
FBtr0077358	CG17600-RA			3742.081	1688.479	0.00295	0.0262
FBtr0077401	CG2837-RB			664.597	2687.425	0.000253	0.00707
FBtr0077402	CG2837-RC			377.233	1330.379	0.00236	0.0231
FBtr0077420	CG15632-RA	Taf12L	TBP-associated factor 30kD subunit α-2	68.24	500.206	1.08E-05	0.00146
FBtr0077434	CG33003-RA			7753.962	2725.566	5.05E-05	0.00301
FBtr0077446	CG15444-RB	ine	inebriated	4852.183	2349.165	0.000266	0.00713
FBtr0077478	CG3352-RA	ft	fat	9546.379	4751.199	0.0023	0.0227

FBtr0077489	CG31772-RA			534.121	258.737	0.00283	0.0258
FBtr0077506	CG15423-RA			517.71	3086.816	0.000201	0.00626
FBtr0077532	CG2788-RA	Dot	Dorothy	2009.985	992.961	0.000377	0.00851
FBtr0077542	CG31777-RA			4536.002	1922.02	0.00633	0.0419
FBtr0077543	CG31778-RA			335.227	147.598	0.00191	0.0206
FBtr0077557	CG3851-RA	odd	odd skipped	3858.008	1609.444	0.00107	0.0147
FBtr0077558	CG3242-RA	sob	sister of odd and bowl	2211.622	896.026	0.000873	0.0132
FBtr0077568	CG15414-RA			206.444	487.255	0.00022	0.00658
FBtr0077586	CG3285-RA			1646.527	635.218	0.000364	0.00839
FBtr0077595	CG15412			330.463	162.705	0.000311	0.0076
FBtr0077647	CG17264-RA			750.137	271.191	0.0025	0.024
FBtr0077657	CG3524-RA	v(2)k05816		210.448	1688.475	1.61E-05	0.00179
FBtr0077705	CG31689-RC			2886.975	6042.276	7.15E-05	0.00364
FBtr0077807	CG31682-RA			28.806	212.517	0.000371	0.00849
FBtr0077809	CG31679-RA			28.88	57.82	0.00053	0.0102
FBtr0077820	CG4238			325.898	1301.81	0.000182	0.006
FBtr0077844	CG4265-RA	Uch	Ubiquitin carboxy-terminal hydrolase	1522.321	3378.817	8.83x10^-6	0.0013
FBtr0077859		lectin-22C		2656.881	1175.948	0.00744	0.047
FBtr0077893	CG31663-RA			685.671	255.693	2.06E-05	0.00199
FBtr0077894	CG15623-RA	c-cup	calcutta cup	31.25	135.522	0.000361	0.00839
FBtr0077920	CG5397-RA			463.457	193.018	0.00436	0.0335
FBtr0077924	CG5450-RA	Cdlc2	Cytoplasmic dynein light chain 2	35.039	164.988	5.24E-05	0.00305
FBtr0077925	CG5450-RB	Cdlc2	Cytoplasmic dynein light chain 2	52.301	112.913	0.00119	0.0154
FBtr0077926	CG14346-RA			540.422	1841.868	8.30x10^-7	0.000347
FBtr0077927	CG14346-RB			211.946	887.633	1.35E-05	0.00165
FBtr0077942	CG33126-RA	Nlaz	Neural Lazarillo	879.534	371.215	0.00076	0.0124
FBtr0077973	CG5011-RA			497.985	1327.11	1.08x10^-6	0.000385
FBtr0077981	CG5080-RB			17220.225	7639.752	0.00718	0.0458
FBtr0078026		GluRIIC		2310.655	806.173	0.00259	0.0244
FBtr0078043	CG3159-RA	Eaat2	Excitatory amino acid transporter 2	120.495	278.688	9.75E-05	0.00432
FBtr0078064	CG11822-RA	nAcRβ-21C	nicotinic acetylcholine receptor beta 21C	2865.185	1227.845	0.00172	0.0192
FBtr0078066	CG2789-RA			2408.352	6811.776	0.000891	0.0134
FBtr0078070	CG2819-RA	Pph13	PvuII-PstI homology 13	183.239	524.916	2.27E-05	0.00207
FBtr0078072	CG2851-RA	Gsc	Goosecoid	636.851	314.906	0.00542	0.038
FBtr0078079	CG2914-RA	Ets21C	Ets at 21C	279.889	582.239	0.000624	0.0111

FBtr0078093	CG4213-RA			3242.453	1154.054	0.00338	0.0286
FBtr0078149	CG4648			903.543	1840.003	2.16x10^-6	0.000505
FBtr0078182	CG5665			210.656	514.204	0.000461	0.00949
FBtr0078183	CG16993-RA	in	inturned	1962.234	920.423	0.0042	0.0327
FBtr0078184	CG13247-RA			2044.188	795.06	0.00561	0.0387
FBtr0078196	CG5932-RA			83.005	793.203	0.000122	0.00497
FBtr0078212	CG4761-RA	knrl	knirps-like	3188.65	1227.805	0.000802	0.0127
FBtr0078213	CG4786-RA	Rcd2	Reduction in Cnn dots 2	430.485	1482.485	3.68E-05	0.00263
FBtr0078234	CG13248-RA			659.9	1394.836	0.00091	0.0135
FBtr0078306	CG18023-RA	Eip78C	Ecdysone-induced protein 78C	4683.262	2144.66	0.0013	0.0163
FBtr0078344	CG32437-RA			239.24	1881.031	4.42E-05	0.0029
FBtr0078345	CG32440-RA			82.515	604.24	5.80x10^-6	0.00102
FBtr0078380	CG7173-RA			15107.922	6035.578	0.00555	0.0385
FBtr0078402	CG12971			264.027	680.271	0.00456	0.0342
FBtr0078411	CG12974-RB			936.872	2174.896	6.98E-05	0.00358
FBtr0078415	CG9389-RA			47.471	112.818	0.000358	0.00835
FBtr0078416	CG9391			1851.923	3821.576	0.000889	0.0134
FBtr0078418	CG7807-RB	AP-2		1904.829	902.457	0.00022	0.00659
FBtr0078427	CG33291-RA			9781.541	4141.088	0.00166	0.0188
FBtr0078428	CG33292-RA			1102.757	436.388	0.000743	0.0123
FBtr0078434	CG14572-RA			273.358	635.463	0.00172	0.0193
FBtr0078457	CG14570-RA			406.254	3694.928	0.00013	0.00513
FBtr0078460	CG32447-RA			2504.044	1188.91	0.00118	0.0154
FBtr0078463	CG7160-RA	Cpr78E	Cuticular protein 78E	939.376	315.084	0.00048	0.00976
FBtr0078504	CG11438-RA			3457.738	1255.51	0.002	0.021
FBtr0078505	CG11437-RA			3414.263	1167.556	0.00764	0.0476
FBtr0078518	CG14456-RA			286.646	957.413	0.00437	0.0335
FBtr0078555	CG11128-RA	slif	slimfast	1015.965	4489.021	0.000678	0.0116
FBtr0078560	CG12768-RA			7031.689	2907.215	0.00136	0.0166
FBtr0078586	CG31563			902.904	182.411	0.00049	0.00986
FBtr0078591	CG15589-RA			3665.211	1699.35	0.00201	0.0211
FBtr0078602	CG1154-RA	Osi12	Osiris 12	4669.575	1836.408	0.00336	0.0284
FBtr0078610	CG15598-RA	Osi17	Osiris 17	2982.779	1027.51	0.00352	0.0293
FBtr0078615	CG10303-RA	Osi4	Osiris 4	129.766	62.731	0.00388	0.031
FBtr0078616	CG31559-RA			9425.749	3573.617	0.0013	0.0163
FBtr0078618	CG31557-RA	Obp83ef	Odorant-binding protein 83ef	332.485	104.775	0.00814	0.0496
FBtr0078623	CG11459-RA			315.091	80.432	0.000439	0.0092
FBtr0078634	CG10999			162.114	381.625	3.67E-05	0.00263

FBtr0078636	CG10999			145.114	421.161	0.000809	0.0128
FBtr0078661	CG2017-RA			3688.605	7635.587	0.000218	0.00658
FBtr0078737	CG31546-RA			57.328	135.292	0.000077	0.00375
FBtr0078841	CG1124-RA			4365.458	1733.098	0.00573	0.0392
FBtr0078847	CG2016-RB			14905.689	6875.928	0.00303	0.0266
FBtr0078848	CG14661-RA			104.206	278.101	0.00492	0.0359
FBtr0078867	CG32946			1989.147	629.761	2.28E-05	0.00206
FBtr0078881	CG14655-RA			2290.457	858.872	0.00168	0.019
FBtr0078882	CG31530-RA			1895.066	645.038	3.66E-05	0.00264
FBtr0078903	CG1102-RA	MP1	Melanization Protease 1	10710.166	5127.145	0.00247	0.0238
FBtr0078963	CG33294			49.785	173.007	0.00822	0.0499
FBtr0078989	CG18090-RA	Dsk	Drosulfakinin	59.712	158.702	0.000531	0.0102
FBtr0078990	CG14044-RA			57.011	222.09	0.000207	0.00635
FBtr0079106	CG6992-RI	GluRIIA	Glutamate receptor IIA	1065.315	348.742	0.00355	0.0295
FBtr0079133	CG7236-RA			664.367	1553.265	6.95x10^-8	0.000199
FBtr0079141	CG14004			88.319	290.68	0.000509	0.0101
FBtr0079142	CG31645			62.963	159.907	8.04E-05	0.00384
FBtr0079145	CG9019-RA	dsf	dissatisfaction	285.4	142.682	0.000244	0.00693
FBtr0079168	CG11149-RB			532.68	2595.546	5.86x10^-7	0.000314
FBtr0079171	CG9046-RA	Vm26Ab	Vitelline membrane 26Ab	437.053	122.016	0.00016	0.00557
FBtr0079227	CG11607-RA	H2.0	Homeodomain protein 2.0	2009.518	841.813	0.00185	0.0201
FBtr0079241	CG13998-RA			190.128	59.871	0.000138	0.00536
FBtr0079275	CG11527-RA	Tig	Tiggrin	12414.454	6164.763	0.00273	0.0254
FBtr0079276	CG9511			336.797	133.03	0.000351	0.00822
FBtr0079279	CG13981			851.137	342.218	0.00432	0.0333
FBtr0079367	CG18304-RA			2638.547	1051.713	0.00236	0.0231
FBtr0079419	CG4496-RA			57.572	148.731	0.003	0.0265
FBtr0079434	CG4969			1082.118	415.075	0.00599	0.0404
FBtr0079439	CG5171-RB			6069.253	2109.348	0.00371	0.0302
FBtr0079464	CG12789-RA	santa-maria	scavenger receptor acting in neural tissue and majority of rhodopsin is absent	3057.358	1277.596	0.00153	0.0179
FBtr0079468	CG5160-RA			717.618	1561.686	2.99x10^-8	0.000103
FBtr0079472	CG6739-RA			1827.149	662.002	0.000359	0.00836
FBtr0079473	CG6976-RB	Myo28B1		99.197	312.33	0.000663	0.0115
FBtr0079474	CG6976-RC	Myo28B1		300.109	1267.45	0.000186	0.00604

FBtr0079485	CG7191-RA			189.717	2842.64	8.07x10^-6	0.00126
FBtr0079499	CG7214-RA			62.132	179.703	0.00111	0.0149
FBtr0079503	CG13796-RB			1629.331	651.024	0.00643	0.0424
FBtr0079506	CG13795			1996.44	793.381	0.00504	0.0364
FBtr0079510	CG7052-RA	Tepll	Thiolester containing protein II	4593.263	2242.198	0.00421	0.0328
FBtr0079517	CG6772-RB	Slob	Slowpoke binding protein	87.489	724.897	3.98x10^-7	0.000297
FBtr0079520	CG13792-RA			170.991	1806.723	6.82E-05	0.00353
FBtr0079527	CG1706			317.33	944.678	0.00287	0.0259
FBtr0079533	CG7356-RA	Tg	Transglutaminase	3458.67	1292.898	0.00139	0.0168
FBtr0079548	CG12560			2326.366	794.797	0.000267	0.00713
FBtr0079602	CG14275-RA			902.248	161.065	0.00284	0.0258
FBtr0079607	CG31901-RA	Mur29B	Mucin related 29B	222.169	1016.181	0.00557	0.0386
FBtr0079649	CG17292-RA			73.5	193.122	0.000568	0.0106
FBtr0079676	CG33194-RA	CheA29a	Chemosensory protein A 29a	146.217	70.936	0.000653	0.0114
FBtr0079678	CG10595			8032.115	3402.503	0.00183	0.0201
FBtr0079679	CG10595			2603.836	1127.336	0.00113	0.015
FBtr0079680	CG10595			6538.237	2980.742	0.00142	0.017
FBtr0079684	CG13091-RA			54.029	152.832	0.000206	0.00634
FBtr0079701	CG13095-RA	Bace	beta-site APP-cleaving enzyme	133.823	1027.34	0.000618	0.0111
FBtr0079711	CG13397-RA			5191.923	2376.079	0.00387	0.0309
FBtr0079731	CG9314-RA			129.749	261.441	0.000128	0.00511
FBtr0079754	CG9494-RA	Tsp29Fa	Tetraspanin 29Fa	1261.966	4903.48	2.23x10^-6	0.000517
FBtr0079755	CG9496-RB	Tsp29Fb	Tetraspanin 29Fb	5302.14	16440.697	4.69x10^-6	0.000945
FBtr0079756	CG9496-RA	Tsp29Fb	Tetraspanin 29Fb	2210.825	8356.877	3.94x10^-6	0.000813
FBtr0079785	CG9541-RA			160.091	1620.693	3.28x10^-7	0.000255
FBtr0079797	CG3694-RC	Gy30A	G protein γ30A	506.146	1330.196	0.000128	0.00512
FBtr0079816	CG17011-RA	lectin-30A		32.975	181.97	0.000276	0.00721
FBtr0079830	CG17855-RA			265.176	582.047	0.00132	0.0164
FBtr0079837	CG3858-RA	gcm2		2302.206	976.957	0.00187	0.0203
FBtr0079860	CG4405-RB	jp	junctophilin	761.986	306.128	0.00593	0.0401
FBtr0079902	CG13124-RA			4916.838	2323.319	0.00173	0.0193
FBtr0079934	CG4778-RA	obst-B	obstructor-B	11918.047	5398.384	0.00221	0.0222
FBtr0079943	CG4839-RB			318.341	1140.53	7.03x10^-6	0.00116

FBtr0079963		Sur		1022.092	402.434	0.000388	0.00861
FBtr0080058	CG5375-RA			418.526	895.595	4.75E-05	0.00293
FBtr0080109	CG6431			173.869	57.626	0.000855	0.0131
FBtr0080124	CG7279-RA	Lip1	Lipase 1	3832.825	8245.565	0.000378	0.00851
FBtr0080125	CG7300-RB			2247.807	573.068	0.000511	0.0102
FBtr0080131	CG7329			44.217	91.61	0.00294	0.0262
FBtr0080184	CG17137-RA	Porin2		41.393	116.101	0.00328	0.028
FBtr0080194	CG16854			285.046	94.157	0.00118	0.0154
FBtr0080201	CG4779-RA	hgo	homogentisate 1,2-dioxygenase	1762.944	596.465	0.00368	0.0301
FBtr0080258		Pde1c		388.665	976.755	5.21x10^-7	0.000308
FBtr0080273	CG31704-RA			183.848	851.79	0.000165	0.00562
FBtr0080275	CG14934-RA	Mal-B1	Maltase B1	832.186	3700.644	0.000225	0.00664
FBtr0080281	CG16963-RA	Cry	Crystallin	110.027	824.141	0.00197	0.0209
FBtr0080294	CG14945-RB			2279.862	954.042	0.00257	0.0244
FBtr0080297	CG14947-RA			111.511	1235.656	1.62x10^-6	0.00044
FBtr0080307	CG6785-RA			5646.589	2732.754	0.000362	0.00837
FBtr0080321	CG31757			765.384	2132.179	7.13E-05	0.00364
FBtr0080324	CG31758			1475.491	3370.002	0.000606	0.0109
FBtr0080336	CG17211-RA			7660.672	3314.019	0.00125	0.016
FBtr0080338	CG31760-RA			52.67	128.787	0.00133	0.0164
FBtr0080362	CG6618-RA	Patsas		651.161	1508.911	0.000685	0.0117
FBtr0080371	CG17024-RA			186.243	465.624	0.000851	0.0131
FBtr0080389	CG31764-RB	vir-1	virus-induced RNA 1	3589.372	7788.166	0.00162	0.0186
FBtr0080391	CG31764-RC	vir-1	virus-induced RNA 1	2147.297	7663.062	0.00138	0.0167
FBtr0080408	CG17036-RA			162.953	585.425	0.00332	0.0283
FBtr0080433	CG5204-RA			98.377	198.561	0.000376	0.00851
FBtr0080450	CG5945-RA			29.409	90.796	0.00363	0.0298
FBtr0080452	CG16820-RA			726.306	2220.513	0.000912	0.0136
FBtr0080487	CG15482-RA			65.496	385.272	5.66x10^-7	0.000313
FBtr0080503	CG16849			54.079	253.471	0.00576	0.0394
FBtr0080504	CG31846			75.107	555.769	7.87E-05	0.00378
FBtr0080505	CG16850			128.941	556.282	0.000266	0.00713
FBtr0080523	CG16957-RA			56.583	162.241	0.000146	0.00535
FBtr0080549	CG7916-RA			662.901	3525.954	0.000461	0.0095
FBtr0080550	CG7953-RA			1139.779	3652.137	0.00753	0.0472
FBtr0080551	CG7968-RA			277.729	1780.484	0.000501	0.01
FBtr0080554	CG16869-RA	Ance-2		165.536	473.269	0.000211	0.00644
FBtr0080563	CG8997-RA			1346.799	9243.867	0.000474	0.00968

FBtr0080580	CG31814-RA			59.17	149.691	0.00318	0.0274
FBtr0080583	CG31841			167.453	80.424	0.0051	0.0366
FBtr0080584	CG31765			198.344	92.966	0.00485	0.0356
FBtr0080585	CG33119-RA	nimB1	nimrod B1	1085.616	353.815	0.00582	0.0398
FBtr0080590	CG4501-RA	bgm	bubblegum	3176.583	1563.477	0.00278	0.0256
FBtr0080596	CG16879-RA			2040.317	633.41	0.000951	0.0138
FBtr0080607	CG31840			103.243	30.65	0.00529	0.0374
FBtr0080608		I(2)32Fa		463.018	119.635	0.000914	0.0136
FBtr0080610	CG8930-RA	rk	rickets	471.089	228.852	0.00083	0.013
FBtr0080656	CG15282-RA			3828.103	1738.511	0.0061	0.0409
FBtr0080670	CG4691-RA			28.962	67.523	0.00015	0.00546
FBtr0080685	CG15279-RB			785.101	2128.15	0.000375	0.00851
FBtr0080690	CG4650			81.572	39.996	0.00178	0.0198
FBtr0080697	CG15274			915.773	1945.575	0.000563	0.0105
FBtr0080701	CG3506			716.941	3261.176	2.23E-05	0.00206
FBtr0080704	CG15269-RA			1376.924	450.278	0.000362	0.00838
FBtr0080714	CG3994-RA	ZnT35C		5052.705	2385.737	0.00306	0.0268
FBtr0080716	CG4168			98.071	205.634	0.000529	0.0102
FBtr0080753	CG11865-RA			123.481	37.759	1.21E-05	0.00156
FBtr0080763	CG18801-RA	Ku80		749.805	1654.069	0.000318	0.00769
FBtr0080785	CG15255-RA			151.878	1681.41	0.000111	0.00466
FBtr0080794	CG4793			348.454	57.873	0.000178	0.00594
FBtr0080869	CG13260			100.231	625.912	7.46E-05	0.00375
FBtr0080888	CG13263-RA	Cyt-c-d	Cytochrome c distal	244.635	657.465	5.54E-05	0.00313
FBtr0080909	CG13270-RA	Ugt36Ba		3217.934	7930.803	4.54E-05	0.00289
FBtr0080923	CG6012-RA			150.461	1177.171	9.09x10^-6	0.0013
FBtr0080925	CG31810-RA			356.402	745.336	0.00292	0.0262
FBtr0080951		beat-IIIb		190.941	484.698	7.07x10^-8	0.000173
FBtr0080961	CG12621			485.179	1062.312	0.000197	0.00621
FBtr0080981	CG5050-RA			63.429	135.626	0.000165	0.00562
FBtr0081004	CG6639-RA			45.786	145.409	0.000963	0.0139
FBtr0081035	CG5758-RC			662.86	2834.126	2.04x10^-8	0.000117
FBtr0081036	CG5758-RA			1106.098	4521.696	4.65x10^-7	0.000307
FBtr0081044	CG31785			56.657	199.917	0.00112	0.015
FBtr0081068	CG10178-RA			2994.474	1304.229	0.000943	0.0138
FBtr0081105	CG17322-RA			950.883	225.505	0.00119	0.0154
FBtr0081118	CG33120-RA			354.296	130.694	0.00642	0.0423

FBtr0081124	CG10348			3013.006	980.231	0.003	0.0265
FBtr0081136	CG15169-RA			440.163	58.522	1.52x10^-6	0.000434
FBtr0081149	CG10493-RA	Phlpp	PH domain leucine-rich repeat protein phosphatase	651.726	1636.705	0.000232	0.00678
FBtr0081184	CG15170-RA			30.151	77.029	0.00632	0.0419
FBtr0081197	CG13086-RA			145.157	333.26	0.00599	0.0405
FBtr0081206	CG9994-RA	Rab9		513.586	6340.248	1.53x10^-7	0.000218
FBtr0081208	CG10237-RB			879.71	361.579	0.00699	0.045
FBtr0081228	CG17566-RA	γTub37C	γ-Tubulin at 37C	116.849	265.403	0.00111	0.0149
FBtr0081241	CG13083			1323.334	230.136	4.53x10^-7	0.00031
FBtr0081242	CG13083-RB			2003.591	296.963	4.30x10^-7	0.000307
FBtr0081251	CG13082-RA			9022.819	3714.495	0.00613	0.041
FBtr0081252	CG13081-RA			152.506	59.954	0.000463	0.00951
FBtr0081256	CG13078-RA			41.222	96.4	0.00113	0.0151
FBtr0081302	CG16772-RA			62.312	180.137	0.0035	0.0292
FBtr0081326	CG13968			294.75	6900.03	7.73x10^-9	0.000133
FBtr0081334	CG10722-RB	nesd	nessun dorma	1966.812	4856.548	4.55E-05	0.00289
FBtr0081336	CG10723-RA	Kua		549.565	1731.216	5.48x10^-7	0.000313
FBtr0081350	CG10659-RA			157.323	1805.424	1.76E-05	0.00187
FBtr0081359	CG11019			760.029	1764.858	0.000202	0.00628
FBtr0081366	CG15130			112.054	226.155	0.00704	0.0453
FBtr0081368	CG10947			355.763	1461.098	0.000053	0.00306
FBtr0081371	CG16798-RA			4419.747	1944.257	0.000244	0.00697
FBtr0081397	CG1864-RB	Hr38	Hormone receptor-like in 38	68.876	231.291	0.00306	0.0268
FBtr0081398	CG1864-RC	Hr38	Hormone receptor-like in 38	96.952	233.726	0.000808	0.0128
FBtr0081406	CG17470-RA			341.019	126.091	0.00406	0.0321
FBtr0081430	CG14401-RA			666.656	311.037	0.00524	0.0371
FBtr0081449	CG14400-RA			155.569	51.103	1.34E-05	0.00166
FBtr0081517	CG8665-RA			2220.218	5101.703	1.88E-05	0.00189
FBtr0081519	CG8663-RC	nrv3	nervana 3	1837.714	4348.506	0.00111	0.0149
FBtr0081520	CG8663-RD	nrv3	nervana 3	457.222	938.339	0.00517	0.0368
FBtr0081521	CG8663-RB	nrv3	nervana 3	449.394	1003.3	0.000741	0.0123
FBtr0081541	CG31146-RD	Nlg1	Neuroligin 1	1919.131	610.771	0.000774	0.0126
FBtr0081542	CG14597			244.13	804.849	0.000754	0.0124
FBtr0081543	CG32465			248.272	810.177	0.000272	0.00718

FBtr0081545	CG1257-RA	α-Est3	α-Esterase-3	1120.327	3646.163	3.14E-05	0.00241
FBtr0081554	CG1287-RA			87.211	300.513	0.00187	0.0203
FBtr0081555	CG1128			931.467	4614.674	1.41E-05	0.00167
FBtr0081628	CG1979-RA			26.676	99.457	1.41E-05	0.00167
FBtr0081672	CG15186-RA			744.398	306.958	0.00113	0.015
FBtr0081674	CG15186-RC			700.842	283.523	0.00141	0.017
FBtr0081704	CG33202-RB	drp11		155.919	514.033	5.66E-05	0.00316
FBtr0081744	CG10086-RA			361.004	1394.945	2.65E-05	0.0022
FBtr0081762	CG10445			75.915	155.286	0.000491	0.00986
FBtr0081773	CG3014-RA			246.165	95.582	0.00146	0.0172
FBtr0081774	CG18744			49.206	260.275	0.000378	0.0085
FBtr0081775	CG18746-RA			93.061	614.377	4.77E-05	0.00292
FBtr0081777	CG18745-RA			135.757	345.228	0.00542	0.038
FBtr0081780	CG3027-RA	pyd3		4482.722	1730.749	0.00223	0.0223
FBtr0081781	CG3250			331.94	138.636	0.00326	0.0278
FBtr0081857		Poxm		923.372	390.485	0.00227	0.0225
FBtr0081875	CG7994			77.636	473.27	0.000066	0.00345
FBtr0081876	CG8007			54.121	441.323	8.41x10^-6	0.00127
FBtr0081877	CG8007			213.641	705.585	0.000966	0.0139
FBtr0081942	CG13318-RA			226.782	710.996	0.000785	0.0126
FBtr0081943	CG11768-RA			249.692	1324.921	0.000122	0.00496
FBtr0081961	CG11977			238.544	111.943	0.000842	0.0131
FBtr0082011	CG31100-RA			1944.984	941.227	0.00226	0.0225
FBtr0082014	CG11966-RA			13951.999	6798.656	0.000329	0.00783
FBtr0082025	CG18473-RA			2310.33	932.099	0.000923	0.0136
FBtr0082041	CG9363-RB			257.972	725.031	0.00142	0.017
FBtr0082042	CG9363-RA			146.513	312.304	0.00137	0.0167
FBtr0082080	CG8348-RA	Dh44	Diuretic hormone 44	113.05	619.092	9.55E-05	0.0043
FBtr0082151	CG12806-RA	Teh1	tipE homolog 1	322.399	1285.922	0.000508	0.0101
FBtr0082159	CG12946-RA	Whamy		383.403	1442.011	0.000203	0.0063
FBtr0082195	CG6208-RA			141.633	412.263	0.000108	0.00457
FBtr0082203	CG12812-RA	Fancl		109.423	309.694	0.000221	0.00657
FBtr0082249	CG14680			150.031	329.257	0.000259	0.00709
FBtr0082315	CG6515-RA	Takr86C	Tachykinin-like receptor at 86C	96.951	444.103	0.000756	0.0124
FBtr0082323	CG6465-RA			3463.264	1322.47	0.00179	0.0198
FBtr0082335	CG14695-RA			180.283	654.057	0.00285	0.0258
FBtr0082337	CG4739-RA	Ugt86Dc		168.174	651.596	1.68E-05	0.00181
FBtr0082340	CG4772-RA	Ugt86Dh		533.854	2873.509	4.33E-05	0.00287
FBtr0082341	CG18577-RA			351.775	731.853	0.00171	0.0191

FBtr0082374	CG6644-RA	Ugt35a		2675.151	11736.407	1.12x10^-6	0.000366
FBtr0082375	CG6649-RA	Ugt35b		195.316	83.996	0.000885	0.0134
FBtr0082378	CG6658-RA	Ugt86Di		38.432	93.232	0.00155	0.018
FBtr0082385	CG5247-RA	Irbp	Inverted repeat-binding protein	907.695	2108.617	1.06x10^-6	0.000384
FBtr0082428	CG14720-RA			1054.277	264.823	0.000938	0.0137
FBtr0082436	CG18765			304.54	1739.954	1.26E-05	0.0016
FBtr0082439	CG6830-RA			898.694	6254.408	1.30x10^-6	0.000419
FBtr0082470	CG14723-RA	HisCl1	Histamine-gated chloride channel subunit 1	55.521	770.884	2.42E-05	0.00211
FBtr0082471	CG14723-RB	HisCl1	Histamine-gated chloride channel subunit 1	85.446	1057.975	3.04E-05	0.00239
FBtr0082472	CG14723-RC	HisCl1	Histamine-gated chloride channel subunit 1	48.606	709.503	2.16E-05	0.00205
FBtr0082531	CG17360-RA			1266.821	2669.873	0.000263	0.00713
FBtr0082550	CG4702-RA			20954.041	10451.499	0.00378	0.0305
FBtr0082551	CG14741			648.19	3194.57	1.27E-05	0.0016
FBtr0082564	CG11502-RB	svp	seven up	1048.151	501.997	0.000693	0.0118
FBtr0082569	CG4181-RA	GstD2	Glutathione S transferase D2	938.226	20451.816	1.64x10^-8	0.000141
FBtr0082570	CG4381-RA	GstD3	Glutathione S transferase D3	3994.702	9796.483	0.000529	0.0102
FBtr0082571	CG11512-RA	GstD4	Glutathione S transferase D4	325.306	994.57	0.000177	0.00592
FBtr0082573	CG4423-RA	GstD6	Glutathione S transferase D6	104.987	3353.07	9.42x10^-6	0.00133
FBtr0082574	CG4371-RA	GstD7	Glutathione S transferase D7	798.173	10562.622	9.53x10^-7	0.000355
FBtr0082575	CG4421-RA	GstD8	Glutathione S transferase D8	179.997	1446.985	0.000077	0.00376
FBtr0082582	CG4940			40.03	101.048	0.000886	0.0134
FBtr0082598	CG11466-RA	Cyp9f2		3672.054	8236.055	2.19E-05	0.00207
FBtr0082599	CG11466-RB	Cyp9f2		688.237	2128.992	1.58E-05	0.00178
FBtr0082603	CG10096-RA			84.272	203.753	0.000705	0.0119
FBtr0082607	CG10045-RA	GstD1	Glutathione S transferase D1	10266.338	26293.084	8.42x10^-6	0.00126
FBtr0082608	CG10091-RA	GstD9	Glutathione S transferase D9	1429.798	4515.095	0.0026	0.0246
FBtr0082609	CG18548-RA	GstD10	Glutathione S transferase D10	809.643	2503.336	0.00121	0.0156
FBtr0082610	CG10090-RA	Tim17a1		43.053	288.699	0.00079	0.0126
FBtr0082613	CG10041-RA			39.333	96.587	4.15E-05	0.00279
FBtr0082636	CG5834-RA	Hsp70Bb		4232.817	8525.526	0.00165	0.0187

		b					
FBtr0082650	CG14395			10221.039	3584.357	0.000268	0.00715
FBtr0082657	CG5724-RA			328.887	3925.562	5.37E-05	0.00309
FBtr0082659	CG5999			61.383	10565.303	9.20x10^-6	0.00131
FBtr0082660	CG10120-RB	Men	Malic enzyme	12415.408	26893.655	2.22E-05	0.00207
FBtr0082684	CG31298-RA	beat-Vb		137.664	62.153	0.00571	0.0391
FBtr0082689	CG31345-RA			559.918	5428.338	3.62E-05	0.00262
FBtr0082725	CG7381			1006.651	4457.543	9.50x10^-7	0.000362
FBtr0082740	CG8774-RB			1682.51	3895.355	0.000989	0.014
FBtr0082757	CG9792-RA	yellow-e		338.656	2172.029	9.49E-05	0.0043
FBtr0082758	CG17044			4917.845	1809.09	0.00287	0.0259
FBtr0082762	CG14375-RA	CCHa2	CCHamide-2	860.261	2036.262	0.000408	0.00887
FBtr0082773	CG8795-RA			657.976	178.502	0.000242	0.00694
FBtr0082775	CG8458-RA	wntD	wnt inhibitor of Dorsal	185.091	499.2	0.0035	0.0292
FBtr0082786	CG18290-RB	Act87E	Actin 87E	499.549	221.283	0.00143	0.0171
FBtr0082789	CG14369-RA			55.89	318.941	0.0048	0.0354
FBtr0082790	CG31337-RA			665.603	229.841	0.00608	0.0408
FBtr0082821	CG9345-RA	Adgf-C	Adenosine deaminase-related growth factor C	98.922	213.083	0.000968	0.0138
FBtr0082837	CG14363			65.261	28.975	0.000366	0.00843
FBtr0082888	CG3153-RB	Npc2b	Niemann-Pick type C-2b	4768.596	2279.192	0.00264	0.0247
FBtr0082890	CG14360-RA	Or88a	Odorant receptor 88a	66.591	156.199	0.00699	0.045
FBtr0082911	CG9913			115.169	4621.107	2.21x10^-8	0.0000945
FBtr0082913	CG14357			43.92	101.174	0.00409	0.0322
FBtr0082926	CG31321-RB			955.789	317.965	0.00435	0.0334
FBtr0082960	CG14853-RB			326.505	768.636	0.000519	0.0102
FBtr0082966	CG3505-RA			1373.914	664.129	0.00142	0.017
FBtr0082982	CG31313-RA			5575.17	2381.116	0.00462	0.0345
FBtr0083012	CG17304-RA			151.745	384.075	0.00357	0.0295
FBtr0083080	CG4843-RC	Tm2	Tropomyosin 2	819.628	334.161	0.00279	0.0257
FBtr0083102	CG6118			15136.278	6389.256	0.00376	0.0304
FBtr0083152	CG18519-RA			2248.106	931.712	0.00589	0.04
FBtr0083155	CG31296-RA			22.295	119.952	0.000668	0.0116
FBtr0083157	CG14872-RA			393.775	1342.149	0.00118	0.0154
FBtr0083248	CG9734-RD	glob1	globin 1	488.209	243.576	0.000139	0.00535
FBtr0083249	CG14877-RA			83.946	277.522	0.000732	0.0122
FBtr0083250	CG4316-RA	Sb	Stubble	1441.516	601.164	0.000438	0.0092
FBtr0083253	CG8925-RA			1140.937	514.799	0.00118	0.0154

FBtr0083254	CG8927-RA			630.972	1567.605	0.000199	0.00626
FBtr0083266	CG6898-RA	Zip3	Zinc/iron regulated transporter-related protein 3	1865.765	845.615	0.00468	0.0348
FBtr0083271	CG17930-RA			1114.244	3684.553	0.000164	0.00565
FBtr0083306	CG14900			3997.226	1330.028	0.00114	0.015
FBtr0083329	CG17562-RA			1308.624	372.847	0.00144	0.0171
FBtr0083330	CG17560-RA			934.132	318.365	0.00506	0.0365
FBtr0083354	CG14907-RA			1214.571	5008.832	2.56x10^-6	0.000569
FBtr0083355	CG14906			494.192	1895.097	5.15E-05	0.00303
FBtr0083367	CG31447-RA	MESK4	Misexpression suppressor of KSR 4	5067.846	2260.664	0.00723	0.046
FBtr0083372	CG8907-RA			1376.004	4691.793	2.55E-05	0.00213
FBtr0083379	CG8956-RD	Ahcy89E	Adenosylhomocysteinase 89E	940.933	469.244	0.00402	0.0318
FBtr0083512	CG16766-RA	TyrRII	Tyramine receptor II	107.964	401.791	0.000068	0.00353
FBtr0083530	CG14318			2611.017	930.95	0.00654	0.0429
FBtr0083532	CG7431-RA	TyrR	Tyramine receptor	231.584	624.877	2.48E-05	0.00213
FBtr0083542	CG7847-RA	sr	stripe	3607.646	1685.239	0.000555	0.0104
FBtr0083581	CG7675-RA			21720.595	10248.854	0.00672	0.0439
FBtr0083582	CG7675-RB			1969.004	655.238	0.00369	0.0301
FBtr0083584	CG7672-RA	gl	glass	207.331	505.257	0.000659	0.0115
FBtr0083587	CG15803			178.668	411.008	0.00275	0.0255
FBtr0083588	CG31235-RA			2803.856	991.727	0.00515	0.0368
FBtr0083589	CG7125-RA	PKD	Protein Kinase D	9546.382	4497.729	0.000607	0.0109
FBtr0083617	CG7208-RA			164.561	503.595	0.00487	0.0357
FBtr0083618	CG7208-RB			149.36	439.484	0.000394	0.00867
FBtr0083624	CG7676-RA	cona	corona	127.48	256.436	0.000684	0.0117
FBtr0083654	CG10864-RA			1542.411	707.905	5.11x10^-6	0.000982
FBtr0083678	CG7720-RB			2615.917	1047.655	0.00188	0.0203
FBtr0083694	CG7695-RA			760.353	212.6	0.000316	0.00766
FBtr0083711	CG14285-RA			2086.589	729.403	0.00124	0.0159
FBtr0083729	CG6040-RA			8288.925	3873.911	0.000265	0.00713
FBtr0083730	CG11821-RA	Cyp12a5		195.439	1119.297	0.00201	0.0211
FBtr0083736	CG3772-RA	cry	cryptochrome	322.368	3056.951	1.89x10^-6	0.000491
FBtr0083755	CG3734-RA			1007.307	3930.556	0.0014	0.0169
FBtr0083756	CG18493-RA			1833.732	8241.409	5.09E-05	0.00301
FBtr0083762	CG31221-RA			125.064	987.23	0.000246	0.00694
FBtr0083788	CG7535-RB	GluClα		750.588	359.336	0.00459	0.0343
FBtr0083791	CG11453-RA			868.971	6189.535	9.59E-05	0.00427
FBtr0083820	CG4733			4173.217	1468.67	0.00249	0.0239

FBtr0083852	CG4468-RA			158.414	690.034	0.000164	0.00564
FBtr0083868	CG5030			294.127	608.36	0.000148	0.0054
FBtr0083886	CG5115			79.056	180.706	4.47E-05	0.00289
FBtr0083894	CG4335-RA			1232.007	449.394	0.000293	0.00742
FBtr0083923	CG31203			148.013	325.873	0.000529	0.0102
FBtr0083932	CG3856-RA	Oamb	Octopamine receptor in mushroom bodies	59.962	310.441	4.64E-05	0.00289
FBtr0083933	CG3856-RB	Oamb	Octopamine receptor in mushroom bodies	85.188	205.494	0.00752	0.0472
FBtr0083934	CG3856-RC	Oamb	Octopamine receptor in mushroom bodies	41.752	367.108	1.62E-05	0.00177
FBtr0083936	CG4058-RB	Nep4	Neprilysin 4	1368	560.913	0.000969	0.0138
FBtr0083938	CG18039-RA	KaiRIA		4036.541	1934.315	0.00517	0.0368
FBtr0083957	CG15690			492.945	1033.67	0.00109	0.0148
FBtr0083968	CG15696-RA			553.578	188.775	6.09E-05	0.00329
FBtr0083987	CG3822-RA			3510.644	1281.579	0.00145	0.0172
FBtr0084001	CG5697-RA			512.641	194.806	0.000218	0.00657
FBtr0084044	CG31207-RA			41.355	118.269	1.93x10^-6	0.000487
FBtr0084053	CG5911-RB	ETHR		406.312	1001.318	5.65E-05	0.00317
FBtr0084054	CG5911-RA	ETHR		320.303	644.209	0.000631	0.0112
FBtr0084098	CG10823-RA	SIFR	SIFamide receptor	62.47	136.744	0.000581	0.0106
FBtr0084101	CG3301-RB			43.662	109.344	0.00168	0.0189
FBtr0084123	CG6534-RA	slou	slouch	2716.74	1245.223	0.00113	0.015
FBtr0084128	CG31198-RA			4507.782	12851.177	0.00243	0.0236
FBtr0084137	CG31431-RA			6715.448	14611.871	0.000146	0.00536
FBtr0084138	CG31178-RA			95.018	290.01	0.000541	0.0103
FBtr0084140	CG33092-RA	P5CDh2	delta-1-Pyrroline-5-carboxylate dehydrogenase 2	57.697	431.263	0.000101	0.00435
FBtr0084147	CG31465-RA			42.322	182.236	0.000036	0.00263
FBtr0084150	CG17843-RA			4988.687	2148.432	0.00175	0.0195
FBtr0084153	CG17820-RA	fit	female-specific independent of transformer	120.906	12867.788	9.83x10^-8	0.000211
FBtr0084154	CG31174-RA			83.445	213.473	0.00254	0.0242
FBtr0084169	CG18389-RA	Eip93F		87.421	534.17	2.05E-05	0.002
FBtr0084179	CG13408-RA			226.498	552.531	9.18E-05	0.00425
FBtr0084180	CG5791-RA			125.568	336.803	0.00127	0.0161
FBtr0084194	CG33334			1771.29	710.888	0.00332	0.0282
FBtr0084195	CG5740			2654.299	1058.386	0.00125	0.016
FBtr0084215	CG7069-RA			42.431	88.668	0.00661	0.0433
FBtr0084234	CG13857-RA			773.426	278.111	0.00132	0.0164
FBtr0084240	CG5386-RA			224.753	85.478	0.000204	0.00631
FBtr0084242	CG5391-RA			999.741	392.249	0.00375	0.0304

FBtr0084243	CG13858			819.393	249.407	9.04E-05	0.00422
FBtr0084244	CG13859			1272.809	372.52	0.00138	0.0167
FBtr0084245	CG13860			1220.51	376.557	0.00137	0.0167
FBtr0084246	CG13861			1842.113	615.471	0.00188	0.0203
FBtr0084259	CG7046-RA			609.057	236.01	0.00536	0.0377
FBtr0084260	CG6919-RA	oa2	octopamine receptor 2	211.869	1242.079	8.84E-05	0.00414
FBtr0084292	CG5376-RA			2707.028	1044.828	0.00748	0.047
FBtr0084296	CG13847			1525.503	564.927	0.00104	0.0144
FBtr0084297	CG13848-RA	pinta	prolonged depolarization afterpotential (PDA) is not apparent	1591.801	3493.625	0.00209	0.0215
FBtr0084304	CG12800-RA	Cyp6d4		1414.572	5729.763	0.000474	0.00967
FBtr0084305	CG6972-RA			6569.077	2856.901	0.00713	0.0456
FBtr0084343	CG6688-RA			928.786	332.919	0.00243	0.0236
FBtr0084351	CG17109-RA			2860.917	14950.953	6.52x10^-6	0.0011
FBtr0084354	CG13830			1032.979	2172.93	0.000281	0.0073
FBtr0084355	CG17111			562.12	198.948	0.00348	0.0291
FBtr0084361	CG17121-RA			10867.194	4748.457	0.0036	0.0297
FBtr0084365	CG13834			213.009	486.967	0.00668	0.0436
FBtr0084419	CG16732-RA			86.738	409.159	0.00128	0.0161
FBtr0084420	CG10170-RA			755.78	4708.877	2.56E-05	0.00213
FBtr0084427	CG4374			2135.081	804.613	0.00018	0.00595
FBtr0084431	CG4408-RA			859.234	2409.268	2.87E-05	0.0023
FBtr0084433	CG10152-RA	beat-IV		268.936	662.468	0.000045	0.0029
FBtr0084434	CG13822-RA			1268.405	261.759	0.00354	0.0294
FBtr0084439	CG18754			111.495	349.65	0.000298	0.00748
FBtr0084440	CG16705-RA	SPE	Spatzle-Processing Enzyme	3973.746	1940.428	0.00734	0.0466
FBtr0084444	CG10301			257.881	116.704	0.00437	0.0335
FBtr0084454	CG10371-RA	Plip	PTEN-like phosphatase	217.541	87.114	0.00311	0.0271
FBtr0084457	CG10374-RB	Lsd-1	Lipid storage droplet-1	3582.759	1592.908	0.00751	0.0471
FBtr0084472	CG10250-RA	nau	nautilus	2257.608	735.263	0.00182	0.02
FBtr0084474	CG10251			129.011	259.226	0.000266	0.00713
FBtr0084484	CG16723			24.165	111.683	0.000675	0.0116
FBtr0084519	CG5338-RB	RpS19b	Ribosomal protein S19b	523.396	1052.07	0.000691	0.0117
FBtr0084549	CG6173-RA	Kal1	Kallmann syndrome 1 ortholog	1141.145	512.513	0.0002	0.00626
FBtr0084589	CG5436-RA	Hsp68	Heat shock protein 68	1067.784	2542.53	0.000257	0.00712
FBtr0084610	CG33339			1092.431	265.127	0.000536	0.0102
FBtr0084611	CG33340-RA			459.623	135.437	6.23E-05	0.00334

FBtr0084612	CG13613			411.606	106.01	0.000094	0.00428
FBtr0084613	CG33341-RA			226.439	88.203	0.000204	0.00631
FBtr0084614	CG13614-RA			2217.904	697.942	6.53E-05	0.00344
FBtr0084615	CG13614			1671.127	513.875	3.21E-05	0.00243
FBtr0084617	CG13615-RA			3340.714	1032.695	0.000792	0.0126
FBtr0084618	CG13616-RA			2999.646	1155.919	0.00676	0.044
FBtr0084619	CG5610-RA	nAcRα-96Aa	nicotinic Acetylcholine Receptor alpha 96Aa	648.412	270.484	0.00425	0.033
FBtr0084620	CG5768-RA			1988.568	577.548	0.000958	0.0139
FBtr0084621	CG17780-RB			416.313	122.953	0.00195	0.0208
FBtr0084622	CG17780-RA			3790.824	1179.376	2.74E-05	0.00224
FBtr0084623	CG17781-RA			2499.228	737.34	7.71E-05	0.00374
FBtr0084624	CG17782-RA			2983.107	903.135	0.0017	0.0191
FBtr0084625	CG18669			260.787	75.266	0.000216	0.00656
FBtr0084626	CG17784-RA			808.321	187.37	0.000326	0.0078
FBtr0084627	CG5762-RA			1241.184	326.618	0.000752	0.0124
FBtr0084634	CG5715-RA			200.02	472.704	0.00568	0.039
FBtr0084639	CG6844-RA	nAcRα-96Ab	nicotinic Acetylcholine Receptor alpha 96Ab	823.499	400.05	0.00588	0.04
FBtr0084643	CG13618-RA			372.494	1527.915	0.00395	0.0315
FBtr0084659	CG6677-RB	ash2	absent, small, or homeotic discs 2	199.483	467.113	0.00451	0.0339
FBtr0084665	CG31125-RA			991.83	2145.418	0.000775	0.0126
FBtr0084680	CG13622			2225.534	920	0.00321	0.0276
FBtr0084689	CG6863-RB	tok	tolkin	3502.604	1377.123	0.00179	0.0198
FBtr0084691	CG6868-RA	tld	tolloid	425.985	1069.66	0.000144	0.0054
FBtr0084694	CG13632			1599.255	473.375	0.000321	0.00772
FBtr0084695	CG6879			6414.171	2471.233	0.00201	0.0211
FBtr0084702	CG13636-RA			259.12	771.544	0.00177	0.0196
FBtr0084703	CG7005-RA	Esp	Epidermal stripes and patches	7849.756	3666.604	0.00467	0.0347
FBtr0084707	CG7016-RA			1532.108	603.766	0.000892	0.0134
FBtr0084722	CG13643			426.855	197.08	0.00487	0.0357
FBtr0084723	CG31121-RA			5531.827	2636.636	0.00199	0.021
FBtr0084742	CG13634-RA			698.855	227.724	0.00146	0.0173
FBtr0084751	CG13646-RA			33.191	139.209	0.000568	0.0105
FBtr0084798	CG31422			468.215	132.937	7.69E-05	0.00377
FBtr0084807	CG31103			1820.307	607.88	0.000821	0.0129
FBtr0084821	CG11878-RA			32.958	66.877	0.00417	0.0325
FBtr0084825	CG31104-RA			79.363	891.54	6.37E-05	0.00337
FBtr0084827	CG11893-RA			48.207	154.64	0.00162	0.0186
FBtr0084828	CG13659-RA			129.108	1417.293	1.58E-05	0.00177

FBtr0084829	CG31370			316.879	844.819	0.00284	0.0258
FBtr0084849	CG10675-RA	CHKov2		1010.154	350.78	0.000156	0.00554
FBtr0084851	CG10562-RA			322.906	4276.733	1.05E-05	0.00144
FBtr0084857	CG10550-RB			3019.017	6096.971	0.000423	0.00909
FBtr0084858	CG10550-RC			302.029	646.984	0.000778	0.0126
FBtr0084859	CG10550			319.438	678.117	0.000214	0.00651
FBtr0084860	CG31288-RA			661.116	2493.482	0.00322	0.0276
FBtr0084861	CG31097			50.14	143.909	0.00368	0.0301
FBtr0084871	CG13664			2022.515	4870.358	0.000236	0.00682
FBtr0084872	CG10421			2734.073	5712.82	0.000312	0.00761
FBtr0084913	CG14545-RA			350.126	820.792	0.00346	0.0291
FBtr0084942	CG31089-RA			43.588	132.021	0.000551	0.0104
FBtr0084950	CG14541			95.206	207.444	0.000387	0.00863
FBtr0084955	CG8333-RA	HLHmy	E(spl) region transcript mγ	7307.704	15213.535	3.93E-05	0.0027
FBtr0084979	CG6096-RA	HLHm5	E(spl) region transcript m5	705.319	288.872	0.00745	0.047
FBtr0085014	CG14238-RA			140.245	315.737	0.00182	0.02
FBtr0085023	CG6490			259.073	669.095	0.000329	0.00784
FBtr0085048	CG6438-RA	amon	amontillado	249.356	564.241	0.00692	0.0447
FBtr0085050		beat-VII		271.094	1235.612	0.000914	0.0135
FBtr0085051		beat-VII		272.247	1267.719	0.000806	0.0128
FBtr0085052	CG14248			155.7	654.185	0.000162	0.00562
FBtr0085110	CG5889-RA	Men-b	Malic enzyme b	2098.308	5534.193	0.00134	0.0165
FBtr0085112	CG5896-RB	grass	Gram-positive Specific Serine protease	1073.368	339.164	0.00311	0.0271
FBtr0085117	CG31066			684.441	278.986	0.00176	0.0195
FBtr0085181	CG5984-RA			2838.645	849.912	0.00755	0.0473
FBtr0085197	CG31057-RA	tau		1901.222	4071.077	0.0037	0.0302
FBtr0085198	CG31058-RA			507.363	2582.8	0.00151	0.0177
FBtr0085202	CG5639-RA			1015.392	2479.294	0.000499	0.00999
FBtr0085307	CG9989-RA			1133.67	407.517	0.00784	0.0483
FBtr0085348	CG33203-RC			109.866	220.159	0.00028	0.0073
FBtr0085349	CG14523-RA			1559.173	646.061	0.00203	0.0212
FBtr0085390	CG11899-RA			770.73	3447.092	3.73E-05	0.00263
FBtr0085403	CG11951-RA			681.74	270.793	0.000025	0.00215
FBtr0085408	CG14509			1562.564	3641.108	4.65E-05	0.00289
FBtr0085427	CG2010-RB			1916.762	631.306	0.0019	0.0205
FBtr0085451	CG18287-RA	ppk19	pickpocket 19	120.282	48.501	0.00751	0.0471
FBtr0085455	CG15505-RA	Obp99d	Odorant-binding protein 99d	415.877	128.322	0.00532	0.0376
FBtr0085462	CG7592-RA	Obp99b	Odorant-binding protein 99b	584.23	166.294	0.00723	0.046
FBtr0085466	CG7577-RA	ppk20	pickpocket 20	103.271	40.17	0.00536	0.0377

FBtr0085485	CG7802-RA	neo	neyo	12141.813	5779.596	0.000307	0.00755
FBtr0085488	CG31009-RA	Cad99C		7836.407	3833.751	0.00109	0.0148
FBtr0085494	CG31038-RA			8592.789	3745.945	0.00098	0.0139
FBtr0085495	CG31038-RB			481.909	175.937	0.0017	0.0191
FBtr0085497	CG31038-RC			3985.147	1816.859	0.00132	0.0164
FBtr0085503	CG15522-RA			83.536	1317.322	2.10x10^-6	0.000513
FBtr0085545	CG7896-RA			6632.671	2376.115	0.00101	0.0141
FBtr0085567	CG15529-RA			398.139	187.595	0.00168	0.0189
FBtr0085601	CG15527-RA	RpS28a	Ribosomal protein S28a	38.883	108.122	0.000405	0.00883
FBtr0085653	CG1546-RA	PH4αSG2	prolyl-4-hydroxylase-alpha SG2	5325.563	1427.007	0.000573	0.0106
FBtr0085683	CG2239-RC	jdp		881.576	360.021	0.00229	0.0226
FBtr0085687	CG31371			1921.824	729.919	0.00625	0.0416
FBtr0085688	CG9728-RA	PH4αNE1	prolyl-4-hydroxylase-alpha NE1	643.846	256.978	0.00398	0.0316
FBtr0085698	CG1342-RA	Spn100A	Serpin 100A	20423.444	9629.781	0.00115	0.0152
FBtr0085708	CG15544-RA			154.147	73.781	0.00133	0.0164
FBtr0085715	CG15547-RA			1662.806	3356.561	0.00254	0.0242
FBtr0085737	CG15556-RA			460.617	226.937	0.00192	0.0206
FBtr0085739	CG11318-RA			341.765	917.873	0.00329	0.0281
FBtr0085753	CG1470-RA	Gycβ100B	Guanylyl cyclase β-subunit at 100B	273.556	974.198	2.28E-05	0.00207
FBtr0085761	CG3669			281.356	115.182	0.004	0.0317
FBtr0085769	CG31005-RA	qless		2779.908	1312.746	0.000833	0.013
FBtr0085785	CG1607-RA			4348.254	2013.89	0.00113	0.0151
FBtr0085867	CG11550-RA			398.835	172.001	0.00561	0.0387
FBtr0085990	CG8335-RA			80.089	193.226	0.000177	0.00591
FBtr0086046	CG7796			856.924	1901.536	0.000107	0.00455
FBtr0086142	CG30446-RA	Tdc2	Tyrosine decarboxylase 2	741.585	352.263	5.23E-05	0.00305
FBtr0086160	CG15236-RB			96.067	47.689	0.00537	0.0377
FBtr0086163	CG9456			950.777	337.496	0.0022	0.0222
FBtr0086164	CG9460-RA	Spn42De	Serpin 42De	4296.325	1731.832	0.00665	0.0435
FBtr0086179	CG12847-RA	Tsp42Ec	Tetraspanin 42Ec	1005.396	4381.176	0.000514	0.0102
FBtr0086218	CG13424-RA	lms	lateral muscles scarcer	956.997	339.535	0.00355	0.0295
FBtr0086235	CG13437-RA			112.386	278.851	0.000973	0.0138
FBtr0086238	CG13439-RA	dpr	defective proboscis extension response	849.778	3662.651	3.81E-05	0.00266
FBtr0086253	CG11175-RA	Rcd6	Reduction in Cnn dots 6	7397.346	2726.214	0.00062	0.0111
FBtr0086266	CG30148-RA			224.565	90.018	0.000155	0.00551
FBtr0086275	CG8908-RB			79.63	274.85	0.000484	0.00983
FBtr0086290	CG33041			693.221	247.521	0.000536	0.0102

FBtr0086316	CG11048-RA	Efhc1.2	EFHC1 homologue 2	200.159	85.506	9.83E-05	0.0043
FBtr0086321	CG11209-RA	ppk6	pickpocket 6	42.141	281.066	1.79x10^-6	0.000477
FBtr0086323	CG13869-RA			415.62	124.924	0.00361	0.0298
FBtr0086325	CG16898-RA			163.633	1896.045	0.000102	0.00437
FBtr0086344	CG12501-RA	Or56a	Odorant receptor 56a	28.087	80.88	0.000304	0.0075
FBtr0086463	CG15120-RA			366.622	4839.617	1.75x10^-7	0.0002
FBtr0086469	CG18367-RA			147.652	56.637	0.00607	0.0408
FBtr0086471	CG15125-RA			33.285	80.733	0.00117	0.0153
FBtr0086491	CG15905			1831.25	720.008	0.00431	0.0333
FBtr0086522	CG10062-RA			243.238	692.187	0.00126	0.016
FBtr0086524	CG10081-RA			29.177	1896.657	9.47x10^-7	0.000369
FBtr0086555	CG9416-RA			9926.273	4320.114	0.00348	0.0291
FBtr0086556	CG30127			474.904	1843.462	0.000249	0.00699
FBtr0086572	CG15105-RB	abba	another B-box affiliate	3285.62	1156.744	0.00337	0.0285
FBtr0086610		Mctp		209.575	746.385	0.000186	0.00602
FBtr0086672	CG17525-RA	GstE4	Glutathione S transferase E4	101.633	465.302	0.000258	0.00711
FBtr0086675	CG17531-RA	GstE7	Glutathione S transferase E7	2152.066	4357.258	0.00131	0.0164
FBtr0086676	CG17533-RA	GstE8	Glutathione S transferase E8	1538.238	9663.673	2.09x10^-6	0.000518
FBtr0086677	CG17534-RA	GstE9	Glutathione S transferase E9	1037.905	4805.701	2.42x10^-6	0.000544
FBtr0086698	CG5226			1376.311	3513.346	0.00063	0.0112
FBtr0086726	CG17522-RA	GstE10	Glutathione S transferase E10	1003.807	485.62	0.00592	0.0401
FBtr0086794	CG30111			2277.523	846.446	0.00208	0.0215
FBtr0086802	CG5076-RA	elk	eag-like K^+ channel	121.616	286.018	0.00423	0.0329
FBtr0086808	CG10911-RA			818.129	3926.277	0.00289	0.0259
FBtr0086826	CG15844			292.69	1665.083	4.52E-05	0.00289
FBtr0086955	CG6530-RA	mthl3	methuselah-like 3	352.762	993.689	0.00532	0.0376
FBtr0086956	CG6536			147.434	836.125	2.35E-05	0.00208
FBtr0086975	CG6953-RA	fat-spondin		9024.325	4128.538	0.000269	0.00715
FBtr0086982	CG15611			275.888	617.02	0.00496	0.0362
FBtr0086987	CG11395-RA			3021.014	1368.813	0.00193	0.0207
FBtr0087005	CG8938-RB	GstS1	Glutathione S transferase S1	16233.75	44221.014	2.52E-05	0.00215
FBtr0087047	CG6518-RA	inaC	inactivation no afterpotential C	115.428	433.858	0.00084	0.0131
FBtr0087048	CG6622-RB	Pkc53E	Protein C kinase 53E	388.77	896.159	8.72x10^-6	0.00129

FBtr0087056	CG6702-RA	Cbp53E	Calbindin 53E	285.246	820.218	0.00223	0.0223
FBtr0087071	CG8910-RA			238.823	556.035	0.00268	0.025
FBtr0087076	CG8652-RA	Ugt37c1	UDP-glycosyltransferase 37c1	2408.67	983.536	0.000825	0.0129
FBtr0087098	CG4945-RA			2374.807	950.153	0.00117	0.0153
FBtr0087099	CG4945-RB			2145.03	855.526	0.00306	0.0268
FBtr0087107	CG5089-RA			138.467	68.41	0.000931	0.0137
FBtr0087137	CG15705-RA			263.458	125.6	0.00603	0.0406
FBtr0087142	CG15924			480.973	175.665	0.00611	0.0409
FBtr0087143	CG3896			1785.604	672.278	0.00372	0.0302
FBtr0087157	CG4398-RA			1030.608	477.348	0.000696	0.0118
FBtr0087221	CG8421			3469.879	1627.803	0.0073	0.0464
FBtr0087248		Ptp52F		709.058	1479.403	4.08E-05	0.00275
FBtr0087276	CG18255-RG	Strn-Mlck	Stretchin-Mlck	805.983	243.064	0.00122	0.0157
FBtr0087310	CG8249-RA			2585.201	1181.107	0.00449	0.0338
FBtr0087311	CG8246-RA	Poxn	Pox neuro	1742.277	830.444	0.00234	0.023
FBtr0087319	CG30080-RA			3114.483	1394.434	0.00184	0.0201
FBtr0087323	CG12958			85.462	339.997	0.000764	0.0125
FBtr0087324	CG12959			72.735	231.768	0.00622	0.0415
FBtr0087325	CG8179-RA			264.87	1199.693	0.000275	0.00722
FBtr0087326	CG30470			207.88	621.738	0.00447	0.0338
FBtr0087338	CG12963			84.056	204.808	0.00219	0.0222
FBtr0087361	CG18285-RA	igl	igloo	610.345	2236.804	0.00318	0.0274
FBtr0087371	CG16827-RA	αPS4		96.386	298.794	0.0022	0.0222
FBtr0087401	CG8093-RA			67.33	3876.264	1.34x10^-6	0.000416
FBtr0087408	CG10257-RA			621.809	247.507	0.00389	0.031
FBtr0087445	CG10200-RA			1115.661	555.393	0.00229	0.0226
FBtr0087452	CG10242-RA	Cyp6a23		1318.031	4402.433	0.00352	0.0293
FBtr0087457	CG10246			243.066	669.558	0.00428	0.0331
FBtr0087504	CG33469-RA			43.364	231.128	0.00424	0.033
FBtr0087536	CG8503-RA			8806.241	4002.617	0.00438	0.0335
FBtr0087537	CG8523-RA	Mdr50	Multi drug resistance 50	160.459	1628.362	9.94E-05	0.00431
FBtr0087547	CG13941-RA	Arc2		499.658	3097.419	1.95E-05	0.00195
FBtr0087551	CG30070			457.541	151.406	0.00129	0.0163
FBtr0087556	CG13939-RA	Obp50e	Odorant-binding protein 50e	32.914	2407.565	1.79x10^-6	0.00047
FBtr0087559	CG10102			7324.993	30505.15	1.57E-05	0.00178
FBtr0087560	CG12505-RA	Arc1		4643.487	27357.479	1.90x10^-6	0.000486
FBtr0087566	CG8547			5603.067	2783.054	0.0028	0.0257

FBtr0087609	CG6704-RA			2279.375	956.428	0.00195	0.0208
FBtr0087628	CG6280-RA			168.91	2078.369	7.63E-05	0.00378
FBtr0087664	CG4812-RA	Ser8		302.578	626.196	0.0036	0.0297
FBtr0087722	CG13325-RA			40.037	140.832	0.00242	0.0235
FBtr0087753	CG17047-RA			5551.119	2126.382	0.00105	0.0145
FBtr0087754	CG4734-RA			1071.039	2960.365	0.000498	0.00998
FBtr0087766	CG12251-RA	AQP	aquaporin	296.938	145.76	0.00415	0.0324
FBtr0087785	CG3830-RA	vg	vestigial	1864.666	812.178	0.00221	0.0222
FBtr0087799	CG3884-RB			2120.882	9958.686	0.000221	0.00658
FBtr0087800	CG3884-RA			547.791	5478.612	7.82E-05	0.00378
FBtr0087817	CG30486-RA			72.552	267.964	6.21E-05	0.00334
FBtr0087818	CG30488-RA			185.158	569.068	1.01E-05	0.00141
FBtr0087847	CG13148-RB			1367.596	593.238	0.000843	0.013
FBtr0087848	CG13148-RA			522.348	216.335	0.00251	0.024
FBtr0087855	CG17579-RA			2181.88	5753.982	0.000217	0.00657
FBtr0087856	CG17579-RB			1140.427	3395.187	0.00004	0.00272
FBtr0087881	CG8785-RA			1540.783	3273.436	0.000433	0.00915
FBtr0087892	CG13165			73.667	480.383	2.24E-05	0.00206
FBtr0087895	CG30046-RB			1066.77	482.885	1.61x10^-6	0.000443
FBtr0087914	CG30042-RA	Cpr49Ab		213.579	61.047	0.00372	0.0302
FBtr0087925	CG13157-RA			493.39	246.068	0.000388	0.00863
FBtr0087972	CG8850-RB			1562.209	550.925	0.000525	0.0102
FBtr0087984	CG12367-RA	Hen1		283.236	621.022	0.00042	0.00905
FBtr0087992	CG8453-RA	Cyp6g1		90.855	253.905	0.00391	0.0312
FBtr0088019	CG13178-RA			280.547	3017.022	1.23x10^-7	0.000191
FBtr0088021	CG30040-RA	jeb	jelly belly	81.643	213.891	0.00376	0.0304
FBtr0088061	CG18188-RA	Damm	Death associated molecule related to Mch2	207.087	614.379	0.00198	0.0209
FBtr0088064	CG8991-RA	Sobp	Sine oculis-binding protein	4103.399	1869.06	0.00234	0.023
FBtr0088077	CG8238-RA	Buffy		1054.556	2124.507	9.92E-05	0.00432
FBtr0088120	CG13209-RA	sha	shavenoid	10135.613	4102.226	0.000431	0.00914
FBtr0088133	CG7759-RA			7358.044	2986.554	0.00778	0.0482
FBtr0088136	CG7777-RB			381.26	905.699	5.39x10^-6	0.000971
FBtr0088137	CG7777-RA			3055.765	7084.332	1.87E-05	0.0019
FBtr0088141	CG9023-RA	Drip		1736.808	4241.983	0.000963	0.0139
FBtr0088142	CG9023-RB	Drip		852.235	2174.17	1.83E-05	0.00189
FBtr0088151	CG9033-RB	Tsp47F	Tetraspanin 47F	794.21	1821.45	0.000978	0.0139
FBtr0088152	CG9033			1057.689	2236.628	0.00385	0.0309

FBtr0088186	CG13214			196.587	58.225	0.000991	0.014
FBtr0088187	CG13214			189.732	56.864	0.000894	0.0134
FBtr0088197	CG9084-RB			521.966	2713.826	1.77E-05	0.00186
FBtr0088246	CG12344-RA			126.98	864.481	1.10x10^-6	0.000382
FBtr0088309	CG30320			577.166	241.557	0.00217	0.022
FBtr0088390	CG2328-RA	eve	even skipped	1168.488	489.452	5.21E-05	0.00305
FBtr0088407	CG2269-RC			292.616	988.056	0.00305	0.0268
FBtr0088467	CG1773-RA			596.227	213.347	0.00143	0.0171
FBtr0088475	CG1652-RA	lectin-46Cb		1174.584	393.27	0.000547	0.0104
FBtr0088476	CG1656-RA	lectin-46Ca		1761.529	600.352	0.00102	0.0142
FBtr0088494	CG1648-RB			1329.636	485.515	0.000387	0.00863
FBtr0088498	CG30004			3691.508	1625.228	0.00121	0.0156
FBtr0088502	CG12926-RA			3086.524	8028.436	5.63E-05	0.00316
FBtr0088584	CG30345			262.999	621.31	0.00766	0.0477
FBtr0088620	CG8046-RA			423.682	198.564	0.0047	0.0349
FBtr0088622	CG8008-RA			252.769	531.138	0.000375	0.00852
FBtr0088636	CG30350-RA			388.361	160.532	0.000754	0.0124
FBtr0088660	CG13747-RA			190.317	42.665	0.000349	0.00817
FBtr0088662	CG13743-RA			59.422	135.55	0.00324	0.0277
FBtr0088666	CG13744-RA			1918.537	611.467	0.00306	0.0268
FBtr0088671	CG8216-RA			50.142	179.853	0.000979	0.0139
FBtr0088687	CG30352			412.379	179.586	0.00114	0.0151
FBtr0088690	CG2397-RA	Cyp6a13		321.315	3828.303	3.09x10^-6	0.000661
FBtr0088698	CG30353			495.105	221.4	0.006	0.0405
FBtr0088705	CG8738-RA			554.742	177.694	0.000436	0.0092
FBtr0088725	CG8586-RA			793.268	230.2	0.00412	0.0324
FBtr0088729	CG8642			328.433	138.055	9.56E-05	0.00429
FBtr0088734	CG8687			72.118	2462.584	9.06E-05	0.00422
FBtr0088735	CG8687			198.068	6978.219	1.47E-05	0.00169
FBtr0088746	CG2062-RA	Cyp4e1	Cytochrome P450-4e1	2784.988	809.075	0.000947	0.0138
FBtr0088747	CG8694-RA	Mal-A2	Maltase A2	248.695	2457.264	0.000114	0.00476
FBtr0088748	CG8693-RA	Mal-A4	Maltase A4	260.43	2512.901	5.49E-05	0.00313
FBtr0088749	CG30359-RA	Mal-A5	Maltase A5	2890.921	1221.623	0.00148	0.0175
FBtr0088757	CG11669-RA	Mal-A7	Maltase A7	26.077	266.915	1.63E-05	0.00178
FBtr0088760	CG2110-RA	Cyp4ad1		452.6	5028.172	5.21x10^-6	0.00098
FBtr0088780	CG8713-RA			2917.759	1226.919	0.00288	0.0259
FBtr0088794	CG14760-RA			189.644	80.127	0.000165	0.00562

FBtr0088808	CG8708			600.005	236.371	0.00204	0.0212
FBtr0088810	CG30374			41.943	142.29	0.000153	0.0055
FBtr0088827	CG12769-RB			8243.293	3592.973	0.00732	0.0465
FBtr0088867	CG14762-RA			751.418	3454.232	1.07E-05	0.00146
FBtr0088868	CG11191-RA			279.798	1466.696	6.00x10^-6	0.00103
FBtr0088922	CG2065-RA			1365.707	4279.96	0.00468	0.0348
FBtr0088927	CG1941-RA			1255.768	3210.73	6.55E-05	0.00344
FBtr0089004	CG11145-RA			303.982	137.863	0.00427	0.0331
FBtr0089025	CG12844			362.752	145.859	0.000447	0.00928
FBtr0089026	CG12844-RB	Tsp42Eh	Tetraspanin 42Eh	1290.344	447.888	0.00436	0.0335
FBtr0089027	CG12844			832.014	225.72	0.00706	0.0454
FBtr0089028	CG12843-RA	Tsp42Ei	Tetraspanin 42Ei	2581.502	882.944	0.00824	0.05
FBtr0089052	CG1857-RA	nec	necrotic	4212.59	1947.117	4.46E-05	0.00289
FBtr0089054	CG1865-RA	Spn43Ab	Serine protease inhibitor 43Ab	521.049	259.131	0.00312	0.0271
FBtr0089055	CG4486-RA	Cyp9b2	Cytochrome P450-9b2	919.157	5365.576	0.00185	0.0202
FBtr0089056	CG4485-RA	Cyp9b1	Cytochrome P450-9b1	173.071	440.294	0.00216	0.022
FBtr0089118	CG1674			1004.128	353.098	0.00232	0.0229
FBtr0089119	CG1674-RD			489.246	117.756	0.000157	0.00555
FBtr0089123	CG32850-RA			1721.652	4223.851	7.64E-05	0.00377
FBtr0089287	CG3477-RA	Pxd	Peroxidase	1011.685	3009	0.000139	0.00536
FBtr0089292	CG8799			299.213	1094.307	0.00115	0.0151
FBtr0089319	CG10604-RA	bsh	brain-specific homeobox	443.719	211.733	0.000948	0.0138
FBtr0089324	CG6806-RA	Lsp2	Larval serum protein 2	280.494	108.996	0.00287	0.0259
FBtr0089326	CG11538			176.671	55.66	0.000145	0.00538
FBtr0089327	CG11049-RA	sv	shaven	1194.212	2701.332	0.00109	0.0148
FBtr0089329	CG11143-RA	Inos		1737.226	3518.482	0.00275	0.0255
FBtr0089376	CG33485-RA	dpr9		306.207	934.821	1.43E-05	0.00167
FBtr0089427	CG2411-RA	ptc	patched	5971.374	2937.655	0.00236	0.0231
FBtr0089490	CG4432-RA	PGRP-LC	Peptidoglycan recognition protein LC	2508.372	899.512	0.000627	0.0111
FBtr0089491	CG4432-RB	PGRP-LC	Peptidoglycan recognition protein LC	1505.226	555.692	0.00306	0.0268
FBtr0089492	CG4432-RC	PGRP-LC	Peptidoglycan recognition protein LC	1642.909	683.646	0.00542	0.038
FBtr0089500	CG5472-RA	Pal2	Peptidyl-α-hydroxyglycine-α-amidating lyase 2	543.465	1766.01	0.00706	0.0454
FBtr0089502	CG5472			1222.616	5230.481	0.000197	0.0062
FBtr0089560	CG6385-RA			1548.121	757.607	0.000306	0.00753

FBtr0089569	CG6449-RA	NijA	Ninjurin A	363.338	95.79	0.00502	0.0364
FBtr0089570	CG6449-RB	NijA	Ninjurin A	1792.399	828.856	0.00155	0.018
FBtr0089571	CG6449-RC	NijA	Ninjurin A	1620.408	710.404	0.000288	0.00737
FBtr0089577	CG7234-RI	GluRIIB	Glutamate receptor IIB	1771.551	501.41	0.00213	0.0217
FBtr0089599	CG9398-RA	king-tubby		2228.42	4710.653	0.000675	0.0116
FBtr0089608	CG33495-RA	Dup99B	Ductus ejaculatorius peptide 99B	134.336	43.508	0.000779	0.0126
FBtr0089695	CG14901-RA	Gr89a		32.81	114.789	0.00717	0.0458
FBtr0089789	CG31795			904.59	2283.364	0.00212	0.0217
FBtr0089790	CG31795			1757.181	4008.634	0.00223	0.0223
FBtr0089804	CG32688			172.966	369.465	0.000487	0.00985
FBtr0089812	CG3277			561.125	1924.192	0.00031	0.00758
FBtr0089813	CG3277			223.46	887.152	9.26E-05	0.00427
FBtr0089931	CG8024-RB	Itd	lightoid	7356.838	3433.146	0.00169	0.019
FBtr0089937	CG8852-RA			508.893	248.338	0.00242	0.0235
FBtr0089956	CG9932-RA			3622.112	1449.49	0.000416	0.00901
FBtr0089969	CG15102			2104.929	6769.214	4.19E-05	0.00281
FBtr0089970	CG15102-RA	Jheh2	Juvenile hormone epoxide hydrolase 2	2406.313	7170.17	7.85E-05	0.00378
FBtr0091456	CG33514-RA			1261.179	2588.641	0.00193	0.0207
FBtr0091458	CG33516			80.484	205.967	0.00448	0.0338
FBtr0091491	CG33528-RE	Vmat	Vesicular monoamine transporter	593.975	226.525	0.00413	0.0324
FBtr0091497	CG33531-RA	Ddr	Discoidin domain receptor	483.612	1603.57	8.01x10^-6	0.00126
FBtr0091508		upd3		40.389	336.101	0.000146	0.00535
FBtr0091534	CG33557-RA			351.525	166.262	0.0069	0.0447
FBtr0091616	CG33639-RA			145.465	311.547	0.00143	0.0171
FBtr0091658	CG33678			83.339	280.283	0.00283	0.0258
FBtr0091765	CG33764-RA			897.057	272.592	0.000139	0.00537
FBtr0091796	CG33792-RA			56.995	256.012	1.86E-05	0.00189
FBtr0091915	CG33911			353.261	108.579	0.00115	0.0152
FBtr0091930	CG33926-RA			70.241	3069.858	0.000039	0.00271
FBtr0099998		Octbeta3R		442.931	942.8	4.72E-05	0.00292
FBtr0100035	CG33989-RD	pHCl		80.853	971.006	0.000235	0.00681
FBtr0100036	CG33989-RE	pHCl		98.324	689.612	4.91x10^-6	0.000967
FBtr0100037	CG33989-RF	pHCl		80.43	755.563	0.000456	0.00943
FBtr0100060	CG34005			123.638	469.634	0.00232	0.0229
FBtr0100068	CG34013			254.106	110.958	0.00399	0.0316

FBtr0100086	CG34031			125.606	926.919	1.12x10^-7	0.000212
FBtr0100087	CG34032-RA			41.785	141.677	0.000686	0.0117
FBtr0100093	CG34038			967.433	361.841	0.000272	0.00717
FBtr0100101	CG34046			211.565	61.181	0.000111	0.00467
FBtr0100110	CG8927-RB			490.658	1197.995	0.00016	0.00558
FBtr0100117	CG14681			325.207	99.414	0.000122	0.00497
FBtr0100118	CG14681			1615.342	738.546	0.00586	0.0399
FBtr0100125	CG31764-RD	vir-1	virus-induced RNA 1	32.418	118.671	2.46E-05	0.00213
FBtr0100131	CG9918-RD	Pk1r	Pyrokinin 1 receptor	179.305	74.594	0.00188	0.0203
FBtr0100158	CG6772-RD	Slob	Slowpoke binding protein	86.939	1271.413	0.000011	0.00147
FBtr0100225	CG7399-RB	Hn	Henna	3720.967	1586.081	0.000246	0.00695
FBtr0100258	CG8938-RC	GstS1	Glutathione S transferase S1	9156.039	36054.215	8.84x10^-6	0.00129
FBtr0100264	CG15279			710.297	1666.562	0.000277	0.00723
FBtr0100290	CG14946			5756.493	12998.247	2.31E-05	0.00208
FBtr0100344	CG11049-RF	sv	shaven	5098.3	13266.336	0.000184	0.00602
FBtr0100345	CG11049-RG	sv	shaven	2390.216	7457.296	5.96E-05	0.00327
FBtr0100410	CG10045-RB	GstD1	Glutathione S transferase D1	390.18	1108.065	0.000523	0.0102
FBtr0100506	CG4637-RB	hh	hedgehog	2076.027	793.895	0.00386	0.0309
FBtr0100524	CG10097-RA			204.813	440.583	0.00398	0.0316
FBtr0100525	CG10097-RB			155.963	453.959	0.000549	0.0104
FBtr0100600	CG11153-RB	Sox102F		1040.752	497.669	0.00006	0.00329
FBtr0100857	CG34063-RA	mt:ND2	mitochondrial NADH-ubiquinone oxidoreductase chain 2	7875.08	3668.335	0.00534	0.0376
FBtr0110821	CG17205			146.212	770.356	3.16E-05	0.00241
FBtr0110837	CG31201-RB	GluRIIE	Glutamate receptor IIE	886.54	293.152	0.00118	0.0154
FBtr0110849	CG14597			504.8	1317.832	1.04E-05	0.00144
FBtr0110881	CG7255-RH			768.455	285.666	0.00196	0.0209
FBtr0110955	CG31499			167.716	399.146	0.00125	0.0159
FBtr0110963	CG14885-RC	Gyc-89Da	Guanylyl cyclase at 89Da	282.699	130.748	0.00517	0.0368
FBtr0110970	CG15078-RA	Mctp	Multiple C2 domain and transmembrane region protein	313.17	1388.03	4.84x10^-6	0.000963
FBtr0111026	CG9610-RC	Poxm	Pox meso	1726.735	79.004	0.00746	0.047
FBtr0111188	CG40486-RB			61.52	598.667	0.000124	0.00499
FBtr0112536	CG34334-RA			154.603	395.538	5.81E-05	0.00321
FBtr0112566	CG34356-RC			199.733	509.51	0.000182	0.00599
FBtr0112607	CG34375-RA			564.856	1206.016	0.00214	0.0219
FBtr0112610	CG34377-RA			1364.888	488.315	0.00033	0.00785

FBtr0112619	CG34381-RB			73.374	181.48	0.00117	0.0153
FBtr0112626	CG14469			858.466	2042.586	0.00197	0.0209
FBtr0112645	CG34396-RD			1854.109	606.229	0.00258	0.0244
FBtr0112648	CG34398-RA			1236.417	533.66	0.00675	0.044
FBtr0112650	CG34399-RC	Nox	NADPH oxidase	1110.815	370.101	0.00219	0.0222
FBtr0112729	CG34428-RA			383.949	119.434	0.00226	0.0225
FBtr0112747	CG34443-RA			753.561	188.902	0.000924	0.0136
FBtr0112750	CG34446-RA			490.159	135.854	0.00434	0.0334
FBtr0113018	CG15412-RB			265.118	103.121	0.0023	0.0227
FBtr0113108	CG6044-RD			397.634	1542.841	7.23x10^-6	0.00117
FBtr0113163	CG7512-RB			1643.317	3910.023	2.81E-05	0.00228
FBtr0113174	CG11905-RI			14252.4	6935.335	0.00115	0.0151
FBtr0113177	CG13027-RB	Obp73a	Odorant-binding protein 73a	51.778	207.118	0.0021	0.0216
FBtr0113266	CG17622			29.777	92.574	0.000423	0.00908
FBtr0113278	CG13613			228.146	59.6	0.00247	0.0237
FBtr0113313	CG3669-RB			250.373	87.283	0.000521	0.0102
FBtr0113329	CG18669			829.248	202.882	0.00253	0.0241
FBtr0113345	CG18748-RC			748.589	1702.015	3.32E-05	0.00247
FBtr0113346	CG18765-RB			733.326	3035.243	2.03E-05	0.00199
FBtr0113347	CG10251-RB			75.405	182.07	0.00563	0.0388
FBtr0113389	CG31103-RB			1599.304	455.378	0.00356	0.0295
FBtr0113424	CG32121-RB			99.536	34.16	0.00123	0.0157
FBtr0113429	CG32204-RB			99.803	396.614	0.00222	0.0223
FBtr0113465	CG33542-RB	upd3	unpaired 3	89.716	681.848	2.69E-05	0.0022
FBtr0113769	CG2893-RD			8220.388	3937.402	0.00663	0.0434
FBtr0113803	CG40122			1985.349	5860.401	0.00027	0.00716
FBtr0113992	CG41113			80.259	463.079	0.00714	0.0457
FBtr0114043	CG41284			556.869	1121.771	0.000441	0.00922
FBtr0114456	CG16801-RC	Hr51	Hormone receptor 51	495.197	201.903	0.00166	0.0188
FBtr0114460	CG3277-RC			490.345	1356.101	0.00163	0.0187
FBtr0114504	CG10301-RB			503.421	240.403	0.00129	0.0162
FBtr0114515	CG18531-RB	Gr2a	Gustatory receptor 2a	331.877	721.145	0.000244	0.00694
FBtr0114516	CG18744-RB			72.933	434.535	0.00153	0.0179
FBtr0114525	CG32036-RC			198.654	52.39	0.00162	0.0186
FBtr0114535	CG4382-RB			299.642	66.206	0.00308	0.0269
FBtr0114541	CG5428-RB			7142.822	2561.425	0.00449	0.0338
FBtr0273227	CG3502-RB			1083.371	225.764	0.00357	0.0296
FBtr0273244	CG4226-RC	GluRIIC	Glutamate receptor IIC	2488.503	836.191	0.00272	0.0253
FBtr0273260	CG11898-RB			96.785	279.48	8.47E-05	0.00401

FBtr0273295	CG5751			123.684	8253.471	2.70x10^-7	0.000243
FBtr0273308	CG30263-RB			45.161	804.128	2.39E-05	0.0021
FBtr0273399	CG8588-RF	pst	pastrel	3215.018	6516.272	0.000556	0.0104
FBtr0273416	CG32335-RB			691.167	3439.606	8.17x10^-6	0.00127
FBtr0273450	CG33179-RC	beat-IIIb		49.136	211.952	0.00171	0.0191
FBtr0289971	CG13622-RB			2003.594	831.905	0.00199	0.021
FBtr0290001	CG32381-RB	unc-13-4A		208.118	569.174	0.00507	0.0365
FBtr0290002	CG32547-RC			136.868	729.594	7.75E-05	0.00376
FBtr0290021	CG5321-RB			5852.553	2536.334	0.00439	0.0335
FBtr0290044	CG9449-RF			6061.955	2138.659	0.0011	0.0149
FBtr0290055	CG31370-RB			478.47	1188.405	0.00292	0.0262
FBtr0290087	CG12507-RB			983.979	4665.691	0.000145	0.00539
FBtr0290126	CG34400-RC			210.159	1069.005	0.00138	0.0167
FBtr0290129	CG34400-RE			392.246	1693.177	0.00108	0.0148
FBtr0290131	CG6938-RB			84.093	461.547	0.00184	0.0201
FBtr0290223	CG14837-RC			40.529	91.483	0.00316	0.0273
FBtr0290268	CG5772-RB	Sur	Sulfonylurea receptor	1085.874	447.038	0.00757	0.0474
FBtr0290276	CG7440-RD	tgy	twiggy	1552.341	761.386	0.000114	0.00477
FBtr0290328	CG42242-RD	beat-VII		192.519	1113.823	0.000528	0.0102
FBtr0290335	CG42244-RG	Octβ3R		232.314	486.791	0.000217	0.00656
FBtr0299509	CG42247-RC	DCX-EMAP	Doublecortin-domain-containing echinoderm-microtubule-associated protein ortholog	46.662	95.519	0.00701	0.0452
FBtr0299541	CG12996			923.094	327.93	0.00528	0.0374
FBtr0299575	CG42261-RA			342.758	700.838	0.0017	0.0191
FBtr0299576	CG42262-RA			700.898	2101.681	0.000389	0.00859
FBtr0299649	CG42280-RE	ome	omega	3798.856	1293.307	0.000813	0.0128
FBtr0299663	CG42284-RC			244.922	828.161	2.67x10^-6	0.000587
FBtr0299676	CG42296-RA			2863.051	1404.609	0.00322	0.0276
FBtr0299697	CG42309-RB	Mlp60A	Muscle LIM protein at 60A	248.747	66.073	0.00475	0.0351
FBtr0299707	CG42311-RK	grh	grainy head	4086.598	1950.314	0.00136	0.0167
FBtr0299785	CG42325-RF	Pde1c	Phosphodiesterase 1c	1299.363	3487.2	0.000946	0.0138
FBtr0299786	CG42325-RG	Pde1c	Phosphodiesterase 1c	1038.487	2768.807	4.76E-05	0.00293
FBtr0299842	CG42331-RB			2648.182	700.624	2.35E-05	0.00209
FBtr0299843	CG42331-RC			7813.099	3174.48	0.00207	0.0214
FBtr0299862	CG42339-RB			415.685	1044.923	4.11x10^-6	0.000838

FBtr0299879	CG3635-RB			1041.433	114.065	0.0033	0.0281
FBtr0299926	CG40305-RB	FucTC		964.688	2050.746	2.82E-05	0.00227
FBtr0299930	CG42347-RC			6155.811	3057.292	0.00288	0.0259
FBtr0299934	CG42348			278.181	825.55	5.12E-05	0.00302
FBtr0299937	CG42349-RD	Pkcδ	Protein kinase C δ	1002.843	397.034	0.00438	0.0335
modified_GFP_1				381.054	38016.171	0.00184	0.0201

Appendix C. Microarray analysis comparing Hindsight Depleted embryos with the Control

Transcript Fbtr ID	Gene ID	Official Symbol	Official Name	Control - linear value	Knockdown - linear value	P value before FDR	P value after FDR
FBtr0070003	CG32825-RA	Or19b	Odorant receptor 19b	2561.851	89.264	0.000309	0.0365
FBtr0070032	CG9571-RA	fd19B	forkhead domain 19B	283.48	41.77	0.000115	0.0203
FBtr0070234	CG11420-RA	png	pan gu	444.974	181.153	4.36E-05	0.0106
FBtr0070349	CG3857-RA			1781.162	880.167	0.000332	0.0374
FBtr0070490	CG2759-RA	w	white	1313.361	9026.976	5.91x10^-7	0.00102
FBtr0070534	CG12535-RB			191.401	531.041	0.00056	0.049
FBtr0070535				207.563	569.189	0.000472	0.0444
FBtr0070881	CG5928-RA			1923.211	348.455	1.19E-05	0.00498
FBtr0070890	CG4746-RA	mab-21		141.544	44.634	9.15E-05	0.0175
FBtr0070893	CG14445-RA			146.933	607.147	1.04E-05	0.00467
FBtr0071201	CG15350-RA	Cp7Fb	Chorion protein b at 7F	85.997	31.192	3.90x10^-6	0.00257
FBtr0071311	CG15371-RA	Gr8a	Gustatory receptor 8a	268.337	30.914	6.73x10^-7	0.000886
FBtr0071335	CG12120-RA	t	tan	3576.465	1554.193	2.68x10^-6	0.00219
FBtr0071386	CG32698-RA			428.459	947.771	0.000311	0.0364
FBtr0071870	CG13517-RB	Obp59a	Odorant-binding protein 59a	151.54	60.627	0.000411	0.0415
FBtr0071871	CG13518-RA	Obp59b	Odorant-binding protein 59b	282.117	106.679	1.63E-05	0.00605
FBtr0071872	CG13519-RA	Obp59d	Odorant-binding protein 59d	304.653	22.98	1.98x10^-8	0.000113
FBtr0071920	CG13524-RA	Obp59c	Odorant-binding protein 59c	3844.284	71.111	1.64x10^-6	0.00165
FBtr0071921	CG30259-RA			282.788	79.096	4.07E-05	0.0103
FBtr0071928	CG4373-RA	Cyp6d2		192.701	782.574	0.00028	0.035
FBtr0071952				123.376	47.965	0.000303	0.0368
FBtr0071967	CG30192-RA			76.815	27.914	0.000591	0.0489
FBtr0072049	CG9871-RA	RpL22-like	Ribosomal protein L22-like	135.12	775.781	4.03x10^-6	0.00256
FBtr0073062	CG10812-RA	dro5	drosomycin-5	4338.918	57.443	3.56x10^-9	0.000061
FBtr0073094	CG17746-RB			680.926	328.442	5.37E-05	0.0121
FBtr0073111	CG14963-RA			623.391	288.944	4.37x10^-6	0.00267

FBtr0073511	CG11697-RA			60.446	4625.189	1.18x10^-7	0.000335
FBtr0074703	CG15882-RA			31.154	77.127	8.37E-05	0.0167
FBtr0074790	CG14234-RA			69.981	162.574	0.000223	0.0306
FBtr0074797	CG11941-RA	skpC		166.027	544.701	0.000362	0.039
FBtr0074876				694.317	174.083	3.18E-05	0.00878
FBtr0075316	CG13032-RA			57.696	839.168	1.18x10^-7	0.000289
FBtr0075361	CG4098-RA			1051.603	363	9.08E-05	0.0175
FBtr0075588				573.81	262.463	6.44E-05	0.0137
FBtr0075618	CG12327-RA	Best3	Bestrophin 3	366.93	41.638	3.01E-05	0.00844
FBtr0076701	CG8023-RA	eIF4E-3		992.76	2559.475	9.71E-05	0.0181
FBtr0076805	CG32373-RA			734.735	259.267	0.000129	0.0218
FBtr0076823				1840.402	843.363	0.000409	0.0414
FBtr0076831	CG8539-RA			132.164	49.443	1.58E-05	0.00599
FBtr0076893				631.754	298.154	0.000181	0.0267
FBtr0076918	CG8620-RA			114.855	755.566	1.55E-05	0.00604
FBtr0076920				46.558	121.094	0.000312	0.0364
FBtr0077047	CG6602-RA			291.801	98.586	2.78x10^-6	0.00217
FBtr0077087				167.771	49.039	3.51E-05	0.00955
FBtr0077152	CG10630-RA	blanks		548.599	1772.647	2.33E-05	0.00753
FBtr0077271	CG1304-RA			20.276	725.988	6.39x10^-7	0.000912
FBtr0077420	CG15632-RA	Taf12L	TBP-associated factor 30kD subunit α-2	68.24	168.533	0.000282	0.0348
FBtr0077523	CG31956-RA	pgant4	polypeptide GalNAc transferase 4	516.05	1118.149	0.000402	0.0413
FBtr0077924	CG5450-RA	Cdlc2	Cytoplasmic dynein light chain 2	35.039	108.953	0.000116	0.0202
FBtr0077926	CG14346-RA			540.422	2139.851	2.24E-05	0.00738
FBtr0077927	CG14346-RB			211.946	1074.247	7.28x10^-6	0.0039
FBtr0078344	CG32437-RA			239.24	911.829	0.000306	0.0367
FBtr0078345	CG32440-RA			82.515	356.347	3.62E-05	0.00938
FBtr0078567	CG32461-RA			51.469	114.652	0.000312	0.0362
FBtr0078861	CG12001-RA			392.895	67.639	1.35x10^-6	0.00154
FBtr0078867				1989.147	621.798	8.01x10^-6	0.00404
FBtr0078882	CG31530-RA			1895.066	673.098	8.76E-05	0.0171
FBtr0079062	CG10833-RA	Cyp28d1		1981.125	4124.493	0.000198	0.0282

FBtr0079171	CG9046-RA	Vm26Ab	Vitelline membrane 26Ab	437.053	43.373	8.69x10^-8	0.000298
FBtr0079241	CG13998-RA			190.128	35.361	8.93x10^-6	0.00425
FBtr0079516	CG18585-RA			1805.472	782.21	2.56E-05	0.00781
FBtr0079548				2326.366	1052.496	1.60x10^-8	0.000137
FBtr0080281	CG16963-RA	Cry	Crystallin	110.027	475.228	0.000149	0.0243
FBtr0080670	CG4691-RA			28.962	167.274	2.62E-05	0.00786
FBtr0080753	CG11865-RA			123.481	35.032	0.000145	0.0239
FBtr0080821	CG31819-RA			21.81	76.871	4.36E-05	0.0107
FBtr0081136	CG15169-RA			440.163	55.61	6.17x10^-6	0.00352
FBtr0081241				1323.334	118.17	3.51x10^-8	0.000151
FBtr0081242	CG13083-RB			2003.591	195.636	1.20x10^-6	0.00147
FBtr0081309	CG33117-RA	Victoria		2426.257	1121.74	0.000393	0.0413
FBtr0081406	CG17470-RA			341.019	46.697	1.73x10^-6	0.00164
FBtr0081435				2061.212	436.962	7.93x10^-6	0.00412
FBtr0081514	CG8667-RA	dimm	dimmed	482.031	217.855	0.000486	0.045
FBtr0081603	CG14606-RA			104.302	308.62	0.000241	0.0325
FBtr0082428	CG14720-RA			1054.277	523.599	0.000576	0.0494
FBtr0082571	CG11512-RA	GstD4	Glutathione S transferase D4	325.306	805.361	4.74E-05	0.0112
FBtr0083790	CG11407-RA			183.779	1146.993	0.00021	0.0292
FBtr0083968	CG15696-RA			553.578	199.401	6.18E-05	0.0136
FBtr0084003	CG12278-RA			288.601	67.945	2.55E-05	0.00792
FBtr0084243				819.393	388.261	0.000358	0.039
FBtr0084420	CG10170-RA			755.78	1928.483	0.000362	0.0392
FBtr0084431	CG4408-RA			859.234	3629.057	6.18x10^-7	0.000961
FBtr0085860	CG2191-RA	Smvt	Sodium-dependent multivitamin transporter	842.85	2286.264	5.16E-05	0.0118
FBtr0085962				44.657	274.341	4.48x10^-7	0.000852
FBtr0086215	CG30154-RA			776.784	353.525	0.000467	0.0444
FBtr0086662	CG18108-RA	IM1	Immune induced molecule 1	45.575	237.696	0.00032	0.0366
FBtr0086665	CG16844-RA	IM3	Immune induced molecule 3	96.231	673.418	0.000516	0.047

FBtr0086956				147.434	574.72	0.000063	0.0137
FBtr0087137	CG15705-RA			263.458	745.228	1.98x10^-6	0.00178
FBtr0087408	CG10257-RA			621.809	92.857	6.36x10^-6	0.00352
FBtr0087467				430.898	1003.889	0.000142	0.0237
FBtr0087560	CG12505-RA	Arc1	Activity-regulated cytoskeleton associated protein 1	4643.487	13957.684	7.43E-05	0.0152
FBtr0087640	CG30485-RA			125.226	40.41	0.000058	0.0129
FBtr0087642	CG6553-RA			201.092	49.158	3.19x10^-7	0.000683
FBtr0087643	CG6543-RA			668.007	287.22	0.000132	0.0222
FBtr0087644	CG6543-RB			92.322	39.915	4.57E-05	0.0109
FBtr0087909	CG33012-RA			91.66	196.911	0.000398	0.0411
FBtr0088190	CG9079-RA	Cpr47Ea		48.168	384.422	3.92E-05	0.0101
FBtr0088591	CG1944-RA	Cyp4p2		3861.651	225.132	2.85x10^-6	0.00203
FBtr0088660	CG13747-RA			190.317	43.02	0.000263	0.0341
FBtr0089563	CG6416-RF	Zasp66	Z band alternatively spliced PDZ-motif protein 66	248.588	569.835	0.000111	0.02
FBtr0089569	CG6449-RA	NijA	Ninjurin A	363.338	48.259	2.82x10^-6	0.0021
FBtr0089570	CG6449-RB	NijA	Ninjurin A	1792.399	330.56	1.17E-05	0.005
FBtr0089571	CG6449-RC	NijA	Ninjurin A	1620.408	349.201	5.00x10^-6	0.00296
FBtr0089804				172.966	352.331	8.80x10^-6	0.00431
FBtr0091448	CG33508-RA	ppk13	pickpocket 13	194.013	50.262	1.36x10^-6	0.00145
FBtr0100357				358.352	123.17	0.000511	0.0468
FBtr0100835	CG34057-RB			379.469	176.441	9.22E-05	0.0174
FBtr0112747	CG34443-RA			753.561	271.663	0.000348	0.0385
FBtr0113170	CG13481-RB			111.459	262.957	0.000238	0.0323
FBtr0114530	CG33276-RB			1487.78	709.946	0.000118	0.0201
FBtr0273260	CG11898-RB			96.785	238.161	0.000438	0.0438
FBtr0299926	CG40305-RB	FucTC		964.688	2793.575	0.000028	0.00811
FBtr0299946				58.655	354.651	2.57x10^-6	0.0022